IMAGE FUSION, IMAGE REGISTRATION, AND RADIOMETRIC NORMALIZATION FOR HIGH RESOLUTION IMAGE PROCESSING

GANG HONG

April 2007

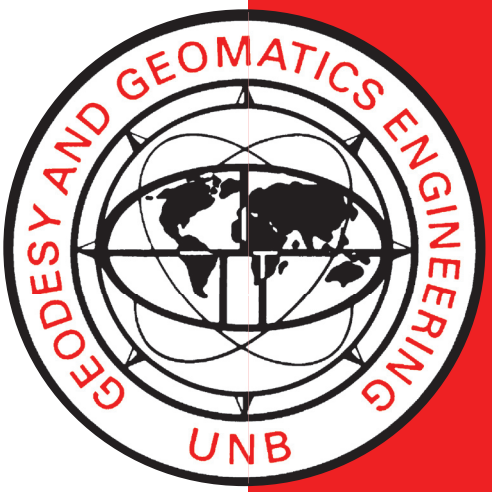

TECHNICAL REPORT
NO. 247

IMAGE FUSION, IMAGE REGISTRATION, AND RADIOMETRIC NORMALIZATION FOR HIGH RESOLUTION IMAGE PROCESSING

Gang Hong

Department of Geodesy and Geomatics Engineering
University of New Brunswick
P.O. Box 4400
Fredericton, N.B.
Canada
E3B 5A3

April 2007

PREFACE

This technical report is a reproduction of a dissertation submitted in partial fulfillment of the requirements for the degree of Doctor of Philosophy in the Department of Geodesy and Geomatics Engineering, April 2007. The research was supervised by Dr. Yun Zhang, and funding was provided by the GEOIDE Network of Centres of Excellence.

As with any copyrighted material, permission to reprint or quote extensively from this report must be received from the author. The citation to this work should appear as follows:

Hong, Gang (2007). *Image Fusion, Image Registration, and Radiometric Normalization for High Resolution Image Processing*. Ph.D. dissertation, Department of Geodesy and Geomatics Engineering, Technical Report No. 247, University of New Brunswick, Fredericton, New Brunswick, Canada, 198 pp.

ABSTRACT

High resolution multi-temporal, multi-sensor remotely sensed data are often used in Earth observation applications. Image fusion is a widely used method to integrate those data, while image registration and radiometric normalization are two necessary procedures in transforming multi-temporal or multi-sensor data into identical geometric and radiometric bases respectively. This Ph.D research attempts to solve problems and develop improved techniques in these three aspects.

A new image fusion method based on the wavelet and IHS integration is proposed to reduce the color distortion in fusing high resolution images. This method was successfully evaluated using optical images (IKONOS and QucikBird) and microwave images (airborne SAR and Radarsat with commonly used multi-spectral images). This research also discusses the wavelet-based fusion problems, improvement approaches, and the factors that should be considered in fusion process.

Further using the multi-resolution property of wavelet, a new image registration method has been proposed. It uses the wavelet multi-resolution property to extract feature points; the normalized cross-correlation and relax-based probability matching techniques to find similarity between feature points in reference image and sensed image; and the triangle-based local transformation model to resample the sensed image. The method was evaluated using two sets of data. The evaluations show that the method can semi-automatically select enough control points and reduce the local distortions caused by terrain relief.

For image normalization, improved strategies are provided for normalizing the high resolution images through modifications to the existing image normalization methods, because existing image normalization methods designed for the Landsat TM/MSS image cannot be directly applied to high resolution images. It is shown the improved strategies to be very helpful in normalizing high resolution images.

ACKNOWLEDGEMENTS

I would like to thank my supervisor, Dr. Yun Zhang, for his financial support, chances to get access to several projects, and his valuable guidance and tremendous support in preparation of the papers for publication and this dissertation, throughout my Ph.D program. I am very grateful to Dr. David Coleman for his help in organizing my minor examination, and reviewing my Ph.D research proposal and dissertation. Thanks are also given to Dr. Francois Anton for reviewing my paper and making suggestive comments.

I want to give thanks to the following people: David Fraser, for his help in writing my papers, good suggestions in my projects and also his jokes to make me feel happy while struggling for my Ph.D; Krista Amolins, for her critical reviewing part of my thesis, and making my thesis more concise and logical; Felix McCarthy and Dan Edwards, for their giving me a lot help about data used in the experiments; and Teresa Tang and Richard Chan, for their help in resolving problems met in the GIS application. I also want to thank my colleagues and friends, Xiaolun Yi, Garrret Duffy, Shaheen Ghayourmanesh, Reza Ghoddousi-Fard, Zeng Xiong, and Sheng Gao; it is you guys who help me live a wonderful life in Fredericton.

I would like to thank GEOIDE which partly supported my Ph.D research and Intermap Corporate Lt. for giving me the chance to evaluate my algorithm in high resolution SAR application.

Finally, I would like to give a special thanks to my wife. Thank you very much for your spiritual support, understanding, and unconditional love. I also give thanks to my

parents and my parents-in-law. Thank you very much for your understanding and support over so many years.

Table of Contents

List of Tables

List of Figures

Acronym

ABM	Area-Based Matching
ATRO	fusion based on the “à TROus” wavelet
BIOR	BIORthogonal wavelet fusion with decimation
CRI	Color Reference Image
DB	Dark and Bright set
DSM	Digital Surface Model
DWT	Discrete Wavelet Transform
FBM	Feature-Based Matching
FFT	Fast Fourier Transform
GEOIDE	GEOmatics for Informed Decisions
GLP	Gaussian Laplacian Pyramid
HM	Histogram Matching
HPF	High Pass Filtering
IFSAR	InterFerometric SAR
IHS	Intensity-Hue-Saturation
PCA	Principal Component Analysis
PIF	PseudoInvariant Features
MS	MultiSpectral
NC	No-Change set
ORI	Orthorectified Radar Image
ORTH	ORTHogonal wavelet fusion with decimation
PMF	Polynomial Mapping Function
RE	Ratio Enhancement
SAR	Synthetic Aperture Radar
SNC	Simulated Natural Colour
SR	Simple Regression
SVR	Synthetic Variable Ratio
TMF	Triangle-based Mapping Function
UBIOR	biorthogonal wavelet fusion without decimation
UORTH	orthogonal wavelet fusion without decimation

UNB	University of New Brunswick
WIHS	Wavelet and IHS transformation integration
WPCA	Wavelet and PCA transformation integration

Co-Authorship

The thesis contains materials that have been published, accepted or submitted for publication in scholarly journals as co-authored papers with the supervisor Dr. Yun Zhang. For Chapter 2, the author proposed the algorithm, wrote the program to implement it, did the experiments, wrote the initial draft of the paper, and answered the reviewers' questions. For other chapters, the author was the primary contributor and the first author of the papers.

Chapter 1. INTRODUCTION

1.1 Selection of Topics

The research topics for this research originated from GEOIDE project "Automating 3D feature extraction and change detection from very high resolution satellite imagery with lidar and maps (MNG#TAO)". This GEOIDE project involved researchers from several academic institutions including the University of New Brunswick (UNB). The main research objectives of this GEOIDE project were: to explore a new avenue to make use of the new generation of high resolution satellite imagery and to develop automated (automatic or semi-automatic), fast and robust algorithms for 3D feature extraction and change detection by integrating Lidar DEM/intensity data and existing Map/GIS information for GIS updating, disaster management, urban planning, telecom and transportation applications [AUTOMAP, 2001]. One of UNB's subprojects was to explore an effective and low cost way for precise change detection using fused panchromatic and multispectral high resolution satellite images.

Change detection using high resolution satellite images is a broad, complex research topic and requires investigation into many different image processing methodologies including**:** data preparation methods like image fusion; preprocessing techniques such as geometric correction, and radiometric correction; different change detection algorithms, such as per-pixel based and objected oriented methods (object-oriented is of particular interest for high resolution image because it offers the potential to resolve spatial variability problems in homogenous areas); different image

classification algorithms such as statistical-based classification method and intelligence-based method [Jensen, 2005].

For this research, it was decided to focus on three image preprocessing techniques for precise change detection, namely: image fusion, image registration and image normalization for the following reasons:

- Image fusion of high resolution satellite images can improve the classification accuracy because the fused image combines complementary information from different sensors that helps in discriminating the different classes [Pohl and Van Gendren, 1998; Colditz et al., 2006]. The high accuracy classified image improves the final change detection result.
- If the images are not properly coregistered, the change detection algorithm will produce incorrect results around the boundaries of homogeneous regions. The errors resulting from the inaccurate co-registration of the images will be attributed to thematic or categorical errors [Coppin et al., 2004].
- Differences in sensor, solar illumination or atmospheric conditions make it difficult to accurately compare satellite images acquired on different dates and/or different platforms. Radiometric normalization serves to remove the effects that alter the spectral characteristics of land features, except for actual changes in ground target, and is necessary step for multi-sensor, multi-date studies, like change detection [Paolini, et al., 2006].

Research in the above three image processing techniques is also important for many different remote sensing applications. A brief summary of the importance of research for image fusion as well as image registration and image normalization is included in sections 1.1.1 and 1.1.2, respectively.

1.1.1 Image fusion

The launch of IKONOS in 1999 marked the beginning of a new era of high-resolution satellite imagery with a spatial resolution of 1 meter. High resolution satellite imagery offers high spatial accuracy suitable for large scale (>1:5,000) urban applications; high temporal resolution and updatability for change detection and base map updating; both stereo and multi-spectral information for automated analysis; cost-effective and affordable pricing for data delivery [AUTOMAP, 2001]. Due to physical constraint, there is a trade off between spatial resolution and spectral resolution of a high resolution satellite sensor [Aiazzi et al., 2002], i.e., the panchromatic image has a high spatial resolution at the cost of low spectral resolution, and the multispectral image has high spectral resolution with a low spatial resolution (IKONOS: panchromatic image, 1m, multispectral image 4m; QuickBird: panchromatic image, 0.7m, multispectral image, 2.8 m). To resolve this dilemma, the fusion of multispectral and panchromatic images, with complementary spectral and spatial characteristics, is becoming a promising technique to obtain images with high spatial and spectral resolution simultaneously [Gonzalez-Audicana et al., 2004]. Image fusion is widely used to integrate these types of data for full exploitation of these data, because fused images may provide increased interpretation capabilities and more reliable results since data

with different characteristics are combined. The images varying in spectral, spatial and temporal resolution may give a more comprehensive view of the observed objects [Pohl and Van Genderen, 1998].

1.1.2 Image registration and image normalization

The information provided by individual sensor is incomplete, inconsistent, or imprecise for many applications. Additional sources may provide complementary data, and fusion of different information can produce a better understanding of the observed site, by decreasing the uncertainty related to the single source [Simone et al., 2003]. Mulitemporal and multisenor high resolution data are often fused together to acquire complementary information to interpret the objects accurately.

Image registration and image normalization are two important preprocessing operations in processing high resolution, multi-temporal or multi-sensor images. Among aspects of image preprocessing for land cover change detection and other Earth observation monitoring applications, there are two outstanding requirements: image registration and image normalization [Coppin and Baucer, 1996]. Image registration and radiometric normalization can transform multi-temporal or multi-sensor data into identical geometric and radiometric bases respectively, and an identical geometric base and a radiometric base are required in processing those images. Without a common geometric base, the derived information from a single remote sensing image cannot be associated with other spatial information, making precise geo-spatial analyses impossible; even comparisons among remote sensing images cannot be implemented if those images do not have the same geometric base. Applications utilizing multitemporal,

multisensor remotely sensed data are dependent on the accurate registration of the data into a common spatial framework [Roy, 2000].

Without a same radiometric base, it will be difficult or wrong-prone to compare images which were acquired at different illumination, atmospheric, or sensor conditions, because those different conditions cause the grey value difference in those images, while these difference does not reflect the actual object different on the ground.

Based on the project task and the important roles of image fusion, image registration and image normalization in processing multitemporal and multisensor high resolution images, the author was motivated to conduct research in these three areas for this PhD research. The author deeply understands these three research topics are broad research topics. All of the above the work will be concentrated on urban and sub-urban area. This ensures that the research is focused.

1.2 Background

1.2.1 Image fusion

Most remote sensing sensors, such as IKONOS, QuickBird, SPOT, IRS and Landsat, provide one high resolution panchromatic image and several multispectral channels [Svab and Ostir, 2006]. The panchromatic image has a high spatial resolution at the expense of a wide spectral bandwidth, and the multispectral image has a higher spectral resolution at the expense of spatial resolution.

The IHS (intensity, hue and saturation) transform based fusion, PCA (principal component analysis) based fusion, arithmetic combination fusion, and wavelet transform based fusion are the most widely used techniques in image fusion.

1.2.1.1 IHS

IHS is a color space, hue is defined as the predominant wavelength of a color, saturation is defined as the purity or total amount of white light of a color and intensity relates to the total amount of light that reaches the eye [Harris et al., 1990]. IHS largely explains the popularity of perceptual color space and overcomes the commonly used RGB color space drawbacks, which does not relate intuitively to the attribute of human color perception [Schetselaar, 2001].

Because of its simplicity and high sharpening ability, many applications using IHS transform in image fusion have been reported. Harris et al. [1990] described how to use IHS in integrating Radar with diverse types of data such as Landsat TM, airborne geophysical and thematic data. The use of IHS transform was also demonstrated for displaying the results of quantitative analyses such as change detection studies and comparison between images characterized by different sensing parameters. Chavez [1991] compared IHS with PCA and other fusion methods by merging the information contents of the Landsat TM and SPOT panchromatic image. It was claimed that IHS method distorts the spectral characteristics of the data the most. Grasso [1993] used the IHS transform for geologic mapping because the IHS transform could allow diverse forms of spectral and spatial landscape information to be combined into a single data set for analysis. Schetselarr [2001] modified the IHS transform and presented a new method

that preserves the spectral balance of the multispectral image data and modulates the IHS coordinate uniformly. The method takes the limits in the representation of color of the display device into account, which aids in compromising the amount and spatial distribution of the over-range pixels against contrast in intensity and saturation. There are other improvements about IHS such as using wavelet [Nuñez et al., 1999; King and Wang, 2001; Chibani and Houacine, 2003].

The main advantage of the IHS method is that it separates the spatial information as an intensity (I) component from the spectral information represented by the hue (H) and saturation (S) components. The spatial information can be manipulated independently to enhance the image while maintaining the overall colour balance of the original images [Carper et al. 1990]. However, there exists color distortion in the fused image because IHS assumes that the intensity is formed by even contribution from the RGB bands; thus, all the details contained in the high resolution image are directly integrated into the intensity component. The color distortion will become worse when the panchromatic image has a low correlation with the multispectral image. Another limitation of IHS is that it only processes three multispectral bands.

1.2.1.2 PCA

The Principal Component Analysis (PCA) is a statistical technique that transforms a multivariate dataset of correlated variables into a dataset of new uncorrelated linear combinations of the original variables [Pohl, 1998]. PCA is widely used in signal processing, statistics, and many other applications.

Chavez et al. [1991] used principal component analysis to merge six Landsat TM bands and SPOT data and concluded that the color distortion in the fusion result of PCA method is less than the result acquired by IHS fusion method. Teggi et al. [2003] presented a fusion method which combines the principal component analysis and "à trous" wavelet and applied it to a pair of images acquired by Thematic Mapper (TM) and IRS-1C-PAN sensors. González-Audícana et al. [2004] presented a new fusion alternative, which uses the multiresolution wavelet decomposition to extract the details and principal component analysis to inject the spatial detail of the high resolution image into the low resolution multispectral image.

The main advantage of PCA method lies in the unlimited multispectral bands in the fusion process, unlike the IHS method, which uses only three multispectral bands. The PCA also distorts the spectral characteristics of the multispectral image, but distortions were less severe than those in the IHS results because the first component image is more similar to the high resolution than is the intensity image [Chavez et al., 1991]. However, the PCA approach is sensitive to the choice of area to be analyzed. The correlation coefficient reflects the tightness of a relation for a homogeneous sample, while shifts in the band values due to markedly different cover types will influence the correlations and particularly the variances [Pohl, 1998].

1.2.1.3 Arithmetic combination technique

Different arithmetic combinations have been employed for fusing multispectral and panchromatic images. The arithmetic operations of multiplication, division, addition and subtraction have been combined in different ways to achieve a better fusion effect.

The Brovey Transform, RE (Ratio Enhancement), and SVR (Synthetic Variable Ratio) techniques are successful examples for SPOT pan fusion [Zhang, 2002].

The Brovey Transform is based on multiplying ratio images with the panchromatic image. It was developed to visually increase contrast in the low and high ends of an image's histogram. The Brovey Transform is good for producing RGB images with a higher degree of contrast in the low and high ends of the image histogram and for producing visually appealing images. However, it should not be used if it is important to preserve the original scene radiometry [Erdas, 2002], because the Brovey Transform may cause color distortion if the spectral range of the intensity replacement image is different from the spectral range covered by the three bands used in the multispectral image. This limitation cannot be avoided in color composites that do not use consecutive spectral bands. The spectral distortion incurred by this fusion technique is difficult to control and quantify, because the high resolution panchromatic image and the multispectral image are from different sensors or different dates [Alparone et al., 2004].

RE is to maintain the radiometric integrity of the data while increasing the spatial resolution [Pohl, 1998]. SVR is an improvement of RE technique, because of its complication in calculating the parameters used in the fusion process. SVR method used regression analysis between the multispectral and panchromatic image to compute parameters for the process of synthetic low panchromatic image. The first modification of the SVR is that the calculation of the parameters for the synthetic low panchromatic image is directly performed from the resampled TM image (10m) and the original SPOT pan image, instead of from the measured classes. The second modification of the

SVR method is that the synthetic panchromatic image is calculated from those TM bands which are used in the merging instead of from the TM Bands 1, 2, 3 and 4 constantly [Zhang, 1999]. This method is very popular and has been used widely in fusing all kinds of high resolution images; however, this method cannot process the panchromatic image and multispectral image, which have large spectral range differences, very well, for instance, SAR data and optical multispecral image.

1.2.1.4 Wavelet based fusion techniques

The wavelet transform is an advanced mathematical tool developed in the field of signal processing. It can decompose a digital image into a set of multi-resolution images accompanied with wavelet coefficients for each resolution level. The wavelet coefficients for each level contain the spatial (detail) differences between two successive resolution levels.

Because the performance of the wavelet based image fusion technique outperforms the traditional image fusion method, it has caught a lot researchers' interest; thus, there are so many publications about this technique which cannot be listed at one time. The following have listed some typical wavelet based literature.

Yocky [1995] proposed the two-dimensional discrete wavelet transform to image merging. The wavelet technique was compared with IHS transform by using multispectral and panchromatic images. The comparison showed that the wavelet technique performs better in combining and preserving spectral-spatial information. Yocky [1996] proposed a new fusion method based on wavelet transform technique, which is a kind of improvement of the method proposed by him in 1995. The method

has been tested by SPOT and Landsat TM. Garguet-Duport et al. [1996] proposed a new method based on wavelet technique to merge a SPOT panchromatic image and an XS multispectral image. The method was compared with IHS and other methods; it has the least spectral characteristic distortion. The distortions are minimal and difficult to detect.

Zhou et al. [1998] presented a multiresolution orthogonal wavelet transform method to merge the SPOT PAN and TM reflective images. Two destination resolution levels, one quarter and one eighth of the original image resolution, were used for decomposition in evaluating the method. Nunez et al. [1999] developed a multiresolution wavelet decomposition image fusion method, which combines a high-resolution panchromatic image and a low-resolution multispectral image by the addition of some wavelet planes of the panchromatic image to the intensity component of the low-resolution image. The discrete wavelet transform known as “a trous” algorithm, which provides a shift-invariant property that is not available with the orthonormal wavelet system, was used in the wavelet decomposition process. Ranchin and Wald [2000] designed the ARSIS concept based on a multiresolution modeling of the information, to improve the spatial resolution together with a high quality in the spectral content of the synthesized images.

King and Wang [2001] presented a wavelet based fusion method that combines IHS transformation and biorthogonal wavelet decomposition. The Landsat 7 data were used to evaluate the proposed fusion method. Chibani and Houacine [2003] investigated the use of the nonorthogonal (or redundant) wavelet decomposition in image fusion and

concluded that this method is better for image fusion than the standard orthogonal wavelet decomposition.

The major advantage of the wavelet based fusion method lies in the minimal distortion of the spectral characteristics in the fusing result. However, it also has problems. The spectral content of small objects--one or two pixels-- is lost with the multispectral image approximation substitution into the panchromatic pyramid. Also, because the wavelet based fusion acts as high- and low- pass filters, the final fusion image may suffer from ringing. It may also have problems in distributing pixel intensities in large, featureless areas [Yocky, 1996].

1.2.2 Image registration

Image registration is the process of geometrically aligning two or more images of the same scene acquired at different times, or with different sensors, or from different viewpoints [Brown, 1992]. It is one of the crucial image processing operations in remote sensing. The image registration technique has been developed for a long time. Several reviewing image registration algorithm studies have been published [Brown, 1992; Fonseca and Manjunath, 1996; Zitova and Flusser, 2003]. However, to date, it is still rare to find an accurate, robust, and automatic image registration method, and most existing image registration methods are designed for a particular application. Manual registration remains by far the most common way to accurately align their imaging data, although it is often time consuming and inaccurate [Zavorin and Le Moigne, 2005].

1.2.2.1 Area-based matching

Generally, the image registration problems can be divided into two parts: one is how to find enough accurate control point pairs, and the second is how to interpolate the image. The image matching method is used to find the correspondent control points. The existing automated image matching techniques can be broadly classified into two categories: area-based matching (ABM) and feature-based matching (FBM) techniques.

ABM is a classical matching method. In area-based algorithms, a small window of pixels in the sensed image is compared statistically with windows of the same size as the reference image. The centers of the matched windows are treated as control points, which can be used to solve for mapping function parameters between the reference and sensed images [Li et al., 1995]. The normalized cross-correlation and least-squares technique are two kinds of widely used area-based matching techniques. The former is based on the maximum value of the correlation coefficient between the reference image and the sensed image; and the latter is based on minimizing the differences in the gray value between the reference image and sensed image.

There are several publications about area-based matching. Cideciyan et al. [1992] used Fourier transformation and cross-correlation for image registration. Zheng and Chellapa [1993] used the area correlation in the spatial domain to match the feature points that are extracted by the Gabor wavelet decomposition. Hsieh et al. [1997] detected feature points using a wavelet transform algorithm; the cross-correlation was used to match the detected points across the images. Also in other publications about feature extraction, area-base matching is a commonly used method to find the similarity of the features in the reference and sensed images.

1.2.2.2 Feature-based matching

FBM techniques do not use the gray values to describe matching entities, but use image features derived by a feature extraction algorithm. These features include edges, contours, surfaces, other salient features such as corners, line intersections, and points of high curvature, statistical features such as moment invariants or centroids, and higher level structural and syntactic descriptions [Brown, 1992].

There are various methods introduced in feature-based matching. Goshtasby et al. [1986] used the corresponding centers of gravity of regions as corresponding control points to estimate the registration parameters. Ventura et al. [1990] described feature-based matching using structural similarity detection techniques. Flusser and Suk [1994] applied the affine moment invariants principle, a segmentation technique, in registering an image with affine geometric distortion. Li et al. [1995] presented two contour-based methods, which used region boundaries and other strong edges as matching primitives. Dai and Khorram [1999] combined an invariant moment shape descriptor with improved chain-code matching to establish correspondences between the potentially matched regions detected from the two images. Habib and Alruzouq [2004] used the line segments as primitives in a registration process. The method assumed that the line segments are plentiful in the scene under processing.

Wavelet decomposition of the images was used for generating the pyramidal structure because of its multiresolution characteristic. Several researchers have reported their application of wavelet transform in the image registration. Djamdji et al. [1993] used “à trous” algorithm wavelet transformation method for feature extraction. Zheng and Chellappa [1993] used Gabor wavelet decomposition to extract feature points.

Simhadri et al. [1998] applied the modified “à trous” algorithm wavelet transformation in feature extraction. Fonseca and Costa [1997] used the local modulus maxima of the wavelet transform to find feature points and cross-correlation method to build the correspondence between those feature points. Only those best pair-wise fitting, among all pairs of feature points are taken as actual control point pairs. Moigne et al. [2002] utilized maxima of wavelet coefficients to form the basic features of a correlation-based automatic registration algorithm.

1.2.2.3 Comparison between ABM and FBM

ABM can be efficiently used in implementation in the Fourier transform domain using the Fast Fourier Transform (FFT). Some of the Fourier transform can be used to achieve invariance to translation, rotation and scale [Fonseca and Manjunath, 1996]. The precision of ABM is higher compared with FBM. These matching algorithms are easy to implement because of their simple mathematical model. The imperfections are also applicable to ABM. The prerequisite of the ABM is that gray level distribution of the sensed image and reference image must be similar. As known, gray values contain little explicit information about the object space; as a consequence, the area-based matching methods are not reliable enough. Therefore, area-based methods are not well adapted to the problem of multisensor image registration since the gray-level characteristics of images to be matched can vary from sensor to sensor. Compared with ABM, FBM is more robust and reliable [Schenk, 1999].

(1) Features are derived properties of the original gray level images and are inherently unique.

(2) Similarity is based on the attributes and /or relations. It is more invariant to illumination, reflectance, and geometry.

(3) Features are sufficient for describing image content.

However, the precision of FBM is lower compared with ABM. Also FBM often requires sophisticated image processing for feature extraction and depends on the robustness of feature detection for reliable matching.

1.2.3 Image normalization

Due to variations in atmospheric conditions, look/view angles, or sensor parameters that occur between acquisition dates, scenes of the same target area acquired at different times have been nearly impossible to compare in an automated fashion without performing the image normalization. Even visual comparison of these images may be difficult [Scott et al., 1988]. There are two kinds of image radiometric normalization: namely absolute and relative. The absolute radiometric correction can convert the digital counts in satellite image data to radiance at the surface of the Earth [Du et al., 2002]. The images from different sensors can be compared by using the radiance. The absolute radiometric correction tends to be more accurate than the relative correction, but it needs sensor parameters, atmospheric refraction parameters and other data that are difficult to obtain. Thus, the difficulty in obtaining the above accurate atmospheric and sensor parameters, makes relative radiometric normalization an attractive alternative. The relative radiometric normalization applies one image as a reference and adjusts the radiometric properties of the subject image to match the

reference image [Hall et al., 1991]. The normalized image appears to have been acquired under the same solar and atmospheric conditions as the reference image.

A variety of relative radiometric normalization techniques have also been developed.

Simple regression normalization [Jensen, 1983] uses the least-squares equation to derive normalization coefficients.

Scott et al. [1988] introduced the pseudoinvariant feature normalization method, which is based on the statistical invariance of the reflectance of man-made in-scene elements such as concrete, asphalt and rooftops, because they are assumed to change not too much with time. Differences in the gray-level distributions of these invariant objects are assumed to be a linear function and are corrected statistically.

Haze correction [Chavez, 1988; Yuan and Elvidge, 1996] is a simple method that assumes that objects with zero reflectance should have the same minimum digital number (DN) on both reference and subject images and is implemented by subtracting the digital count associated with darkest materials (zero reflectance) present in a scene.

Histogram matching uses the equalization of the histogram of a given image to another or various images to a reference image and is a statistical method based on the cumulative distribution function of the data and does not assure the in-between band relationship [Shimabukuro et al., 2002]. This method does not depend on the geometrically accurate registration images because of their use for the whole image and is useful for matching data of the same scenes acquired on different dates with slightly different sun angle or atmospheric effects.

The minimum-maximum and the mean-standard deviation normalization [Yuan and Elvidge, 1996] are two different methods that both apply statistical parameters, i.e. the minimum and maximum respectively, and the mean and standard deviation to derive normalization coefficients.

Hall et al. [1991] used the average of a set of dark and bright pixels (Dark -bright set), which are extracted from the subject and reference image through Kauth-Thomas greenness-brightness transformation. The underlying assumption of this method is that an image always contains at least some pixels that have the same average surface reflectance among images acquired at different dates.

Elvidge et al. [1995] developed a radiometric normalization method (No change pixel set) through a no-change set determined from the scattergram. The no-change sets are obtained from regions, such as water and stable land clusters, identified as no change in the scattergram between near-infrared bands of the subject image and the reference image. The initial regression line is generated by those no-change sets. A no-change region is determined by setting a threshold around this line. Pixels falling within the no-change region will be used to compute regression lines for all bands.

Du et al. [2002] proposed a procedure which selects the pseudo-invariant features statistically, and uses principal component analysis to find linear relationships between the mulitemporal images of the same area. The procedure is claimed to ensure the conservation of radiometric resolution for the multitemporal images involved.

Ya'allah and Saradjian [2005] presented a method which is based on efficient selection of unchanged pixels through pixels in each band. The capability of the method

can consider the imaging condition differences and effectively exclude real land change pixels from the normalization process.

Using the mean square error calculation as the statistical measure of the goodness of fit between the reference image and subject image, Yuan and Evlidge [1996] evaluated some methods and ranked the methods with the "best" at the top of the list: No change pixel set, Dark-bright set, Simple regression, Haze correction, Mean-standard deviation, Minimum-maximum and pseudoinvariant features. From the visual inspection, the no change pixel set method is the best and the Mean-standard deviation, Minimum-maximum and pseudoinvariant features methods yield poor matches to the reference image. No single approach has universal application because solutions are independent of location, application and image. Analysts must, therefore, be aware of existing procedures and be prepared to use or adapt these, or develop alternative procedures, as appropriate [Heo and Fitzhugh 2000]. The Landsat MSS data of the Washington D.C. area used by Yuan and Elvidge contain a high proportion of clear water and urban area which should favor methods, like the no change pixel set that rely on these ground targets in determining the transformation coefficients [Yang and Lo, 2000].

1.3 Problem statement

High resolution satellite imagery provides researchers with information sources necessary for use in many change detection applications. However, problems occur when applying conventional traditional image processing methods to process and analyze these high resolution images. According to a literature review, the following

problems associated with applying conventional fusion, normalization and registration techniques to high resolution images were identified:

Image fusion. A common problem of existing techniques is the colour distortion that occurs in the resulting fused images [Zhang, 2002]. For high resolution images, such as IKONOS and QuickBird, the wavelength of the panchromatic image is much broader than that of the multispectral bands. This discrepancy between the wavelengths causes considerable color distortion to occur when fusing high resolution panchromatic and multispectral images. To solve the colour distortion problem, methods based on wavelet have been introduced and have demonstrated superior performance [Aiazzi et al., 2006]. However, when applying wavelet based methods, spatial distortions, typically ringing or aliasing effects, and originating shifts or blur of contours and textures may occur [Yocky, 1996]. These problems- which can be as pronounced as colour distortion mentioned above - are emphasized by misregistration between a panchromatic image and its multispecral counterparts, especially if the wavelet is not shift-invariant [Aiazzi et al., 2002; Gonzáles Audícana et al., 2004].

Image registration. Very high spatial resolution data presents a different set of image geometry problems than moderate spatial resolution data. Since the nominal pixel sizes of high resolution images, such as QuickBird and IKONOS, are smaller than 10 m, the altitude of the sensor is lower than other satellite sensors, such as Landsat, SPOT. Relief displacement in high resolution imagery begins to increase due to lower altitude, causing localized distortion related to landscape height [Schowengerdt, 1997]. It is also difficult for operators to accurately locate control points using manual methods. Since a large number of control points are typically required to obtain satisfactory registration

results, selecting ground control may be a very time consuming and tedious task [Moigne, et al., 2002].

Radiometric normalization. Most existing normalization methods were developed for use with moderate resolution images, such as Landsat TM or Landsat MSS data. These image normalization methods cannot be used directly in normalizing high resolution images because of satellite sensor differences. For example, it is difficult to implement radiometric normalization between high resolution images because of the spatial variability in homogenous areas; this increases the complexity of the selection purity of the unchanged targets; also because of channel reduce compared with the moderate resolution data, some normalization methods require two near-infrared bands, while high resolution sensor often has one near-infrared band, this also increases the complexity using some existing normalization methods.

1.4 Objective

The objective of this research is to develop/improve image preprocessing techniques for high resolution change detection, i.e. the image processing operations that are applied before the use of a change detection algorithm. These image preprocessing techniques will be specifically designed for processing high resolution satellite images of urban or sub-urban areas. These new approaches or strategies will be designed to overcome the problems that occur when applying conventional image processing methods to high resolution images. For this thesis, image fusion, image registration, and image normalization techniques will be developed or improved.

The technical objectives of this research for the above three topics and the tasks required to complete this research are outline below.

Image Fusion: The technical objectives for the research conducted for image fusion are:

- Reduce colour distortion that occurs (in the resulting high resolution fused images) when applying image processing methods to high-resolution images
- Remove spatial distortion that occurs (in the resulting high resolution fused images) when applying wavelet-based fusion techniques to fuse high resolution images

To satisfy the above two objectives (i.e. reducing colour and spatial distortion), a new fusion algorithm suitable for use with high resolution satellite images will be developed. The characteristics of this algorithm will be:

- Preserve colour information contained in the original multispectral and panchromatic images
- Maintain the spatial information of the panchromatic image
- Applicable for use with a wide variety of high resolution images (e.g. IKONOS, QuickBird, and high resolution SAR data)

Image Registration: The technical objectives for the research conducted for image registration are:

- Reduce local geometric distortions when applying conventional image registration techniques (polynomial-based model) to high resolution images of areas with significant terrain relief.
- Resolve difficulty in locating control points accurately using manual methods

To satisfy the above objectives, a new image registration algorithm suitable for processing high resolution satellite images will be developed. This algorithm will be implemented using a wavelet-based feature extraction technique, a combination of normalized cross-correlation and probability relaxation matching techniques, and a triangle-based local transformation model. The algorithm will be able to select a number of feature points semi-automatically, and reduce the local distortion that exists in high resolution images of areas with significant terrain relief.

Image Normalization: The technical objectives for the research conducted for image normalization is:

- to resolve the problems encountered using traditional image normalization methods for moderate resolution images in normalizing high resolution image.

To satisfy this objective, strategies to improve existing image normalization methods in normalizing high resolution images will be explored and evaluated.

The metrics used to evaluate the performance of the image fusion, image registration and image normalization methods developed for this thesis are outlined in Table 1.1 below.

Table 1.1. Metrics used to evaluate algorithms developed for this research

Metric	Method Evaluated	Metric Description
Correlation Coefficient	Image fusion	Correlation is widely used in evaluating the quality of the fusion results and is a typical method which is included in almost all the publications in image fusion. The correlation coefficient measures the closeness or similarity between two images; it can vary between -1 and +1. A value close to +1 indicates that two images are very similar, while a value close to -1 indicates that they are highly dissimilar [Pradhan, 2005]. There are two kind comparisons: - The first is: the correlation between each band of the multispectral image and the corresponding band of fused image was computed. Since the multispectral image has spectral information, the correlation between the fused image bands and the multispectral bands is expected to be higher than that between panchromatic image and the original multispectral bands. An increase in the correlation indicates an increase in the spectral information from multispectral image has been included in the corresponding band in fused images. For the fused images, the lower the correlation is, the higher the color distortion is. - The second is: the correlation was computed between each band of the fused image and the panchromatic image. Since the panchromatic image has better spatial information, the correlation between the fused image bands and the panchromatic image is expected to increase compared to that of the original multispectral. An increase in the correlation indicates an increase in the spatial information from panchromatic image has been included in the corresponding band in fused images [Vijayaraj, 2004].
The root-mean-square error (RMS error)	Image registration	RMS error is the distance between the input (source) location of a control point and the retransformed location for the same control point. It reflects the difference between the desired output coordinate for a control point and the actual output coordinate for the same point, when the point is transformed with the geometric transformation [Erdas, 2002]. A small RMS error means that the desired output coordinate for a control point and the actual output coordinate for the same point is close. For the registered images, the higher the total RMS error is, the higher the local geometric distortion is.

(Continued)

The root-mean-square error (RMSE)	Radiometric normalization	The root-mean-square error (RMSE) can be used to measure the statistical agreement of a normalized image with the reference image. It is widely used in quantitatively analysis of the normalized results [Elvidge et al., 1995; Yuan and Elvidge, 1996; Yang and Lo, 2000]. The pixel digital numbers of the radiometrically normalized image are compared with those of the reference image of the same band. If the difference between the digital numbers is small, the RMSE will be small, implying that the subject image is radiometrically more similar to the reference image. For the normalized images, the higher the RMSE is, the higher the radiometric distortion is.

The selected three research topics are not only important for change detection but are also widely used for a variety of other applications. For example: image fusion can be used for image sharpening and image classification; image registration for all types of applications that use multitemporal or multisensor data; and image normalization for creating image mosaics and multiple image composites. Since image fusion, image registration and image normalization are used for many different applications, it was not feasible to validate the proposed image preprocessing techniques for every application. However, the proposed fusion, registration and normalization methods were evaluated independently and were evaluated using quantitative (Table 1.1) and qualitative techniques.

The relationship between the data (or datasets) used to evaluate a particular processing method, the method evaluated and thesis chapter (i.e. the chapter (journal article) that investigates one of the image processing methods examined in this research) is summarized in Table 1.2. For image fusion, except data listed in Table 1.2, other available data sets have also been used to evaluate the proposed image fusion method; the results have not been included in the dissertation.

Table 1.2. Remote sensing datasets, method evaluated and thesis chapter

No.	Data Sets	Evaluated Method	Chapter
1	Two data sets: an IKONOS data set (1m panchromatic and 4m multispectral images; 10,000 by 10,000 pixels; urban area of Fredericton, NB, Canada; acquired in October 2001); and a QuickBird data set (0.7m panchromatic and 2.8m multispectral images; 3,000 by 3,000 pixels; Pyramids area of Egypt; acquired in 2002).	The IHS and wavelet integration image fusion method	Chapter 2 [Zhang, Y., and G. Hong ,2005]
2	Two data sets of Star-3i airborne SAR data (10,000 by 10,000 pixels each), covering two different areas, four different MS images (SPOT, Simulated Natural Color SPOT, ASTER, Landsat TM); one set (4096 by 4096 pixels) of Radarsat image with Landsat TM image.	The IHS and wavelet integration image fusion method	Chapter 3 [Hong et al. ,2006]
3	Two data sets from the urban area of Fredericton NB, Canada: an IKONOS data (4096 by 4096 pixels) acquired in fall, 2001; and a QuickBird data (4096 by 4096 pixels) acquired in summer, 2002.	Several image fusion methods and the IHS and wavelet integration fusion method	Chapter 4 [Hong and Zhang. ,2007]
4	Two sets of data: a multi-temporal panchromatic Ikonos data acquired in 2000 and 2002 (IKONOS panchromatic versus IKONOS panchromatic (2048 by 2048 pixels); and a multi-temporal, multi-sensor, multi-spectral dataset, Quickbird multispectral acquired in 2002 (1024 by 1024 pixels) versus IKONOS panchromatic acquired with the same year.	Image registration method	Chapter 5 [Hong and Zhang, 2006a]
5	Two datasets from the urban area of Fredericton, NB, Canada: IKONOS multispectral data (2048 by 2048 pixels) acquired in July, 2000; and QuickBird multispectral data (2048 by 2048 pixels) acquired in August, 2002.	Radiometric normalization methods	Chapter 6 [Hong and Zhang ,2006b]

1.5 Dissertation outline

This dissertation is an articles-format dissertation. Five journal articles (two published, three submitted for peer review) have been incorporated in the dissertation. The dissertation is divided into seven chapters and includes three research topics: image fusion, image registration, and radiometric normalization. Figure 1.1 illustrates the organization of this dissertation.

The introduction, which includes the topic selection, research motivation, objective, and dissertation outline, is included in the **first chapter**.

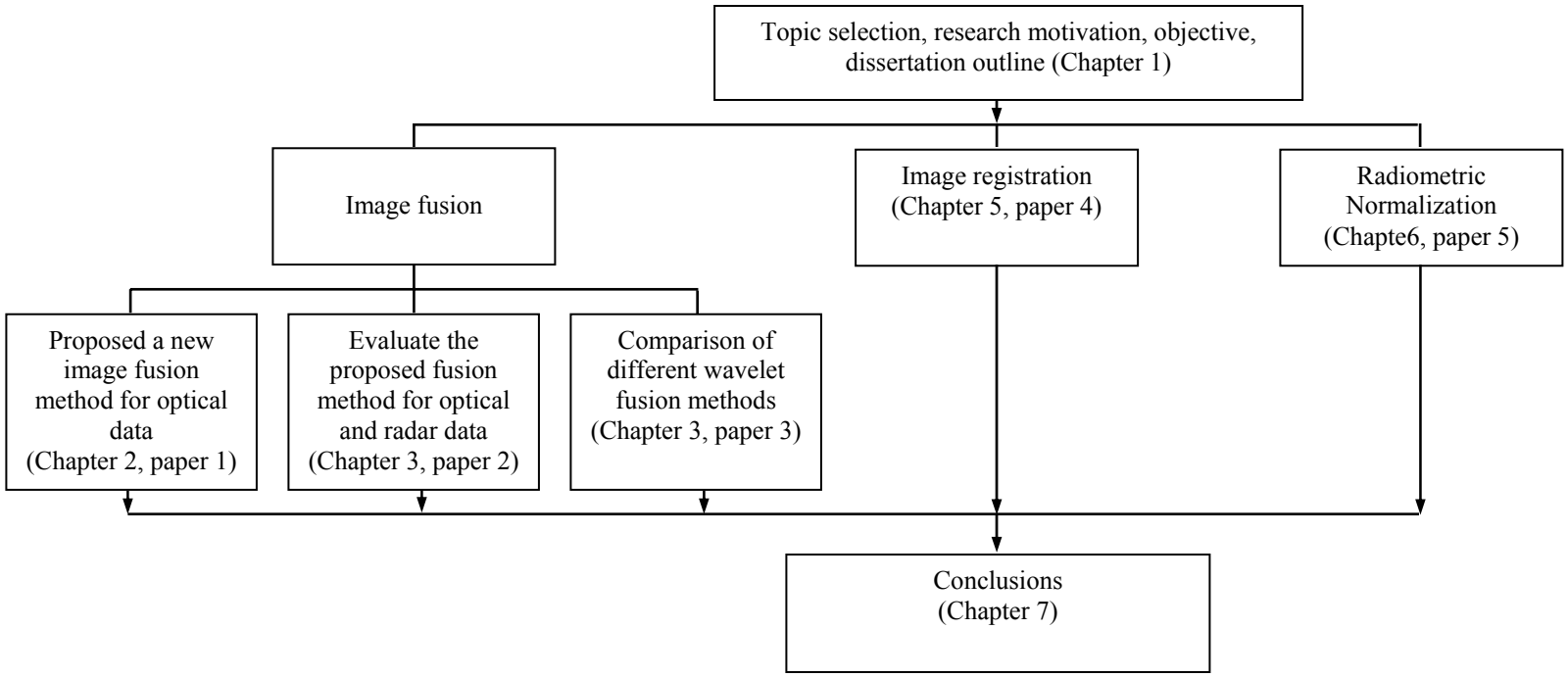

Figure 1.1. Illustrate the organization of this dissertation.

Paper 1: Zhang, Y., and G. Hong (2005). An IHS and wavelet integrated approach to improve pan-sharpening quality of IKONOS and QuickBird images. *Information Fusion*, Vol. 6, No. 3, pp. 225-234.

Paper 2: Hong, G., Zhang, Y., and Mercer, J.B. (2006). A robust technique for fusing SAR data and multisource multispectral images. Submitted to *Photogrammetric Engineering and Remote Sensing*, under review.

Paper 3: Hong, G., and Zhang, Y. (2007). Comparison and improvement of wavelet-based image fusion. Submitted to *International Journal of Remote Sensing*, in press.

Paper 4: Hong, G., and Zhang, Y. (2006a). Wavelet-based image registration technique for high resolution remote sensing image. Submitted to *Computers & Geosciences*, under review.

Paper 5: Hong, G., and Y. Zhang (2006b). A comparative study on radiometric normalization using high resolution satellite images. *International Journal of Remote Sensing*, accepted, in press.

The topic on image fusion occupies three chapters (**Chapters 2, 3, and 4**), resulting in the main contribution in this PhD research. Based on the wavelet multiresolution analysis property, a new image fusion method, which integrates IHS and wavelet transform, is proposed to reduce the color distortion problem met in using current image fusion methods to process high resolution images.

Chapter 2 is a journal chapter, originally published in the journal *Information Fusion* [Zhang and Hong, 2005]. It introduces the theory of the wavelet transform, the IHS transform, and the proposed new image fusion method. Fusion results from IKONOS and QuickBird imagery are provided, and an evaluation of the results is also included in this chapter.

In order to test whether the proposed image fusion method can be applied to multisource data, the multisource SAR and common multispectral images were fused using the proposed method. **Chapter 3** includes the results of this fusion and evaluation of these results; it has been submitted to *Photogrammetric Engineering and Remote Sensing* [Hong et al., 2006].

Because the proposed image fusion method is based on wavelet transform, problems in image fusion related to wavelets are also discussed in order to take advantage of using wavelet in image fusion; both comparison among wavelet-based image fusion and suggested improvements are given in **Chapter 4**, this chapter has also been accepted by *International Journal of Remote Sensing* [Hong and Zhang, 2007].

While the wavelet multiresolution analysis property is used in the proposed image fusion method in the previous chapters (Chapters 2, 3 and 4); it is further explored for the application of image registration based on the knowledge and experience acquired

from the image fusion research. To reduce the local distortion existing in high resolution images with terrain relief, **Chapter 5** introduces a new wavelet-based image registration method for high resolution images. This chapter has been submitted to *Computers & Geosciences* [Hong and Zhang, 2006a]. The proposed method uses the wavelet multi-resolution property to extract feature points; the normalized cross-correlation and relax-based probability matching techniques to find similarity between feature points in reference image and sensed image; and the triangle-based local transformation model to resample the sensed image. The method was evaluated using two sets of data. The evaluations show that the method can semi-automatically select enough control points and reduce the local distortions caused by terrain relief.

On top of the discussion on geometric base problems in Chapter 5, **Chapter 6** discusses a radiomimetic problem, because it is important to have both an identical geometric base and a radiometric base to process multi-temporal or multi-sensor images. Radiometric normalization is necessary in transforming multi-temporal or multi-sensor data into an identical radiometric base. In this chapter, a comparative analysis of image normalization in high resolution images is discussed. Improved strategies are provided for normalizing the high resolution images through modifications to the existing image normalization methods, because existing image normalization methods designed for the Landsat TM/MSS image cannot be directly applied to high resolution images. It is shown the improved strategies to be very helpful in normalizing high resolution images. A journal paper on this topic has been accepted by *International Journal of Remote Sensing* for publication [Hong and Zhang, 2006b].

Chapter 7 summarizes the major work in this research, draws conclusions, and gives recommendations for further research.

REFERENCES

Alparone, L., S. Baronti, A. Garzelli, and F. Nencini (2004). "Landsat ETM+ and SAR image fusion based on generalized intensity Modulation." *IEEE Trans. Geoscience and Remote Sensing*, Vol. 42, No. 12, pp. 2832-2839.

AUTOMAP (2001). "Automating 3D feature extraction and change detection from very high resolution satellite imagery with lidar and maps (automap program) (MNG#TAO)," GEOIDE Research Proposal, October, 2001.

Brown, L.G. (1992). "A survey of image registration techniques." *ACM Computing Surveys*, Vol. 24, No. 4, pp. 325-376.

Carper, W.J., T.M. Lillesand, and R.W. Kiefer (1990). "The use of Intensity-Hue-Saturation transformations for merging SPOT panchromatic and multispectral Image Data." *Photogrametric Engineering and Remote Sensing*, Vol. 56, No. 4, pp. 459-467.

Chavez, P.S., and D.J. Mackinnon (1994). "Automatic detection of vegetation changes in the Southwestern United States using remotely sensed images." *Photogrammetric Engineering and Remote Sensing*, Vol. 60, No. 5, pp. 571-583.

Chavez, P.S., S.C. Slides, and J.A. Anderson (1991). "Comparison of Three Different Methods to Merge Multiresolution and Multispectral Data: Landsat TM and SPOT panchromatic." *Photogrammetric Engineering and Remote Sensing*, Vol. 57, No. 3, pp. 295-303.

Chavez, P.S. (1988). "An improved dark-object subtraction technique for atmospheric scattering correction of multispectral data". *Remote Sensing of Environment*, Vol. 24, pp. 459-479.

Chibani, Y., and A. Houacine (2003). "Redundant versus orthogonal wavelet decomposition for multisensor image fusion." *Pattern Recognition*, Vol. 36, No. 4, pp. 879-887.

Cideciyan, A.V., S.G. Jacobson, C.M. Kemp, R.W. Knighton, and J.H. Nagel (1992). "Registration of high resolution images of the retina", Proceedings of the SPIE-The International Society for Optical Engineering." *Medical Imaging VI. Image processing*, Vol. 1652, pp. 310-322.

Colditz, R.R., T. Wehrmann, M. Bachmann, K. Steinnocher, M. Schmidt, G. Strunz, S. Dech (2006). "Influence of image fusion approaches on classification accuracy: a case study." *International Journal of Remote Sensing*, Vol. 27, No. 15, pp. 3311-3335.

Coppin, P.R. and M.E Bauer (1996). "Digital change detection in forest ecosystems with remote sensing imagery." *Remote Sensing of Reviews*, 13, 207-234.

Coppin, P., I. Jonckheere, K.Nackaerts, B. Muys, and E. Lambin (2004). "Digital Change Detection Methods in Ecosystem Monitoring: A Review." *International Journal of Remote Sensing*, Vol. 25, No. 9, pp. 1565-1596.

Dai, X.L., and S. Khorram (1999). "A feature-based image registration algorithm using improved chain code representation combined with moment invariants." *IEEE Trans. on Geoscience and Remote Sensing*, Vol. 37, No. 5, pp. 2351-2362.

Djamdji, J.P., A. Bijaoui, and R. Maniere (1993). "Geometrical registration of images, the multiresolution approach." *Photogrammetric Engineering and Remote Sensing*, Vol. 59, No. 5, pp. 645-653.

Du, Y., P.M. Tiellet, and J. Cihlar (2002), "Radiometric normalization of multitemporal high-resolution satellite images with quality control for land cover change detection." *Remote sensing of environment*, Vol. 82, No. 1, pp. 123-134.

Eckhardt, D.W., J.P. Verdin, and G.R. Lyford (1990). "Automated update of an irrigated lands GIS using SOPT HRV imagery." *Photogrammetric Engineering and Remote Sensing*, Vol. 56, No. 11, pp. 1515-1522.

Elvidge, C.D., D. Yuan, R.D. Werackoon, and R.S. Lunetta (1995). "Relative radiometric normalization of Landsat Multispectral Scanner (MSS) data using an automated scattergram controlled regression." *Photogrammetric Engineering and Remote Sensing*, Vol. 61, No. 10, pp. 1255-1260.

Erdas. (2002). *ERDAS Field Guide*™. 5th ed., ERDAS Inc, Atlanta, Georgia.

Flusser, J., and T. Suk (1994). "A moment-based approach to registration of images with affine geometric distortion." *IEEE Trans. Geoscience and Remote Sensing*, Vol. 32, No. 2, pp. 382–387.

Fonseca, L.M.G., and M.H. Costa (1997). "Automatic registration of satellite images". *Brazilian Symposium on Graphic Computation and Image Processing*, 10., Campos de Jordão, 1997. Proceedings. Los Alamitos: IEEE Computer Society, 1997. pp. 219-226.

Fonseca, L.M.G., and B.S. Manjunath (1996). "Registration techniques for multisensor remotely sensed imagery." *Photogrammetric Engineering & Remote Sensing*, Vol. 62, No. 9, pp. 1049-1056.

Garguet-Duport, B., J. Girel, J.M. Chassery, and G. Pautou (1996). "The use of multiresolution analysis and wavelets transform for merging SPOT panchromatic and multispectral image data." *Photogrammetric Engineering and Remote Sensing*, Vol. 62, No. 9, pp. 1057-1066.

Gonzalez-Audicana, M., J.L. Saleta, and R.G. Catalan (2004). "Fusion of multispectral and panchromatic images using improved IHS and PCA mergers based on wavelet decomposition." *IEEE Transactions on Geoscience and Remote Sensing*, Vol. 42, No. 6, pp. 1204–1211.

Goshtasby, A., G. Stockman, and C. Page (1986). "A region-based approach to digital image registration with subpixel accuracy." *IEEE Transactions On Geoscience and Remote Sensing*, Vol. 24, No. 3, pp. 390-399.

Grasso, D.N. (1993). "Applications of the IHS color transformation for 1:24,000-scale geologic mapping: A low cost SPOT alternative." *Photogrammetric Engineering & Remote Sensing*, Vol. 59, No. 1, pp. 73-80.

Habib, A.F., and R.I. Alruzouq (2004). "Line-based modified iterated Hough transformation for automatic registration of multi-source imagery." *Photogrammetric Record*, Vol. 19, No. 105, pp. 5-21.

Hall, F.G., D.E. Strebel, J.E. Nickeson, and S.J. Goetz (1991). "Radiometric rectification toward a common radiometric response among multidate, multisensor images." *Remote Sensing of Environment*, Vol. 35, No. 1, pp. 11-27.

Harris, J.R., R. Murray, and T. Hirose (1990). "IHS transform for the integration of radar imagery with other remotely sensed data." *Photogrammetric Engineering and Remote Sensing*, Vol. 56, No. 12, pp. 1631-1641.

Heo, J., and T.W. FitzHugh (2000). "A standardized radiometric normalization method for change detection using remotely sensed imagery." *Photogrammetric Engineering and Remote Sensing,* Vol. 66, No. 2, pp. 173-181.

Hong, G., Y.,Zhang, and J.B., Mercer (2006). "A robust technique for fusing SAR data and multisource multispectral images." Submitted to *Photogrammetric Engineering and Remote Sensing*, under review.

Hong, G., and Y., Zhang (2007). "Comparison and improvement of wavelet-based image fusion." Submitted to *International Journal of Remote Sensing*, in press.

Hong, G., and Y., Zhang (2006a). "Wavelet-based image registration technique for high resolution remote sensing image." Submitted to *Computers & Geosciences*, under review.

Hong, G., and Y. Zhang (2006b). "A comparative study on radiometric normalization using high resolution satellite images." *International Journal of Remote Sensing*, accepted, in press.

Horne, H.J. (2003). "A tasseled cap transformation for IKONOS image." *ASPRS 2003 Annual conference proceedings,* Anchorage, Alaska.

Hsieh, J.W., H.Y.M. Liao, K.C. Fan, M.T. Ko, and Y.P. Hung (1997). "Image registration using a new edge-based approach." *Computer Vision and Image Understanding*, Vol. 67, No. 2, pp. 112-130.

Jensen, J.R. (1983). "Urban/suburban land use analysis." In. R. N. Colwell (Ed.), *Manual of Remote Sensing*, 2nd ed., American Society of Photogrammetry, Falls Church, VA, pp. 1571-1666.

Jensen, J.R. (2005). *Introductory Digital Image Processing: A Remote Sensing Perspective*, Upper Saddle River, NJ: Prentice Hall, 3rd Ed., 526 pages.

King, R.L., and J.W. Wang (2001). "A wavelet based algorithm for pan sharpening Landsat 7 imagery." *Geoscience and Remote Sensing Symposium, IGARSS '01.* IEEE 2001 International Volume 2, 9-13 July 2001, pp.849 – 851.

Li, H., B.S. Manjunath, and S.K. Mitra (1995). "A contour-based approach to multisensor image registration." *IEEE Trans. Image Processing*, Vol.4, pp. 320-334.

Moigne, J.Le, W.J. Campbell, and R.F. Cromp (2002). "An automated parallel image registration technique of multiple source remote sensing data." *IEEE Transactions on Geoscience and Remote Sensing*, Vol. 40, No. 8, pp. 1849-1864.

Munechika, C.K., J.S. Warnick, C. Salvaggio, and J.R. Schott (1993). "Resolution enhancement of multispectral image data to improve classification accuracy."*Photogrammetric Engineering and Remote Sensing*, Vol. 59, pp. 67-72.

Nuñez, J., X. Otazu, O. Fors, A. Prades, V. Palà, and R. Arbiol (1999). "Multiresolution-based image fusion with additive wavelet decomposition." *IEEE Transactions on Geosciences and Remote Sensing*, Vol. 37, No. 3, pp. 1204-1211.

Pajares, G., and J. Manuel de la Cruz (2004). "A wavelet-based image fusion tutorial." *Pattern Recognition*, Vol. 37, No. 9, pp. 1855-1872.

Paolini, L., G. Francisco, S. José, J.M. Juan, K. Haydee (2006). "Radiometric correction effects in Landsat multi-date/multi-sensor change detection studies." *International Journal of Remote Sensing*, Vol. 27, No.4, pp. 685-704.

Pohl, C., and J.L. Van Genderen (1998). "Multisensor image fusion in remote sensing: concepts, methods, and applications." International Journal of Remote Sensing, Vol. 19, No. 5, pp. 823-854.

Pradhan, P. (2005). *Multiresolution based, multisenor, multispectral image fusion*. Ph.D dissertation, Department of Electrical and Computer Engineering, Mississippi State University, Mississippi, Mississippi State, USA, 191 pp.

Ranchin, T., and L. Wald (2000) "Fusion of high spatial and spectral resolution images: The ARSIS concept and its implementation." *Photogrammetric Engineering and Remote Sensing,* Vol. 66, No. 1, pp. 49-61.

Richards, J.A., and X. Jia (1999). *Remote sensing digital image analysis: an introduction*. 3rd ed., Springer-Verlag, New York.

Roy, D.P. (2000). "The impact of misregistration upon composited wide field of view satellite data and implications for change detection." *IEEE Transactions on Geoscience and Remote Sensing*, Vol. 38 No. 4, 2017-2032.

Simone, G., A. Farina, F.C. Morabito, S.B. Serpico and L. Bruzzone, (2002) "Image fusion techniques for remote sensing applications." *Information Fusion,* Vol. 3, No.1, pp. 3–15.

Schenk, T. (1999). *Digital Photogrammetry (volume I).* Ed. TerraScience, Laurelville, Ohio, pp. 232-295.

Schetselaar, E.M. (2001). "On preserving spectral balance in image fusion and its advantages for geological image interpretation." *Photogrammetric Engineering and Remote Sensing*, Vol. 67, No. 8, pp. 925-934.

Schott, J.R., C. Salvaggio, and W.J. Volchok (1988). "Radiometric scene normalization using pseudoinvariant features." *Remote Sensing of Environment*, Vol. 26, No. 1, pp. 1-16.

Schowengerdt, R.A. (1997). *Remote sensing models and methods for image processing*. 2nd ed., Academic Press, Burlington.

Shettigara, V.K. (1992). "A generalized component substitution technique for spatial enhancement of multispectral images using a higher resolution data set." *Photogrammetric Engineering and Remote Sensing*, Vol. 58, No. 5, pp. 561-567.

Shimabukuro, Y.E., E.M. Novo, and L.K. Mertres (2002). "Amazon river mainstem floodplain Landsat TM digital mosaic." *International Journal of Remote Sensing*, Vol 23, No. 1, pp. 57-69.

Simhadri, K.K., S.S. Iyengar, and R.J. Holyer (1998). "Wavelet-based feature extraction from oceanographic images." *IEEE Transactions on Geoscience and Remote Sensing*, Vol. 36, No. 3, pp. 767-778.

Svab, A., and K. Ostir. (2006). "High-resolution image fusion: methods to preserve spectral and spatial resolution." *Photogrammetric Engineering & Remote sensing*, Vol. 72, No. 5, pp. 565-572.

Teggi, S., R. Cecchi, and F. Serafini (2003). "TM and IRS-1C-PAN data fusion using multiresolution decomposition methods based on the 'atrous' algorithm." *International Journal of Remote Sensing*, Vol. 24, pp. 1287-1301.

Ventura, A.D., A. Rampini, and R. Schettini (1990). "Image registration by recognition of corresponding structures." *IEEE Transactions Geoscience and Remote Sensing*, Vol. 28, No. 3, pp. 305-314.

Vijayaraj V. (2004). *A quantitative analysis of pansharpened images*. Master thesis, Department of Electrical and Computer Engineering, Mississippi State University, Mississippi, Mississippi State, USA, 94 pp.

Ya'allah, S.M., and M.R. Saradjian (2005). "Automatic normalization of satellite images using unchanged pixels within urban areas." *Information Fusion*, Vol. 6, pp. 235-241.

Yang, X.J., and C.P. Lo (2000). "Relative radiometric normalization performance for change detection from multi-date satellite images." *Photogrammetric Engineering and Remote Sensing*, Vol. 66, No. 8, pp. 967-980.

Yocky, D.A. (1996). "Multiresolution wavelet decomposition image merger of Landsat Thematic Mapper and SPOT panchromatic Data." *Photogrammetric Engineering and Remote sensing*, Vol. 62, No. 3, pp. 295-303.

Yocky, D.A. (1995). "Image merging and data fusion using the discrete two-dimensional wavelet transform." *J. Opt. Soc. Am. A*, Vol. 12, No. 9, pp. 1834-1841.

Yuan, D., and C.D. Elvidge (1996). "Comparison of relative radiometric normalization techniques." *ISPRS Journal of Photogrammetry and Remote Sensing*, Vol. 51, No. 3, pp. 117-126.

Zavorin, I., and J. Le Moigne (2005). "Use of multiresolution wavelet feature pyramids for automatic registration of multisensor imagery." *IEEE Transactions on Image Processing*, Vol. 14, No. 6, pp. 770-782.

Zhang, Y., and G. Hong (2005). "An IHS and wavelet integrated approach to improve pan-sharpening quality of IKONOS and QuickBird images." *Information Fusion*, Vol. 6, No. 3, pp. 225-234.

Zhang, Y. (2002). "Problems in the fusion of commercial high-resolution satellites Images as well as LANDSAT 7 Images and initial Solutions." *Proceedings of the ISPRS, CIG, and SDH Joint International Symposium on Geospatial Theory, Processing and Applications*, 9-12 July 2002. Ottawa, Canada, unpaginated CD-ROM.

Zhang, Y. (1999). "A new merging method and its spectral and spatial effects." *International Journal of Remote Sensing*, Vol. 20, No. 10, pp. 2003-2014.

Zheng, Q., and R. Chellappa (1993). "A computational vision approach to image registration." *IEEE Trans. Image Processing*, Vol. 2, No. 3, pp. 311–326.

Zhou, J., D.L. Civco, J.A. Silander (1998). "A wavelet transform method to merge Landsat TM and SPOT panchromatic data." *International Journal of Remote Sensing*, Vol. 19, No. 4, pp. 743-757.

Zitova, B., and J. Flusser (2003). "Image registration methods: a survey." *Image and Vision Computing*, Vol. 21, No. 11, pp. 977-1000.

Chapter 2. AN IHS AND WAVELET INTEGRATED APPROACH TO IMPROVE PAN-SHARPENING VISUAL QUALITY OF NATURAL COLOUR IKONOS AND QUICKBIRD IMAGES[♣]

ABSTRACT

Image fusion is an important tool in remote sensing, as many Earth observation satellites provide both high-resolution panchromatic and low-resolution multispectral images. To date, many image fusion techniques have been developed. However, the available algorithms can hardly produce a satisfactory fusion result for IKONOS and QuickBird images. Among the existing fusion algorithms, the IHS technique is the most widely used one, and the wavelet fusion is the most frequently discussed one in recent publications because of its advantages over other fusion techniques. But the colour distortion of these two techniques is often obvious, especially when IKONOS or QuickBird natural colour multispectral images are fused with its panchromatic images. This study presents a new fusion approach that integrates the advantages of both the IHS and the wavelet techniques to reduce the colour distortion of IKONOS and QuickBird fusion results. Different IKONOS and QuickBird images have been fused with this new approach. Visual and statistical analyses prove that the concept of the proposed IHS and wavelet integration is promising, and it does significantly improve the fusion quality compared to conventional IHS and wavelet fusion techniques.

♣ Reprinted from *Information fusion*, Vol. 6, Zhang, Y., G. Hong. "An IHS and wavelet integrated approach to improve pan-sharpening visual quality of natural colour IKONOS and QuickBird images." pp. 225-234.

Key Words: Image fusion, IHS and wavelet integration, IKONOS, QuickBird, natural colour

2.1 Introduction

Most Earth observation satellites, such as SPOT, IRS, Landsat 7, IKONOS, and QuickBird, provide both panchromatic images at a higher spatial resolution and multispectral images at a lower spatial resolution. An image fusion technique that can effectively integrate the spatial detail of the panchromatic image and the spectral characteristics of the multispectral image into one image is important for a variety of remote sensing applications. For example, in geoscience domain image fusion can provide more detailed information for land use classification, change detection, map updating and hazard monitoring; in national defense it is useful for target detection, identification and tracking, and in medical imaging domain for diagnosis, modeling of the human body or treatment planning [Pohl and Van Genderen, 1998; Piella,2002].

Because of the importance of image fusion techniques, many image fusion algorithms have been developed [Qiu, 1990; Chavez et al., 1991; Shettigara, 1992; Yocky, 1995; Zhou et al., 1998; Zhang, 1999; Hill et al., 1999; Ranchin and Wald, 2002]. Pohl and Van Genderen [1998] provided a comprehensive review of most published image fusion techniques by 1998. Successful algorithms for the fusion of Landsat TM and SPOT Pan images, and alike, fall in general into the following three categories: (1) projection and substitution methods, such as IHS colour (Intensity-Hue-Saturation) fusion, and PCA (Principal Component Analysis) fusion; (2) band ratio and arithmetic combination, such as Brovey and SVR (Synthetic Variable Ratio), and (3) the

recently popular wavelet fusion which injects spatial features from panchromatic images into multispectral images, such as ARSIS (an abbreviation of the French definition 'amélioration dela résolution spatial par injection de structures'), and GLP (Gaussian Laplacian Pyramid) techniques. The HPF (High Pass Filtering) method also injects spatial features into MS images, but the spatial features are extracted using high-pass filtering instead of using wavelet transforms.

Among the three categories, the IHS technique has been most widely used in the practical applications, and the wavelet fusion technique has been discussed most frequently in the recent publications due to its advantages over other fusion techniques [Yocky, 1995; Zhou et al., 1998; Ranchin and Wald, 2002; Yocky, 1996; Aiazzi et al. 2002; Shi et al. 2003]. Therefore, this study focuses on the IHS and the wavelet fusion methods, and explores their potential for further improvement.

With the IHS fusion, if the intensity image of the IHS transform has a high correlation to the panchromatic image being fused, it will produce a satisfactory fusion result. The higher the correlation is, the less colour distortion the fused results have. In the practice, however, the intensity image and the panchromatic image often differ from each other to a certain extent. Hence, colour distortion becomes a common problem of the IHS technique. Such a problem has been reported by many authors, such as Chavez et al. [1991] and Pellemans et al. [1993]. The colour distortion is especially significant when the panchromatic and multispectral images of the IKONOS, QuickBird, and Landsat 7 are fused, because the correlation between the panchromatic image and the intensity image is often very low, in particular when the natural colour bands 1, 2 and 3

are fused with the panchromatic image [Zhang, 2002]. However, despite of colour distortion IHS fused images usually show plentiful colour in the fusion results.

The wavelet base fusion technique usually can better preserve the colour information than the IHS does, as the wavelet technique extracts spatial detail information from a high-resolution panchromatic image first, and then injects the spatial information into the multispectral bands, respectively. In this manner, the colour distortion can be reduced. However, the spatial detail information extracted from a high-resolution panchromatic image is not equivalent to that existing in an original high-resolution multispectral band. This difference can also introduce colour distortion into the fusion result, especially when IKONOS, QuickBird, and Landsat 7 images are fused with their panchromatic images. Further, because the spatial detail is injected into individual multispectral bands, the fused image sometimes appears like a fusion result through a high-pass filtering process, e.g., the integration between colour and spatial detail is not smooth. Some ring effects may appear in the image, and small objects may not obtain colour information [Yocky, 1995; Yocky, 1996]. Because of this problem, further research has been done to reduce it [Aiazzi et al., 2002; Aiazzi et al., 2003].

To date, significant colour distortions of the IHS technique for IKONOS or QuickBird image fusions have been reported by many authors [Zhang, 2002]. Only a few satisfactory fusion results have been reported by some authors in which advanced wavelet fusion techniques were involved [Aiazzi et al., 2003; Laporterie-Dejean, 2003].

To overcome the disadvantages of the IHS fusion technique and those of the wavelet fusion technique, and to explore a more effective way to fuse the IKONOS and QuickBird images, especially the natural colour multispectral bands, an IHS and wavelet

integrated fusion approach has been developed in this study. This proposed approach has been implemented with IKONOS and QuickBird images. Visual and statistical analyses demonstrate that the new IHS and wavelet integrated fusion approach does improve the fusion quality of the IKONOS and QuickBird images compared to the original IHS technique and the wavelet technique.

2.2 Conventional IHS and Wavelet Fusion Techniques

2.2.1 IHS fusion technique

The colour system with red, green and blue channels (RGB) is usually used by computer monitors to display a colour image. Another colour system widely used to describe a colour is the system of intensity, hue and saturation (IHS). The intensity represents the total amount of the light in a colour (also called brightness), the hue is the property of the colour determined by its wavelength, and the saturation is the purity of the color. An intensity image of the IHS system usually appears like a panchromatic image. This characteristic is utilized in the image fusion to fuse a high-resolution panchromatic image into a low-resolution colour image.

To conduct an image fusion the three bands of a colour image have to be transferred from the RGB space into the IHS space. Before this, the colour image should be registered to the high-resolution panchromatic image and resampled to the same pixel size with the panchromatic image. The intensity image is then replaced by a high-resolution panchromatic image. To have a better fusion quality, the panchromatic image usually needs to be matched to the intensity image before the replacement. After the

replacement, the panchromatic image together with the hue and saturation images are reversely transferred from the IHS space into the RGB space, resulting in a fused colour image. This process is schematized in Figure 2.1.

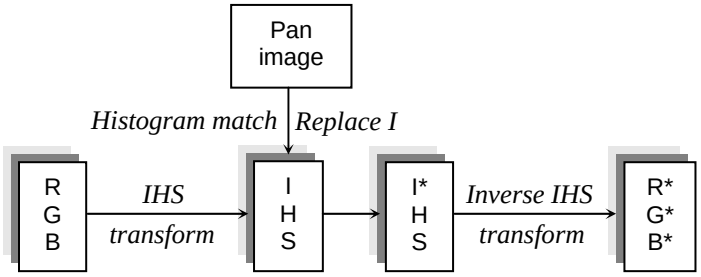

Figure 2.1. IHS image fusion process

Different transformations have been developed to transfer a colour image from the RGB space to the IHS space. One common IHS transformation is based on a cylinder colour model which is described by the following equations [Pohl and Van Genderen, 1998; Shettigara, 1992].

$$\begin{pmatrix} I \\ v1 \\ v2 \end{pmatrix} = \begin{bmatrix} \frac{1}{\sqrt{3}} & \frac{1}{\sqrt{3}} & \frac{1}{\sqrt{3}} \\ \frac{1}{\sqrt{6}} & \frac{1}{\sqrt{6}} & \frac{-2}{\sqrt{6}} \\ \frac{1}{\sqrt{2}} & \frac{-1}{\sqrt{2}} & 0 \end{bmatrix} \begin{pmatrix} R \\ G \\ B \end{pmatrix} \tag{2.1}$$

$$H = \tan^{-1}\left(\frac{v1}{v2}\right) \tag{2.2}$$

$$S = \sqrt{v1^2 + v2^2} \tag{2.3}$$

where $v1$ and $v2$ are two intermediate values.

The corresponding inverse transformation is defined as:

$$v1 = S\cos(H) \tag{2.4}$$

$$v2 = S\sin(H) \tag{2.5}$$

$$\begin{pmatrix} R \\ G \\ B \end{pmatrix} = \begin{bmatrix} \frac{1}{\sqrt{3}} & \frac{1}{\sqrt{6}} & \frac{1}{\sqrt{2}} \\ \frac{1}{\sqrt{3}} & \frac{1}{\sqrt{6}} & \frac{-1}{\sqrt{2}} \\ \frac{1}{\sqrt{3}} & \frac{-2}{\sqrt{6}} & 0 \end{bmatrix} \begin{pmatrix} I \\ v1 \\ v2 \end{pmatrix} \tag{2.6}$$

Another commonly used IHS transformation is based on a triangular colour model. The forward IHS transformation can be described as below [Qiu, 1990]:

$$I = \frac{1}{3} I' \tag{2.7}$$

$$I' = R + G + B \tag{2.8}$$

$$H = \frac{G-3B}{I'-3B},\ S = \frac{I'-3B}{I'}, \text{ when B is the minimum} \tag{2.9}$$

$$H = \frac{B-R}{I'-3R}+1,\ S = \frac{I'-3R}{I'}, \text{ when R is the minimum} \tag{2.10}$$

$$H = \frac{R-G}{I'-3G}+2,\ S = \frac{I'-3G}{I'}, \text{ when G is the minimum} \tag{2.11}$$

The corresponding inverse IHS transformation is:

$$\begin{cases} R = \frac{1}{3} I'(1+2S-3SH) \\ G = \frac{1}{3} I'(1-S+3SH) \\ B = \frac{1}{3} I'(1-S) \end{cases} \text{ when B is the minimum} \tag{2.12}$$

$$\begin{cases} R = \frac{1}{3} I'(1-S) \\ G = \frac{1}{3} I'(1+5S-3SH) \\ B = \frac{1}{3} I'(1-4S+3SH) \end{cases} \text{when R is the minimum} \tag{2.13}$$

$$\begin{cases} R = \frac{1}{3} I'(1 - 7S + 3SH) \\ G = \frac{1}{3} I'(1 - S) \\ B = \frac{1}{3} I'(1 + 8S - 3SH) \end{cases} \quad \text{when G is the minimum} \tag{2.14}$$

2.2.2 Wavelet fusion technique

Wavelet transformation is a mathematical tool that can detect local features in a signal process. It can also be employed to decompose two-dimensional signals – a digital image – into different resolution levels for a multi-resolution analysis. This multi-resolution characteristic is utilized for fusing images at different resolution levels.

Figure 2.2 shows the general concept of a wavelet image fusion process [Nuñez et al., 1999]. First, three new panchromatic images are produced according to the histogram of R, G, B bands of multispectral image respectively. Then each of the new high-resolution panchromatic images is decomposed into a low-resolution approximation image and three wavelet coefficients, also called detail images, which contain information of local spatial details. The decomposed low-resolution panchromatic images are then replaced by the real low-resolution multispectral image bands (B, G, R), respectively. In the last step, a reverse wavelet transform is applied to each of the sets containing the local spatial details and one of the multispectral bands (B, G, and R). After three times of reverse wavelet transforms, the high-resolution spatial details from the panchromatic image are injected into the low resolution multispectral bands resulting in fused high-resolution multispectral bands.

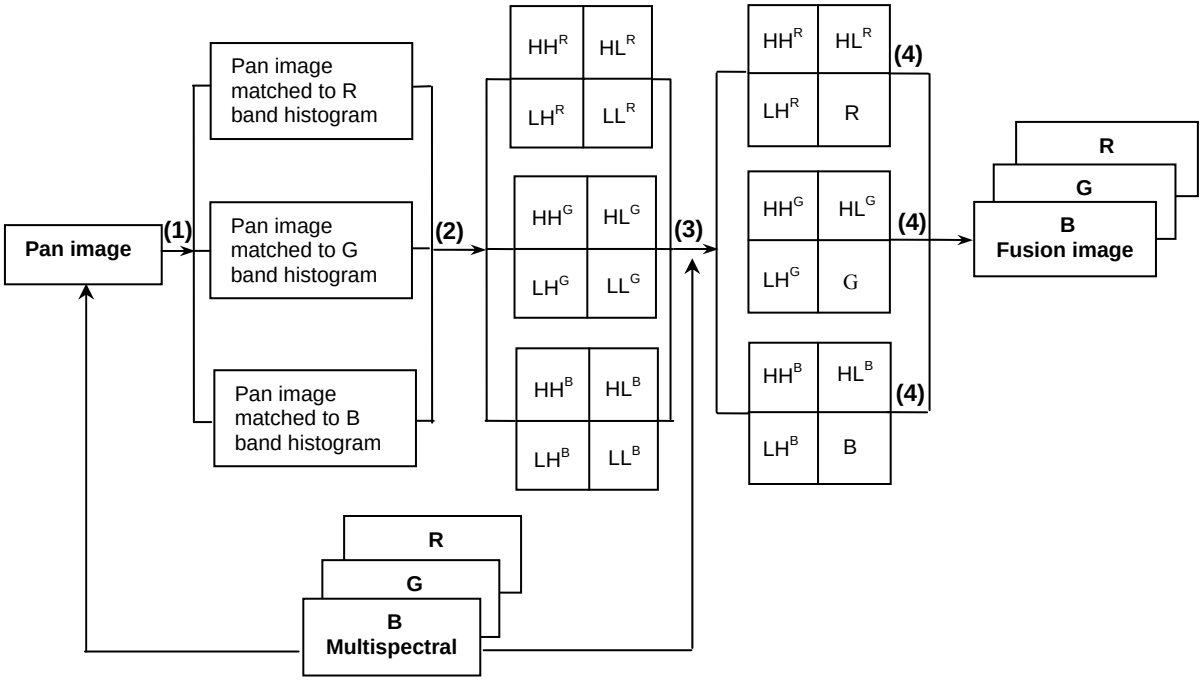

Figure 2.2. General concept of a wavelet image fusion

(1), (2), (3) and (4) indicate the processing steps of histogram matching, wavelet decomposition, band replacement and reverse wavelet transform; R, G and B are three bands of a multispectral image set; and the superscripts R, G and B indicate wavelet decompositions from R, G, or B matched Pan images. LL^R represents an approximation image of pan image according to R band histogram at a lower resolution level. HH^R, HL^R and LH^R represent corresponding wavelet coefficients (or detail images) in diagonal, horizontal and vertical directions. .

The original concept and theory of a wavelet-based multi-resolution analysis comes from Mallat [1989]. Many researchers have applied this theory to different image fusions resulting in promising fusion results [Yocky, 1995; Zhou et al., 1998; Ranchin and Wald, 2002; Aiazzi et al., 2002; Shi et al., 2003]. Let $\left\{ s_{m,n}^{j+1}, m, n \in Z \right\}$ be a two-dimension image at a resolution of j+1 with j being an integer. m and n are the dimensions of the image in row and column directions, which belong to an integer set Z. The wavelet multi-resolution transform can then be expressed as [Shi et al., 2003]:

$$\begin{cases} s_{m,n}^{j} = \frac{1}{2}\sum_{k,l\in Z} s_{k,l}^{j+1} h_{k-2m} h_{l-2n} \\ d_{m,n}^{j1} = \frac{1}{2}\sum_{k,l\in Z} s_{k,l}^{j+1} h_{k-2m} g_{l-2n} \\ d_{m,n}^{j2} = \frac{1}{2}\sum_{k,l\in Z} s_{k,l}^{j+1} g_{k-2m} h_{l-2n} \\ d_{m,n}^{j3} = \frac{1}{2}\sum_{k,l\in Z} s_{k,l}^{j+1} g_{k-2m} g_{l-2n} \end{cases} \tag{2.15}$$

where s^j is an approximation image at a lower resolution j (e.g., LL^P). d^{j1}, d^{j2} and d^{j3} are three wavelet coefficients containing local spatial details (e.g., HH^P, HL^P and LH^P). g_n is a high-pass filter bank, and h_n is a low-pass filter bank.

The reverse wavelet transform for reconstructing a high-resolution image is written as:

$$\begin{aligned} s_{m,n}^{j+1} = \frac{1}{2}\Big(&\sum_{k,l\in Z} s_{k,l}^{j} \tilde{h}_{2k-m} \tilde{h}_{2l-n} + \sum_{k,l\in Z} d_{k,l}^{j1} \tilde{h}_{2k-m} \tilde{g}_{2l-n} + \\ &\sum_{k,l\in Z} d_{k,l}^{j2} \tilde{g}_{2k-m} \tilde{h}_{2l-n} + \sum_{k,l\in Z} d_{k,l}^{j3} \tilde{g}_{2k-m} \tilde{g}_{2l-n}\Big) \end{aligned} \tag{2.16}$$

where $\tilde{g}_n$ and $\tilde{h}_n$ meet the following relationships:

$$\begin{cases} g_n = (-1)^{-1+n} h_{1-n} \\ \tilde{h}_n = h_{1-n} \\ \tilde{g}_n = g_{1-n} \end{cases} \tag{2.17}$$

The Equation set (2.15) applies to the step 1, and the Equation (2.16) applies to the step 3 in Figure 2.2.

2.2.3 The proposed IHS and wavelet integrated fusion

As denoted in the introduction, the IHS fusion method usually can integrate colour and spatial features smoothly. The colour depth (or intensity) of the IHS fusion results is

high (rich in colour). And, if the correlation between the IHS intensity image and the panchromatic image is high, the IHS fusion can well preserve the colour information. In the real cases, however, the colour distortion is significant due to the low correlation between the intensity image and the panchromatic image, especially when the natural colour multispectral bands and panchromatic images from IKONOS and QuickBird are fused.

On the other hand, the wavelet image fusion usually can better preserve colour information than other conventional fusion methods, such as IHS, PCA, and bands arithmetic combination, because the high-resolution spatial information from a panchromatic image is injected into all the three low-resolution multispectral bands. However, the spatial detail from a panchromatic image is often different from that of a multispectral band having the same spatial resolution. This difference may introduce colour distortion into the wavelet fusion results, and sometimes it may make the integration between colour and spatial detail appear unnatural [Yocky, 1996].

To better utilize the advantages of the IHS and the wavelet fusion techniques for the fusion of IKONOS and QuickBird images, and to overcome the shortcomings of the two techniques, we proposed an IHS and wavelet integrated fusion approach. The concept and the process steps of this approach are illustrated in Figure 2.3. In general, it uses the IHS transform to integrate the low-resolution multispectral colour information with the high-resolution panchromatic spatial detail information to achieve a smooth integration of colour and spatial features (part I of Figure 2.3). However, the wavelet transform is utilized to generate a new panchromatic image (new intensity in Figure 2.3)

that has a high correlation to the intensity image and contains the spatial detail of the original panchromatic image (part II in Figure 2.3).

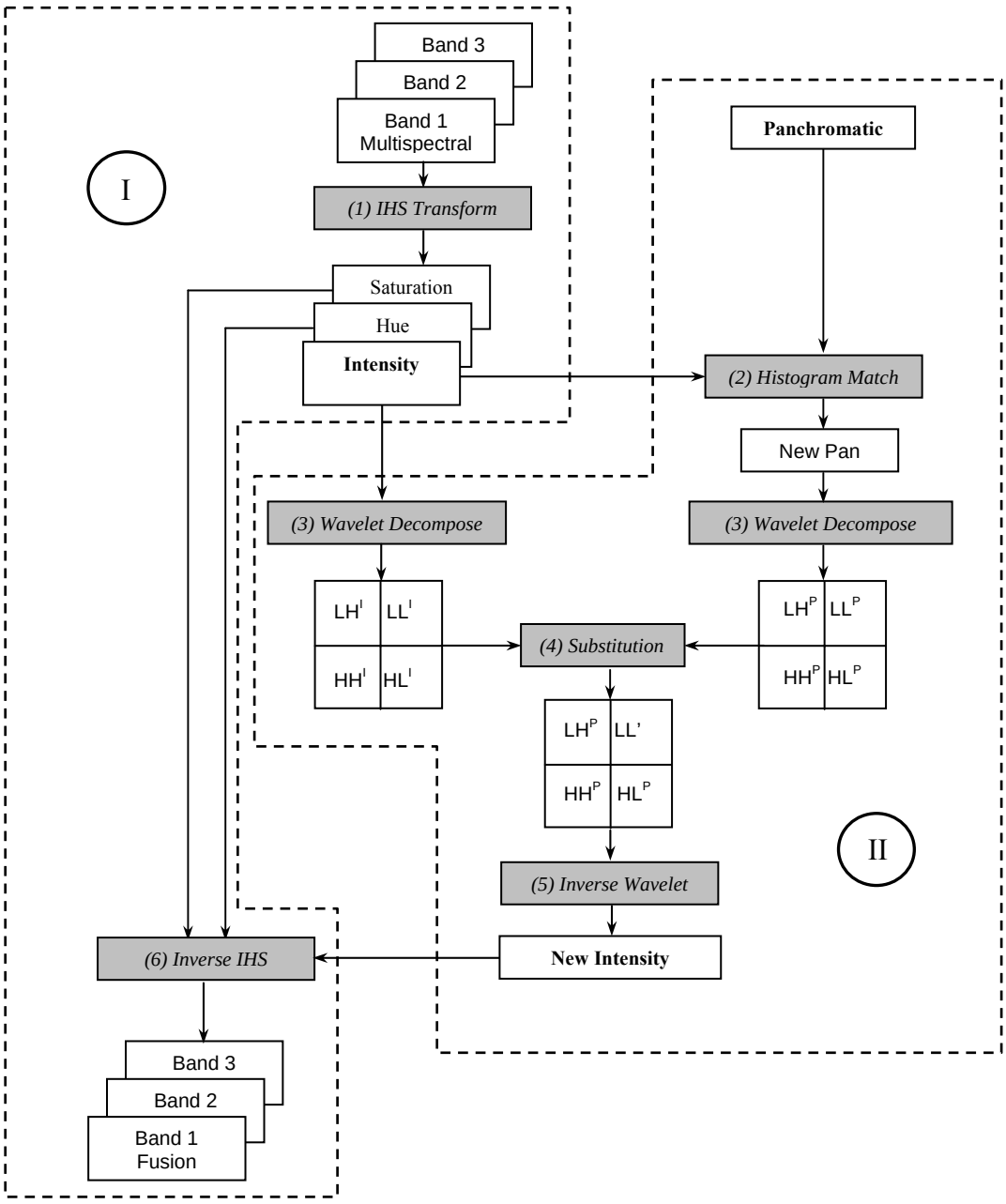

Figure 2.3. Processing flow of the proposed IHS and wavelet transforms integrated fusion method. (Two-level wavelet decomposition is applied to both the intensity image and the panchromatic image. Only one-level decomposition is symbolically drawn in the figure to highlight the overall concept.)

As shown in Figure 2.3, the detailed steps of this integrated fusion method are:

(1) Transforming the multispectral image into the IHS components (Forward IHS transform). Before the IHS transform, the multispectral image must be co-registered to the panchromatic image and resampled to the pixel spacing of the panchromatic image.

(2) Applying histogram matching to match the histogram of the panchromatic image to that of the Intensity component (I), and obtaining a new panchromatic image (New Pan).

(3) Decomposing the new panchromatic image and the intensity component (I) into wavelet planes (a two-level decomposition is applied), respectively. The intensity image has the same pixel size as the panchromatic image.

(4) Replacing the approximation image of the panchromatic decomposition (LL^P) by that of the intensity decomposition (LL^I) to inject grey value information of the intensity image into the panchromatic image. To avoid an over injection of the intensity information, the LL^P at the second decomposition level is not completely, but partially, replaced by the LL^I at the same level, namely a new approximation image (LL') is first generated through a weighted combination of LL^P and LL^I, and then replaces the LL^P of the panchromatic decomposition. The method for the weighted combination is described in Equations 2.18 and 2.19 below.

(5) Performing an inverse wavelet transform to obtain a new intensity image, which has similar grey value distribution to that of the intensity image of IHS transform and contains the same spatial detail of the original panchromatic image.

(6) Transforming the new intensity together with the hue and saturation components back into RGB space (inverse IHS transform).

The triangular model of IHS transform (Equations 2.7 through 2.14) is employed in this proposed IHS and wavelet integrated fusion. The method to generate the new approximation image LL', denoted as *c*, can be expressed as:

$$c = w_1 \times a + w_2 \times b, \tag{2.18}$$

where *a* and *b* are the approximation images LL^I and LL^P, respectively, and w_1 and w_2 are the corresponding weight coefficients, which are determined by:

$$w_1 = Corr(a/b) = \frac{\sum_{i=1}^{N}(a_i - \bar{a})(b_i - \bar{b})}{\sqrt{\sum_{i=1}^{N}(a_i - \bar{a})\sum_{i=1}^{N}(b_i - \bar{b})}}, \quad \text{with } w_1 + w_2 = 1 \tag{2.19}$$

where $\bar{a}$ and $\bar{b}$ are the means of *a* and *b*, and *N* is the total pixel number of the approximation images.

In this proposed approach, the gray value information of the intensity image is partially injected into the panchromatic image to make the new intensity image having similar gray value relationship (high correlation) to the original intensity image and containing enough spatial detail from the panchromatic image. This new intensity image is, then, used to replace the intensity image of the IHS transform. Finally, the spatial detail of the panchromatic image is integrated into the multispectral image bands by a reverse IHS transform.

The correlation coefficient (w_1) between LL^I and LL^P is introduced as the weight to the LL^I. The coefficient w_2 (w_2 = 1-w_1) is applied to the LL^P to control the balance of the partial replacement, i.e. the higher to correlation between LL^I and LL^P, the more weight

to the LL^I in the replacement. This weighted combination of LL^I and LL^P ensures that the modified panchromatic image (New Intensity) has a high correlation to the intensity image and enough spatial detail from the original panchromatic image.

A similar approach by Nunez *et al.* [1999] was identified after the completion of the research resulting in the proposed approach above. But, significant differences can be found between the two approaches. In Nunez's approach, an "*a trous*" ("with holes") algorithm was employed to decompose the panchromatic image, the low-resolution panchromatic approximation image was completely replaced by L image of a LHS transform, and modified Landsat TM R, G and B bands were fused with SPOT panchromatic image [Aiazzi et al., 2003]. Neither natural colour images were tested, nor IKONOS or QuickBird images were fused.

2.3 Testing data and fusion experiments

The testing image data consist of an IKONOS data set with 1m panchromatic and 4m multispectral images, and a QuickBird data set with 0.7m panchromatic and 2.8m multispectral images. The IKONOS data set covers the urban area of Fredericton, NB, Canada. It was taken in October of 2001. The image size is approximately 10,000 by 10,000 pixels at the resolution of 1m. The QuickBird image was taken over the well-known Pyramids area of Egypt in 2002. The image size being tested is approximately 3,000 by 3,000 pixels at the resolution of 0.7m. Before the image fusion, the multispectral images were co-registered to the corresponding panchromatic images and resampled to the same pixel sizes of the panchromatic images.

The cylinder model and triangular model of the IHS transform, the common wavelet fusion transform, and the proposed IHS and wavelet integrated transform were employed to fuse the two image data sets. The fusion results are displayed in Figure 2.4 and 2.5. The same standard stretching method was applied to all the images for the display.

Figure 2.4. IKONOS image in Fredericton, Canada, and different fusion results (256×200 pixel subset)

(a) Original panchromatic image; (b) Original multispectral image with bands 1, 2, and 3; (c) IHS fusion result with the cylindrical model; (d) IHS fusion result with the triangular model; (e) Wavelet fusion result; (f) Result of the proposed IHS and wavelet integrated method.

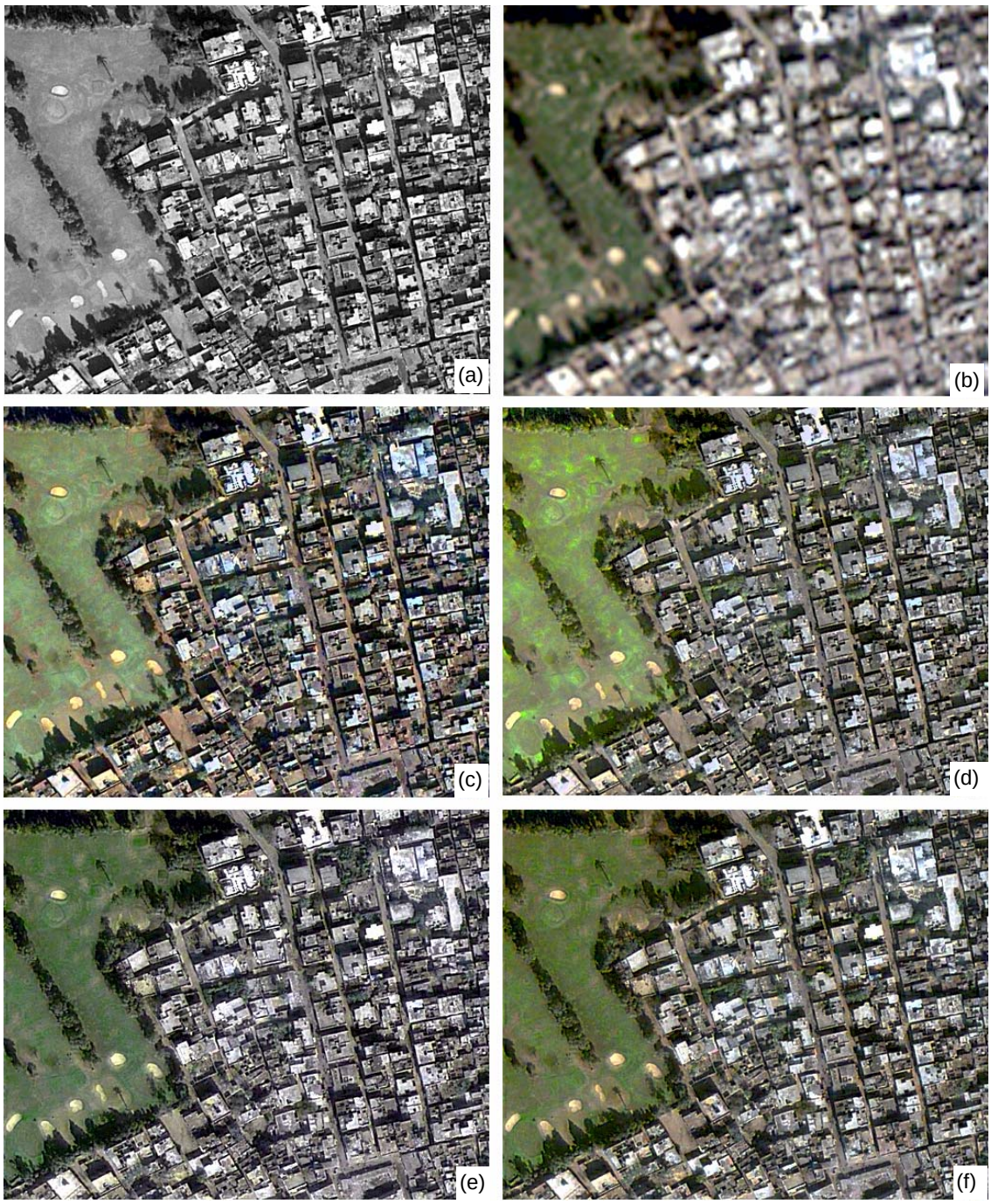

Figure 2.5. Original QuickBird image in the Pyramidal region, Egypt, and different fusion results (256×200 pixels subset)

(a) Original panchromatic image; (b) Original multispectral image with bands 1, 2, and 3; (c) IHS fusion result with the cylindrical model; (d) IHS fusion result with the triangular model; (e) Wavelet fusion result; (f) Result of the proposed IHS and wavelet integrated method.

2.4 Accuracy analyses of the fusion results

2.4.1 Visual analysis

It can be seen in Figure 2.4 that the fusion results of the two models of the IHS transform (Figure 2.4. c and d) are rich in colour, and they have a good colour and spatial feature integration. However, the colour distortions are significant. The colour in vegetation areas was deflected to yellow, and that of the paved areas with high spectral reflectance was distorted from white to purple. The wavelet fused result (Figure 2.4.e) shows clear spatial detail like the original pan image; however, its colour intensity is weak. Much colour information has lost. It is clear to see that the result from the proposed IHS and wavelet integrated fusion method (Figure 2.4.f) appears best among all the results. The colour was least distorted, the spatial detail is as clear as the original pan, and the integration of colour and spatial features is natural.

Figure 2.5 shows the original QuickBird images and the fusion results. The results of the two IHS models (Figure 2.5. c and d) are also rich in colour, but with obvious colour distortions. The colour in vegetation areas was deflected from dark green to light yellow green, and that of highly reflecting roofs was distorted from white to light blue. The magnitudes of the colour distortions are different in the two IHS results and they differ from object to object. The colour of the wavelet fused result (Figure 2.5.e) is close to that of original colour image in vegetation areas, but with obviously weak colour intensity in residence areas. The roads and building roofs have almost the same colour except the brightness variation. Trees in residence areas can be hardly recognized. However, the IHS and wavelet integrated method (Figure 2.5.f) overcomes the disadvantage of the IHS methods – significant colour distortion – and that of the wavelet

method – weak colour intensity. The colour of this integrated method is, in general, closest to that of the original colour image, and it appears like the combination of the colour of the IHS fusion result (Figure 2.5.c) and that of the wavelet fusion result (Figure 2.5.e).

Compared to Figure 2.4 and Figure 2.5 it can also be seen that the colour distortions of the two IHS models and the conventional wavelet fusion are data source dependent. In the IHS fusion results, the colour of highly reflecting building roofs and other paved areas are changed from white, in the original IKONOS colour image (Figure 2.4.b), to purple, in the fusion results (Figure 2.4.c and d), while it is distorted from white to light blue, in QuickBird fusion result (Figure 2.4.e). The colour of the vegetation areas is also distorted in different directions, namely from dark green to yellow green or cyan in the IKONOS fusion results, but to light green in the QuickBird fusion results.

For the wavelet fusion, the colour depth (or intensity) decreases significantly for all the areas in the IKONOS fusion result (Figure 2.4.e), while it just decreases mainly in the build up areas in the QuickBird fusion result (Figure 2.5.e). For the IHS and wavelet integrated fusion approach, however, the colour of fused images can be kept close to that of the original colour images regardless the difference of the data source (compare Figure 2.4.f and 4.b, and Figure 2.5.f and 5.b).

The spatial quality of the fusion results has also been analyzed by enlarging the fused images and the panchromatic images. In all of the fusion results, cars, building corners and other sharp edges can be seen as clear as in the original panchromatic

images. This indicates the spatial qualities of all the fusion techniques being tested are similar, or the same.

2.4.2 Statistical analysis

Two kinds of evaluation models are employed to testify the degree of colour distortion caused by the different fusion methods. (1) The fusion results of the degraded panchromatic and multispectral images (4 times degraded in resolution) are compared with original multispectral images. (2) The fusion results from the original panchromatic and multispectral images are compared with the original multispectral image.

For IKONOS the original panchromatic and multispectral images are degraded to 4m and 16m respectively by the cubic convolution resampling method. Table 2.1 shows the correlation coefficients between the original bands and the corresponding fused bands from the degraded images. C_R, C_G and C_B are the correlation coefficients between the original multispectral bands and their corresponding fused bands.

Table 2.1. Correlation coefficients (C_R, C_G, C_B) between original IKONOS multispectal R, G and B bands and the corresponding fused bands from the degraded images

	IHS(C)	IHS(T)	WAVELET	WAVELET+IHS
C_R	0.587	0. 627	0.718	0. 832
C_G	0. 560	0. 576	0. 705	0. 806
C_B	0. 505	0.508	0. 631	0. 766

From Table 2.1, it can be found that the correlation coefficients C_R, C_G and C_B of IHS cylinder model, IHS(C), are the lowest among all the fusion methods. The second lowest is IHS triangular model, IHS (T), the third lowest is conventional wavelet method, and the highest is the proposed IHS and wavelet integrated method. Therefore,

we can draw a conclusion that IHS(C) fused image has the largest colour distortion, and the fusion result of the IHS and wavelet integrated method has the least colour distortion. These statistical assessment results agree with those of the visual analysis, e.g., the IHS(C) has the largest colour distortion and the proposed IHS and wavelet integrated method has the least colour distortion (see Figure 2.4).

Like for IKONOS, colour QuickBird panchromatic and multispectral images are degraded to 2.8m and 11.2m respectively by the cubic convolution method. The fusion result from the degraded images is used to compare with the original multispectral image. Table 2.2 shows the correlation coefficients between the original bands and the corresponding fused bands from the degraded QuickBird images.

Table 2.2. Correlation coefficients (C_R, C_G, C_B) between original QuickBird multispectral image bands and the fused bands from the degraded images

	IHS(C)	IHS(T)	WAVELET	WAVELET+IHS
C_R	0.709	0. 777	0. 835	0. 913
C_G	0.656	0. 730	0. 823	0. 876
C_B	0.736	0. 846	0. 819	0. 941

It can be seen from Table 2.2 that the IHS(C) technique has the lowest C_R, C_G and C_B, followed by the IHS(T), while the IHS and wavelet integrated method has the highest correlations. This means that the proposed IHS and wavelet integrated method has the smallest colour distortion. It accords with that of visual analysis (Figure 2.5).

The correlation evaluation between the full resolution multispectral images before and after the fusion is also carried out.

Table 2.3 shows the correlation coefficients between the original image bands and the corresponding fused bands for the IKONOS image. The resolution of panchromatic image is 1m, multispectral image is 4m, and fusion result is 1m. From Table 2.3 the

same conclusion as Table 2.1 can be drawn, namely IHS(C) fused image has the largest colour distortion, followed by the IHS(T) fusion result and the wavelet result, respectively. The fusion result of the proposed IHS and wavelet integrated method has the least colour distortion.

Table 2.3. Correlation coefficients (C_R, C_G, C_B) between original IKONOS multispectral image bands and the corresponding fused bands

	IHS(C)	IHS(T)	WAVELET	WAVELET+IHS
C_R	0. 601	0. 737	0. 883	0. 922
C_G	0. 582	0. 693	0. 877	0. 904
C_B	0. 575	0. 672	0. 839	0. 917

Table 2.4 shows the correlation coefficients between the original multispectral bands and the corresponding fused bands for the QuickBird image. The resolution of the panchromatic image is 0.7m, multispectral is 2.8m, and the fusion result is 0.7m.

Table 2.4. Correlation coefficients (C_R, C_G, C_B) between original QuickBird multispectral bands and the fused bands

	IHS(C)	IHS(T)	WAVELET	WAVELET+IHS
C_R	0.644	0. 673	0. 833	0. 930
C_G	0.655	0. 623	0. 826	0. 898
C_B	0.691	0. 801	0. 871	0. 941

From Table 2.4, it can also be found that the same conclusion to Table 2.2 can be drawn, i.e. IHS (C) has the largest colour distortion, followed by the IHS (T) and wavelet, while the IHS and wavelet integrated method has the least distortion.

2.5 Conclusion

The algorithms and fusion results of the most popular IHS fusion techniques and the recently widely discussed wavelet fusion technique are reviewed and analyzed in

this study. To reduce the colour distortion and improve the fusion quality, an IHS and wavelet integrated fusion approach is proposed. This approach utilizes the IHS transform to fuse high-resolution spatial information into the low-resolution multispectral images, and uses the wavelet transform to reduce the colour distortion, in the way of generating a new high-resolution panchromatic image that highly correlates to the intensity image of the IHS transform. The new panchromatic image is, then, used to replace the intensity image for a reverse IHS transform. The fused image is produced after the reverse IHS transform.

IKONOS and QuickBird multispectral and panchromatic images are fused with this proposed approach. The fusion results are compared with those of the conventional IHS fusion methods (the cylinder model and the triangular model) and the conventional wavelet fusion by visual analysis and statistical analysis. The analysis results demonstrate that the proposed IHS and wavelet integrated fusion approach does significantly reduce the colour distortion compared to the conventional, non-adaptive fusion methods. In other words, the results have proved that the concept of the proposed IHS and wavelet integration is promising.

ACKNOWLEDGMENTS

This research was supported by the GEOIDE Network (Geomatics for Informed Decisions) of Canada under the project MNG#TAO, and the NSERC Discovery Grant (Natural Science and Engineering Research Council, Canada). The authors would like to thank Mr. Rob Lunn, GIS supervisor of the City of Fredericton, NB, Canada, for providing the IKONOS multispectral and panchromatic images.

REFERENCES

Aiazzi, B., L. Alparone, S. Baroni, and A. Garzelli (2002). "Context-Driven Fusion of Spatial and Spectral Resolution Images Based on Oversampled Multiresolution Analysis." *IEEE Transaction on Geoscience and Remote Sensing,* Vol. 40, No.10, pp. 2300-2312.

Aiazzi, B., L. Alparone, S. Baroni, A. Garzelli, and M. Selva (2003). "An MTF-Based Spectral Distortion Minimizing Model for Pan-Sharpening of High Resolution Multispectral Images of Urban Areas." *Proceedings of GRSS/ISPRS Joint Workshop on "Data Fusion and Remote Sensing over Urban Areas",* Berlin, Germany, 22-23 May 2003, pp. 90-94.

Chavez, P.S., S.C. Slides, and J.A. Anderson (1991). "Comparison of Three Different Methods to Merge Multiresolution and Multispectral Data: Landsat TM and SPOT panchromatic." *Photogrammetric Engineering and Remote Sensing,* Vol. 57, No. 3, pp. 295-303.

Garguet-Duport, B., J. Girel, J.M.Chassery, and G. Pautou (1996). "The use of multiresolution analysis and wavelets transform for merging SPOT panchromatic and multispectral image data." *Photogrammetric Engineering and Remote Sensing*, Vol. 62, No. 9, pp. 1057-1066.

Hill, J., C. Diemer, O. Stöver, and Th. Udelhoven (1999). "A Local Correlation Approach for the Fusion of Remote Sensing Data with Different Spatial Resolutions in Forestry Applications." *International Archives of Photogrammetry and Remote Sensing*, Vol. 32, Part 7-4-3 W6, Valladolid, Spain, 1999.

Laporterie-Dejean, F., C. Latry and H. De Boissezon (2003). "Evaluation of the quality of panchromatic/multispectral fusion algorithms performed on images simulating the future Pleiades satellites." *Proceedings of GRSS/ISPRS Joint Workshop on "Data Fusion and Remote Sensing over Urban Areas"*, Berlin, Germany, 22-23 May 2003, pp. 95-98.

Mallat, S.G. (1989) "A theory for multiresolution signal decomposition: The wavelet representation." *IEEE Transactions on Pattern Analysis and Machine Intelligence,* Vol. 11, No. 7, pp. 674-693.

Nuñez, J., X. Otazu, O. Fors, A. Prades, V. Palà and R. Arbiol (1999). "Multiresolution-based image fusion with additive wavelet decomposition." *IEEE Transactions on Geosciences and Remote Sensing,* Vol. 37, No. 3, pp.1204-1211.

Pellemans, A., R. Jordans, and R. Allewijn (1993). "Merging Multispectral and Panchromatic SPOT Images with Respect to the Radiometric Properties of the Sensor." *Photogrammetric Engineering and Remote Sensing,* Vol. 59, No. 1, pp. 81-87.

Piella, G. (2002). "A General Framework for Multiresolution Image Fusion: from Pixels to Regions". *Research Report PNA-R0211*, CWI, Amsterdam.

Pohl, C., and J.L. Van Genderen (1998). "Multisensor image fusion in remote sensing: concepts, methods, and applications." *International Journal of Remote Sensing,* Vol. 19, No. 5, pp.823-854.

Qiu, Z.C. (1990). "The Study on the Remote Sensing Data Fusion." *Acta Geodaetica et Cartographica Sinica*, Vol. 19, No. 4, pp.290-296.

Ranchin, T., L. Wald, and M. Mangolini (1996). "The ARSIS method: A general solution for improving special resolution of images by the means of sensor fusion." *Proceedings of the First Conference Fusion of Earth Data: Merging Point Measurements, Raster Maps and Remotely Sensed Images*, Cannes, France, 06-08 February 1996, pp. 53-58.

Ranchin, T., and L. Wald (2000) "Fusion of High Spatial and Spectral Resolution images: The ARSIS Concept and Its Implementation." *Photogrammetric Engineering and Remote Sensing,* Vol. 66, No. 1, pp. 49-61.

Shettigara, V.K. (1992). "A Generalized Component Substitution Technique for Spatial Enhancement of Multispectral Images Using a Higher Resolution Data Set." *Photogrammetric Engineering and Remote Sensing,* Vol. 58, No. 5, pp. 561-567.

Shi, W., Ch. Zhu, C. Zhu, and X. Yang (2003). "Multi-Band Wavelet for Fusing SPOT Panchromatic and Multispectral Images." *Photogrammetric Engineering and Remote Sensing,* Vol. 69, No. 5, pp. 513-520.

Wald, L., T. Ranchin, and M. Mangolini (1997). "Fusion of Satellite Images of Different Spatial Resolutions: Assessing the Quality of Resulting Images." *Photogrammetric Engineering and Remote Sensing,* Vol. 63, No. 6, pp. 691-699.

Yocky, D.A. (1995). "Image merging and data fusion using the discrete two-dimensional wavelet transform." *J. Opt. Soc. Am. A.* Vol. 12, No. 9, pp. 1834-1841.

Yocky, D.A. (1996). "Multiresolution Wavelet Decomposition Image Merger of Landsat Thematic Mapper and SPOT Panchromatic Data." *Photogrammetric Engineering and Remote sensing*, Vol. 62, No. 3, pp. 295-303.

Zhang, Y. (1999). "A new merging method and its spectral and spatial effects." *International Journal of Remote Sensing*, Vol. 20, No. 10, pp. 2003-2014.

Zhang, Y. (2002). "Problems in the Fusion of Commercial High-Resolution Satellites Images as well as LANDSAT 7 Images and Initial Solutions." Proceedings of the ISPRS, CIG, and SDH Joint International Symposium on Geospatial Theory, Processing and Applications, 9-12 July 2002, Ottawa, Canada, unpaginated CD-ROM.

Zhou, J., D.L. Civco, and J.A. Silander (1998). "A wavelet transform method to merge Landsat TM and SPOT panchromatic data." *International Journal of Remote Sensing,* Vol. 19, No. 4, pp. 743-757.

Zhu, S.L., and Z.M. Zhang (2000). *Remote Sensing Data Acquisition and Analysis*. Scientific Press, Beijing, China.

Chapter 3. A ROBUST TECHNIQUE FOR FUSING MULTISOURCE SAR AND MS IMAGES[♣]

ABSTRACT

Synthetic aperture radar (SAR) imaging is independent of solar illumination and weather conditions, which makes it a particularly viable alternative, or complement, to traditional optical remote sensing techniques. Along with the technology advancement, the spatial resolution of SAR is becoming increasingly higher, which makes it possible for high resolution mapping purposes. However, significant problems exist in the interpretation of SAR images. Although image fusion presents an alternative to improve the interpretability of SAR images by fusing the colour information from low resolution multispectral (MS) images, few publications about fusing high resolution SAR and low resolution optical multispectral image can be found in recent literature. In this paper, a new fusion method, based on the integration of wavelet transform and IHS (Intensity, Hue, and Saturation) transform, is proposed for SAR and MS fusion to maintain the spectral content of the original MS image while retaining the spatial detail of the high-resolution SAR image. Three data sets are used to evaluate the proposed fusion method: two of them are airborne SAR images with MS images at different resolutions; the other is a Radarsat image with a Landsat TM image. The fusion results are analyzed visually and statistically.

[♣]This chapter has been submitted.
Hong G., Y. Zhang (2006). "A robust technique for fusing multisource SAR and MS images." *Submitted to Photogrammetric Engineering and Remote Sensing, September, 2006.*

Keywords: synthetic aperture radar, ASTER, SPOT, Landsat, image fusion, wavelet transform

3.1 Introduction

Synthetic aperture radar (SAR) is an active sensor, and its wavelength ranges from 1 millimeter to 1 meter, making it a particularly viable alternative, or complement, to traditional optical remote sensing techniques [Foody, 1988]. For example, SAR imaging is independent of solar illumination and weather conditions; it is not affected by rain, fog, hail, smoke and, most importantly, clouds; it can even penetrate some Earth's surfaces to return information about subsurface features because it has a long wavelength; and SAR instruments can measure both intensity and phase of the backscattered microwaves, resulting not only in a high sensitivity to texture, but also in three-dimensional capabilities [Crisp, 2006].

However, SAR images are difficult to interpret due to their special characteristics: the geometry and the spectral range of SAR are different from optical imagery, and they are different from how the human eye works. In addition, the reflectance of objects in the microwave range depends on the used frequency band and may significantly differ from the usual assumption of more or less diffuse reflection at the Earth's surface. Therefore, mapping staff such as photogrammetric operators often experience difficulties in interpreting SAR imagery for topographic mapping [Hellwich et al., 2001].

Image fusion presents a good alternative for increasing the interpretability of SAR images by integrating colour information from MS images. The colour information in

MS images represents the reflectance of solar energy from a target area, which is easier to interpret. However, the brightness of SAR intensity images is dependent upon the roughness and material contents of the targeted surface and the wavelength of the microwave, which is difficult to interpret but may contain useful information that cannot be found in MS images. Therefore, the fusion of SAR and MS images may contribute to better understanding of the objects of the target areas [Pohl and Van Genderen, 1998].

To date, numerous image fusion algorithms have been developed [e.g., Qiu, 1990; Chavez et al., 1991; Shettigara et al., 1992; Yocky, 1995; Zhou et al., 1998; Zhang, 1999; Hill et al., 1999; Ranchin et al., 2000]. Conventional fusion methods can be generally classified into four groups: classical Intensity-Hue-Saturation (IHS) transform, Principal Component Analysis (PCA), statistical and arithmetic combination, and the recently popular wavelet fusion [Zhang, 2002].

Wavelet transformation, originally a mathematical tool for signal processing, is now widely used in the field of image fusion. Recently, many image fusion methods based on wavelet transformation have been published [Yocky, 1995; Li et al., 1995; Yocky, 1996; Zhou et al., 1998; Núñez et al., 1999; Ranchin et al., 2000; Aiazzi et al., 2002]. The physical principal of wavelet used in image fusion is that wavelet can separate image into high frequency and low frequency components, the separated high frequency from the SAR can be injected into the low resolution multispectral image without changing its color. The objects appearing as high frequency in the SAR image, for example, small metallic objects, look like bright points; while they appear the same as other objects in the optical images, and thus they cannot be discriminated from other

objects easily. If the high frequency of those objects from SAR can be injected into a multispectral image, they can be easily recognized in the fused image.

High resolution orthorectified colour images from aerial photography or satellite are widely desired but often prohibitively expensive particularly over large areas, while monochromatic orthorectfied radar images at 1.25 meter resolution with corresponding horizontal accuracy are now available at relatively low cost over relatively large areas – for instance, the whole of Great Britain. It would be desirable for many applications to create a fused product from the radar orthorectified image and a suitable MS low resolution source [Mercer et al., 2005]. The objective of this paper is to propose an effective image fusion method to fuse a high spatial resolution SAR image with multisource low spatial resolution MS images and obtain a high spatial resolution colorful SAR image. The method itself is based on wavelet and IHS integrations, and the intuition of the fusion method is that the fusion result can maintain the spectral content of original MS image while retaining the spatial detail of the high-resolution SAR image. The justification of the propsed method is listed as follows: the fusion between MS and panchromatic images by only stand-alone wavelet transformation often produces poor image fusion results (artifacts problem) [Yocky, 1996; Aiazzi et al., 2006]. The IHS method is good at preserving the spatial characteristics, but strongly depends on the resemblance between the panchromatic image and the intensity of the MS image [Svab and Ostir, 2006]. To overcome the colour distortion and artifacts problems associated with stand-alone wavelet or IHS methods and to develop a reliable fusion method for SAR and MS fusion, the wavelet transform and IHS transform are integrated in this research. Because the substitution in IHS transform is limited to only

the intensity component, the integration of wavelet transform and IHS transform for SAR and MS fusion can be made simpler and faster. Results demonstrate that this integration can also better preserve color information.

Three data sets are used to evaluate the proposed fusion method: two are airborne SAR data and MS data at different resolutions; the other is a Radarsat image and a Landsat TM image. Successful results are achieved in the fusion of all the SAR images and MS images from a variety of sensors with significant spatial and spectral variations. The ratio of spatial resolution between SAR and MS images varies from 1 to 24 for the case of SAR and Landsat TM fusion, 1 to 16 for SPOT, and 1 to12 for ASTER; and the spectral variations of the test images range through visible, infrared and microwave. The improvements of the proposed method are demonstrated by visual, and statistical evaluations.

3.2 IHS, wavelet and the proposed fusion methods

3.2.1 IHS transform

Different transformations have been developed to transfer a colour image from the RGB space to the IHS space. A commonly used IHS transformation is based on a triangular colour model [Qiu, 1990]. The forward IHS transformation can be described as below:

$$I = \frac{1}{3} I', \quad I' = R + G + B \tag{3.1}$$

$$H = \frac{G - 3B}{I' - 3B}, \; S = \frac{I' - 3B}{I'}, \text{ when B is the minimum} \tag{3.2}$$

$$H = \frac{B-R}{I'-3R}+1,\ S = \frac{I'-3R}{I'}, \text{ when R is the minimum} \tag{3.3}$$

$$H = \frac{R-G}{I'-3G}+2,\ S = \frac{I'-3G}{I'}, \text{ when G is the minimum} \tag{3.4}$$

The corresponding inverse IHS transformation is:

$$\begin{cases} R = \frac{1}{3} I'(1 + 2S - 3SH) \\ G = \frac{1}{3} I'(1 - S + 3SH) \\ B = \frac{1}{3} I'(1 - S) \end{cases} \text{ when B is the minimum} \tag{3.5}$$

$$\begin{cases} R = \frac{1}{3} I'(1 - S) \\ G = \frac{1}{3} I'(1 + 5S - 3SH) \\ B = \frac{1}{3} I'(1 - 4S + 3SH) \end{cases} \text{when R is the minimum} \tag{3.6}$$

$$\begin{cases} R = \frac{1}{3} I'(1 - 7S + 3SH) \\ G = \frac{1}{3} I'(1 - S) \\ B = \frac{1}{3} I'(1 + 8S - 3SH) \end{cases} \text{ when G is the minimum} \tag{3.7}$$

3.2.2 Wavelet transform

The original concept and theory of a wavelet-based multi-resolution analysis comes from Mallat [Mallat, 1989]. Many researchers have applied this theory to different image fusions resulting in promising fusion results [Garguet-Duport et al., 1996; Yocky, 1996; Zhou et al., 1998; Ranchin et al., 2000; Aiazzi et al., 2002].

The discrete wavelet transform can be expressed by following equations: let $\left\{ s_{m,n}^{j+1}, m, n \in Z \right\}$ be a two-dimensional image at a resolution of j+1 with j being an integer. m and n are the dimensions of the image in row and column directions, which

belong to an integer set *Z*. The wavelet multi-resolution transform can then be expressed as [Zhu and Zhang 2000].

$$\begin{cases} s_{m,n}^{j} = \frac{1}{2}\sum_{k,l\in Z} s_{k,l}^{j+1} h_{k-2m} h_{l-2n} \\ d_{m,n}^{j1} = \frac{1}{2}\sum_{k,l\in Z} s_{k,l}^{j+1} h_{k-2m} g_{l-2n} \\ d_{m,n}^{j2} = \frac{1}{2}\sum_{k,l\in Z} s_{k,l}^{j+1} g_{k-2m} h_{l-2n} \\ d_{m,n}^{j3} = \frac{1}{2}\sum_{k,l\in Z} s_{k,l}^{j+1} g_{k-2m} g_{l-2n} \end{cases} \tag{3.8}$$

where s^j is an approximation image at a lower resolution j (LL in Figure 3.1). d^{j1}, d^{j2} and d^{j3} are three wavelet coefficients containing local spatial details (LH, HL, and HH in Figure 3.1). g_n is a high-pass filter bank, and h_n is a low-pass filter bank.

The reverse wavelet transform for reconstructing a high-resolution image is written as:

$$\begin{aligned} s_{m,n}^{j+1} = \frac{1}{2}\Big(&\sum_{k,l\in Z} s_{k,l}^{j} \tilde{h}_{2k-m} \tilde{h}_{2l-n} + \sum_{k,l\in Z} d_{k,l}^{j1} \tilde{h}_{2k-m} \tilde{g}_{2l-n} + \\ &\sum_{k,l\in Z} d_{k,l}^{j2} \tilde{g}_{2k-m} \tilde{h}_{2l-n} + \sum_{k,l\in Z} d_{k,l}^{j3} \tilde{g}_{2k-m} \tilde{g}_{2l-n}\Big) \end{aligned} \tag{3.9}$$

where $\tilde{g}_n$ and $\tilde{h}_n$ meet the following relationships:

$$\begin{cases} g_n = (-1)^{-1+n} h_{1-n} \\ \tilde{h}_n = h_{1-n} \\ \tilde{g}_n = g_{1-n} \end{cases} \tag{3.10}$$

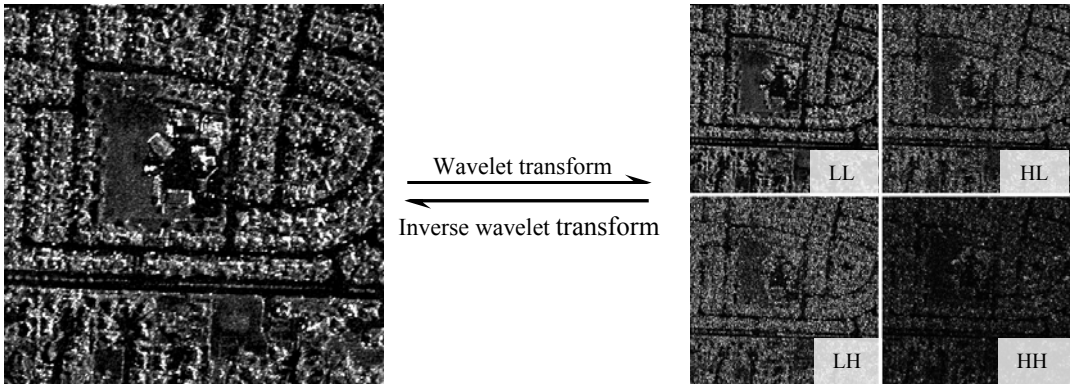

Figure 3.1. Illustration of wavelet transform

3.2.3 The proposed wavelet-IHS fusion method

The stand-alone IHS fusion method can usually integrate colour and spatial features smoothly. If the grey value distribution of the IHS intensity image is close enough to that of the panchromatic image, the IHS fusion method can also well preserve the color information. However, especially when the MS and panchromatic images from a SAR image and a low resolution MS image are fused, the grey value difference between the intensity image and the panchromatic image is obvious. This difference results in a significant colour distortion of the IHS fusion images. The colour distortion is especially significant when the MS bands 1, 2, and 3, like QuickBird and IKONOS, are fused for a natural colour composite [Zhang, 2002].

On the other hand, the stand-alone wavelet image fusion usually can better preserve color information than other conventional fusion methods, such as IHS, PCA, and band arithmetic combination, because the high resolution spatial information from a panchromatic image is injected into all three low resolution MS bands. However, the spatial detail from a panchromatic image is often different from that of a MS band having the same spatial resolution because of their spectral range difference. This difference may introduce colour distortion into the wavelet fusion results, and

sometimes it may make the integration between colour and spatial detail appear unnatural [Yocky, 1996].

To better utilize the advantages of the IHS and the wavelet fusion methods for the fusion of a SAR image and a MS image, and to overcome the shortcomings of the two methods, an IHS and wavelet integration fusion method is proposed. The concept and the process steps of this method are illustrated in Figure 3.2. In general, it uses the IHS transform to integrate the low resolution MS colour information with the high resolution SAR spatial detail information to achieve a smooth integration of colour and spatial features (part I of Figure 3.2). However, the wavelet transform is utilized to generate a new image (New Intensity in Figure 3.2) that has a high correlation with the intensity image and contains the spatial detail of the original SAR image (part II in Figure 3.2).

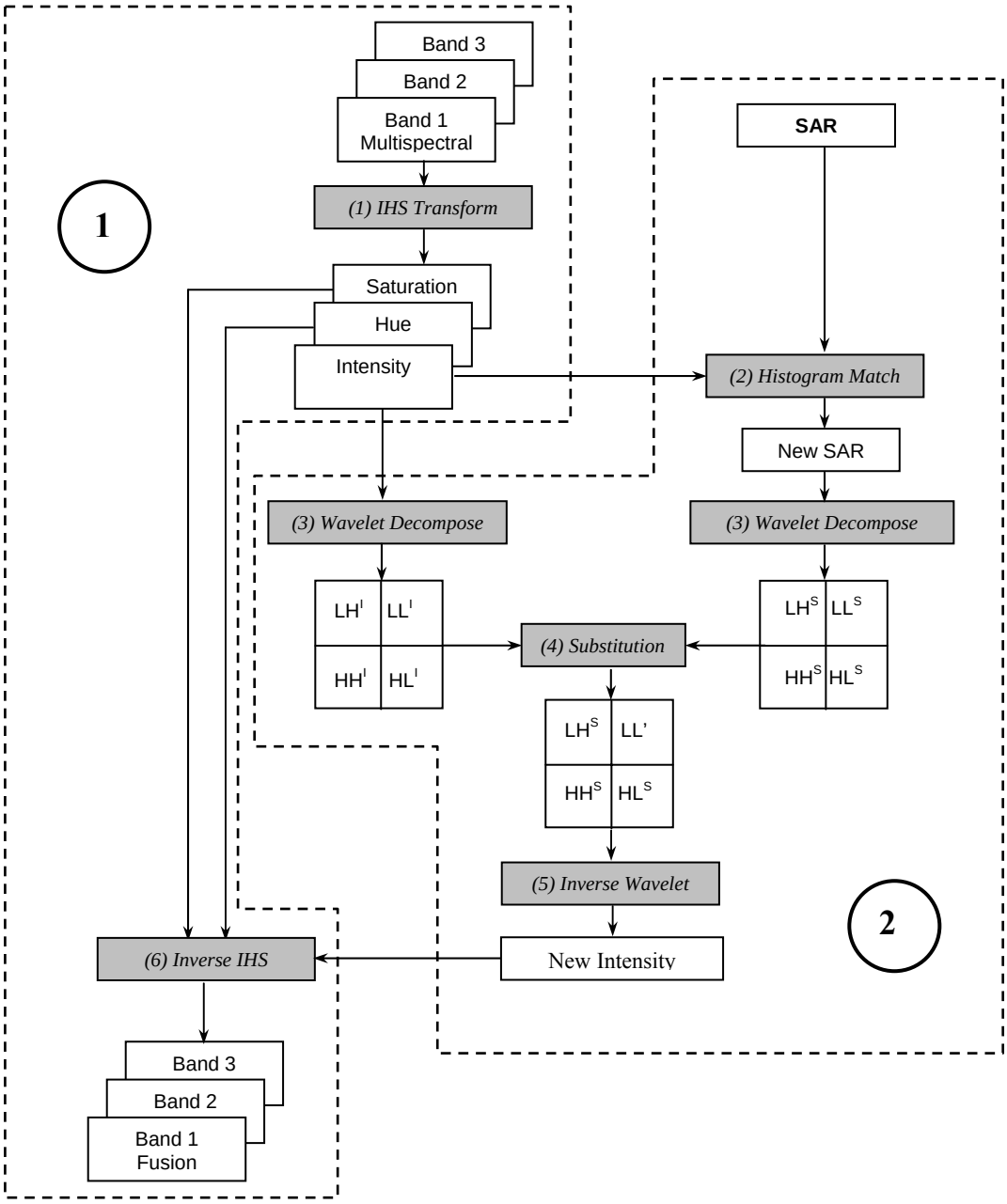

Figure 3.2. Processing flow of the proposed wavelet-IHS fusion method

As shown in Figure 3.2, the detailed steps of this integration fusion method are:

(1) Transforming the MS image into the IHS components (forward IHS transform).

(2) Applying a histogram match between the SAR data and the Intensity component (I), and obtaining a new SAR image (New SAR).

(3) Decomposing the new SAR image and the intensity component (I) into wavelet planes, respectively. The intensity image has the same pixel size as the SAR image.

(4) Replacing the approximation image of the SAR decomposition (LL^S) by that of the intensity decomposition (LL^I) to inject grey value information of the intensity image into the SAR image. To avoid an over injection of the intensity information, the LL^S is not completely, but partially, replaced by the LL^I; namely a new approximation image (LL') is first generated through a weighted combination of LL^S and LL^I, and then replaces the LL^S of the SAR decomposition. The combination could be implemented manually or automatically. The method for the weighted combination is described in Equations 3.11 and 3.12 below.

(5) Performing an inverse wavelet transform to obtain a new intensity image, which has similar grey value distribution to that of the intensity image of the IHS transform and contains the same spatial detail of the original SAR image.

(6) Transforming the new intensity together with the hue and saturation components back into RGB space (inverse IHS transform).

The triangular model of the IHS transform (Equations 3.1 through 3.7) is employed in this proposed IHS and wavelet integrated fusion. The method to generate the new approximation image LL', denoted as *c*, can be expressed as:

$$c = w_1 \times a + w_2 \times b, \tag{3.11}$$

where a and b are the approximation images LL^I and LL^S, respectively, and w_1 and w_2 are the corresponding weight coefficients, which are determined by:

$$w_1 = Corr(a/b) = \frac{\sum_{i=1}^{N}(a_i - \bar{a})(b_i - \bar{b})}{\sqrt{\sum_{i=1}^{N}(a_i - \bar{a})\sum_{i=1}^{N}(b_i - \bar{b})}}, \quad \text{with } w_1 + w_2 = 1 \tag{3.12}$$

where $\bar{a}$ and $\bar{b}$ are the means of a and b, and N is the total pixel number of the approximation images. w_1 and w_2 could certainly be set manually according to the operator's preference, whether high spectral information or high spatial information is required.

3.3 Experiment data and results

3.3.1 Experimental data sets

A variety of SAR and MS images from different sensors are used to evaluate the proposed wavelet-IHS fusion method. The resolution and spectral range of the image data used in this research are listed in Table 3.1.

Table 3.1. Sensor spectral range and resolution

Satellite sensor	Resolution (m)	Spectral range (μm)
SPOT (Band1~Band3)	20	0. 50 ~ 0. 89
SPOT (Simulated natural colour or SNC)	20	—
Landsat5(TM) (Band1~Band5, Band7)	28.5	0. 45~ 1. 75, 2. 08 ~ 2. 35
ASTER(Band1~Band3)	15	0.52 ~ 0.86
Ortho Rectified Star 3i	1.25m	X-band
Radarsat	12.5m	C-band (0.057m)

Data sets from three significantly different areas are used to evaluate the proposed fusion method: two data sets of Star-3i airborne SAR data (10,000 by 10,000 pixels each), covering two different areas, are fused with four different MS images respectively; one set (4096 by 4096 pixels) of Radarsat image is fused with Landsat TM image (band 7, band 4 and band 3).

STAR-3*i* is an X-band interferometric SAR (IFSAR) carried in a Learjet [Mercer and Schnick, 1999] and has been operated commercially by Intermap Technologies since 1997. The core products generated include a Digital Surface Model (DSM) and an Orthorectified Radar Image (ORI). ORI resolution was 2.5 meters but after a major upgrade it was reduced to 1.25 meters. In this study, the resolution of ORI is 1.25 meters.

Three image bands (including one near infrared band) of ASTER data has been used in this study. The resolution of those bands is 15m.

Original SPOT (band1, band2, band3) and simulated natural colour SPOT image (SNC SPOT, converted using Cal2 color transform) have been used in this study. The Cal2 color transform first accepts a reference image, such as a color aerial photograph, as a color reference image (CRI), which defines what "realistic" means; then it uses a Least Squares Estimation to determine the optimum parameter values that will match the multispectral image to CRI [Mercer et al., 2005]. The color transform is very useful for the data, such as SPOT and ASTER, which is short of one natural band. The three MS bands used in this instance, corresponding to SPOT bands 3, 2 and 1 are essentially in the Near IR, Visible Red and Visible Green parts of the spectrum. From a remote sensing perspective, this is well understood and has distinct advantages. However from

the perspective of a prospective user anticipating natural color products, this is a disadvantage.

Landsat TM (band 5, band 4, and band 3) has been fused with the Star 3i data, its resolution is 28.5m.

3.3.2 Experimental results

Figure 3.3 and Figure 3.4 show a sub-scene (1024 by 800 pixels) of the fused images from one of the two Star-3i SAR test areas (10,000 by 10,000 pixels each). Figure 3.5 shows a sub-scene (1024 by 1024 pixels) of the fused images from the Radarsat and Landsat TM fusion (4096 by 4096 pixels).

All the fusion results are produced by the proposed wavelet-IHS integration method, except for Figure 3.3 (e) and (f), which are fused by stand-alone IHS and wavelet methods, respectively, for comparison purpose. In Figure 3.3, (a) is the original Star-3i image, (b) is the SNC SPOT image converted by Cal2 color transform, (c) is the fusion result of Star-3i and SNC SPOT produced by the proposed method, (d) is the fusion result of Star-3i and SNC SPOT by using the IHS fusion method, (e) is the fusion result of the Star-3i and SNC SPOT by using the wavelet fusion method.

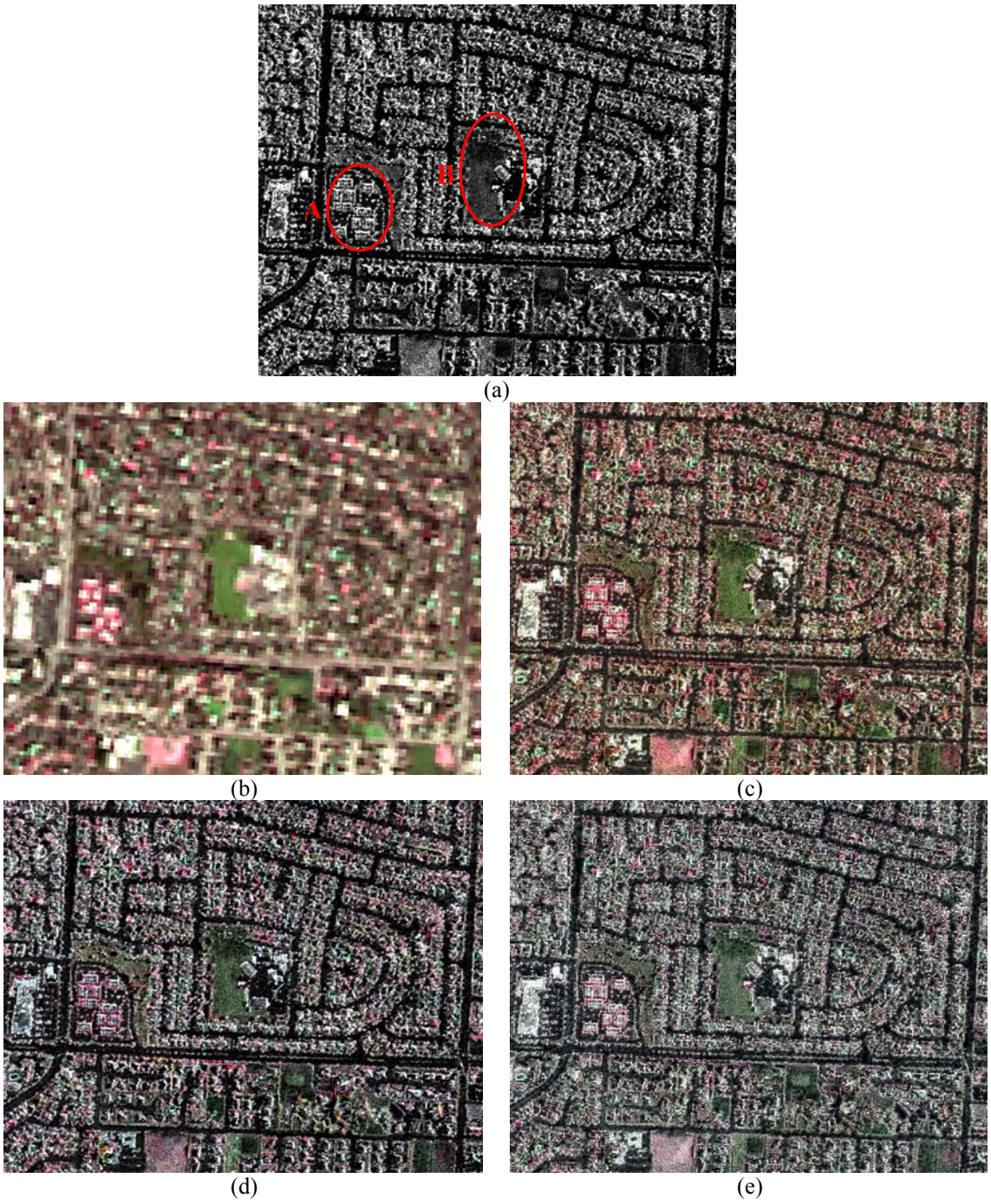

Figure 3.3. SAR, MS images and fusion results of different methods

(a) original Star-3i image, (b) SNC SPOT, (c) fusion result of the proposed wavelet-IHS method, (d) fusion result of stand-alone IHS method, (e) fusion result of stand-alone wavelet fusion method

Figure 3.4 shows the original MS images from different sensors (left column) and the corresponding fusion results of the proposed wavelet-IHS integration method (right column). The high resolution SAR used in the fusion is the same as Figure 3.3(a). In

Figure 3.4, (a) is the original SPOT bands 1, 2 and 3, (b) is the fusion result of the Star-3i with SPOT, (c) is ASTER image bands 1, 2 and 3, (d) is the fusion result of the Star-3i with ASTER, (e) is the Landsat TM image and (f) is the fusion result of the Star-3i with Landsat TM.

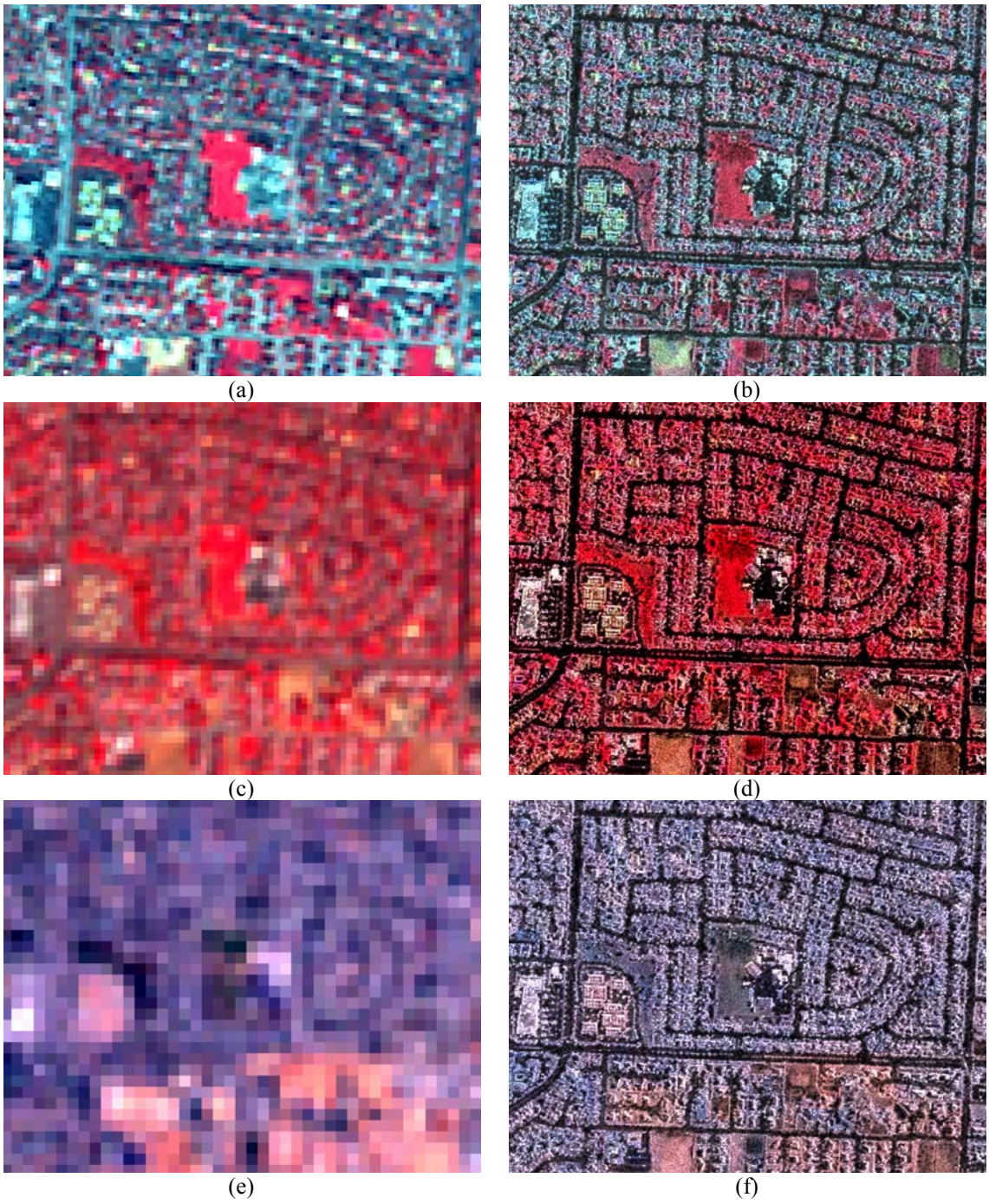

(a) (b) (c) (d) (e) (f)

Figure 3.4. MS images from different sensors as input (left column) and the fusion results of the proposed wavelet-IHS method (right column)

(a) SPOT bands 1, 2 and 3, (b) fusion result of SPOT and Star-3i (Fig. 3 (a)), (c) ASTER bands 1, 2, and 3, (d) fusion result of ASTER and Star-3i, (e) Landsat TM bands (f) fusion result of Landsat TM and Star-3i

In Figure 3.5, (a) is an original Radarsat fine beam amplitude image, (b) is an original Landsat TM and (c) is the fusion result of the Radarsat and Landsat TM of the proposed wavelet-IHS fusion method.

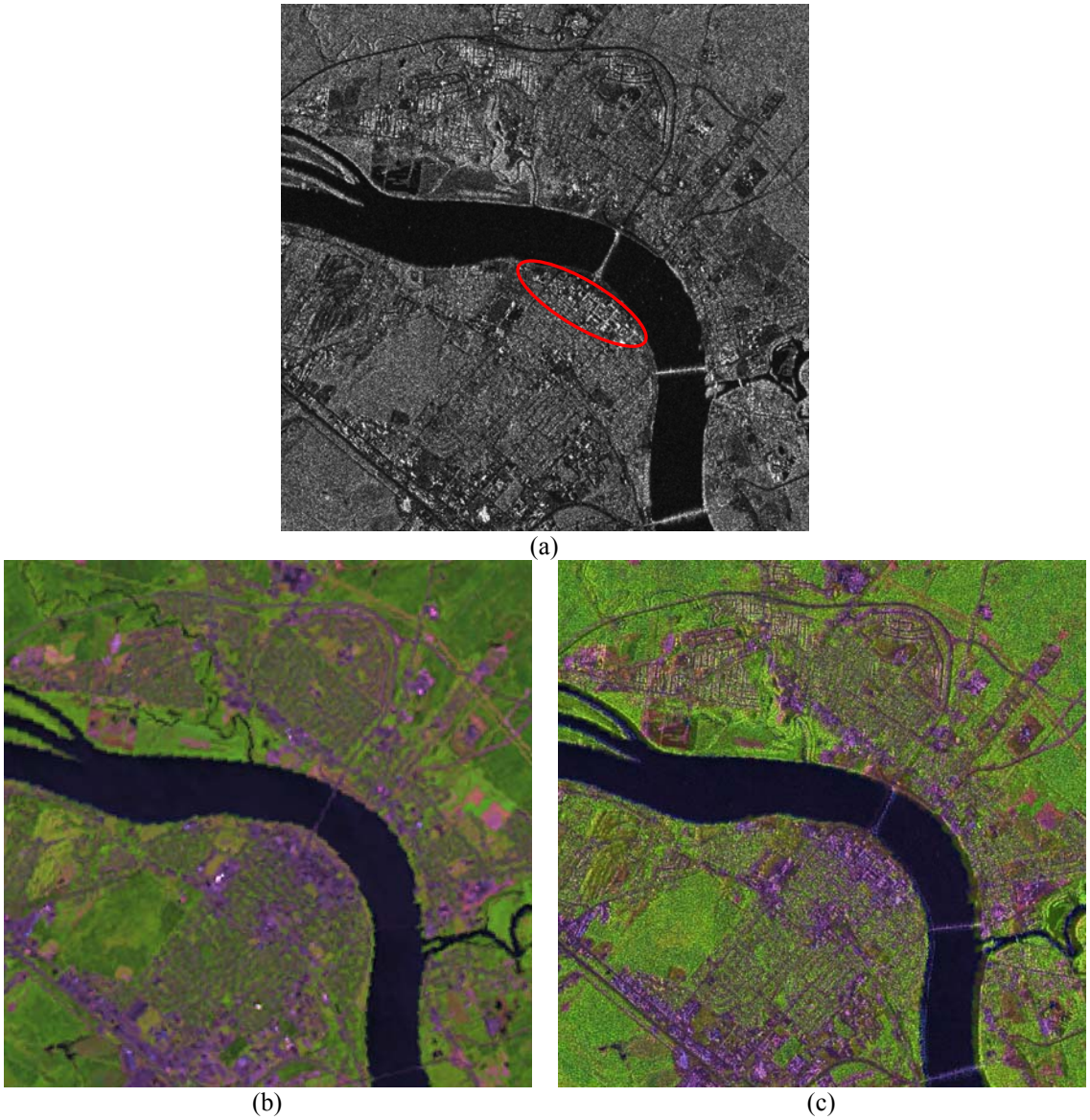

(a)

(b) (c)

Figure 3.5. Radarsat and TM fusion of the proposed wavelet-IHS fusion method
(a) Radarsat fine beam, (b) Landsat TM, (c) fusion result of Radarsat and Landsat TM

3.4 Accuracy analyses and comparison of the fusion results

3.4.1 Visual analysis

The fusion results (Figure 3.3 (c), Figure 3.4 (b), (d), (e) and Figure 3.5 (c)) show that the proposed fusion method can integrate the spatial information of the SAR image and color information of the original image into a single fusion image very well. The proposed method preserves the spatial information of the SAR data and the color information of the original MS image. The colors of the fusion results look close to those of the original MS images; and the fusion results look as detailed as the original SAR image. Compared to the original SAR data, the land cover types in the fusion results can be more easily and accurately interpreted.

Comparing the fusion results (Figure 3.3) indicates that the stand-alone IHS fusion method (Figure 3.3(d)) can integrate the spatial information of the SAR image into the fusion image very well; but obvious color distortion exists when compared with the original MS image (Figure 3.3(b)). The stand-alone wavelet fusion method can enhance the spatial information of the fusion result (Figure 3.3(e)), making the result look clearer than the original MS image, but severe color distortion is also introduced. The whole image looks gray because the SAR image is integrated equally into the individual bands of the MS image.

In Figures 3.3 and 3.4, one SAR image was fused with several MS images. Although a large difference between the spatial resolutions of the SAR and MS images exists, and the correlation between the SAR and MS images is very low, the spatial information of the SAR data can be incorporated into the MS images very well when the SAR image is fused with several MS images. In the MS image, a building is represented

by only a few pixels, making it difficult to be identified very well merely from those MS images. The building in the SAR image is also hard to judge because its appearance is different from traditional optical image. For example, in Figure 3.3(a), it is challenging for those inexperienced in interpreting SAR data to identify location A, but in the fusion images (Figure 3.3 (c), Figure 3.4 (b), (d), (e)), this building can be identified easily. Also for location B in Figure 3.3 (a), it is difficult to identify the type of land cover it is, while in fusion images ((Figure 3.3 (c), Figure 3.4 (b), (d), (e)), it is easily determined to be grass land. The grass land is especially apparent in Figure 3.3 (c), the fusion result of the SAR image and the natural composite of SNC SPOT image.

In Figure 3.5, one Radarsat image was fused with a TM image. The color of the fusion result is very close to the original MS image and the fusion image looks as clear as the SAR data. From this fusion result, it is easy to interpret the land cover. For example, it is easy to differentiate the road from the water. The backscatter of the road and water is very low in the SAR image; they looks similar without considering the context, while in the fusion result, they appear absolutely different. Also the dense built-up area (one sample circled in Figure 3.5 (a)), appears purple in the multispectral image, and appears bright in the SAR image; the fusion result can help people differentiate them from other types of land cover more easily.

3.4.2 Statistical analysis

Visual inspection is a straightforward method for appreciating the quality of a fusion method. However, a statistical comparison is necessary in order to evaluate precisely the performance of each fusion result. The correlation coefficient is often used

to evaluate the spectral resemblance of two images. The value of the correlation coefficient varies between -1 and +1, with zero indicating the absence of correlation. A value close to +1 means that two images are very similar, while a value close to -1 means that they are absolutely dissimilar (i.e. positive image vs. negative image) [Pradhan, 2005]. The correlation coefficient between the fused image and resampled multispectral image can reflect how much a fusion method is capable of improving the quality of the fused product with respect to that of the resampled multispectral image. For example, the microwave SAR image is not correlated closely with the optical multispectral image before image fusion; the correlation coefficient between them is very low. After image fusion, the correlation coefficient between fused image and resampled multispectral image is much higher than that between SAR and resampled multispectral image. From the comparison between pre- and post- fusion, it can be found the information has changed in the fused image.

Table 3.2 shows the correlation coefficients between the original Star-3i and the MS images. In this table, the correlation coefficients are very close to 0; some of them are minus, which means Star 3i is not correlated with the bands of those MS images. Actually, it can be verified from the point of spectral range: the Star 3i does not overlap with the bands of those MS images.

Table 3.2. Correlation coefficients between Star-3i SAR data and individual bands of different MS images

	Band R	**Band G**	**Band B**
SAR (ASTER case)	0.096	0.011	0.023
SAR (SPOT case)	-0.061	-0.059	-0.064
SAR (SNC SPOT case)	-0.079	-0.087	-0.070
SAR (TM case)	-0.059	-0.055	-0.038

Table 3.3 shows the correlation coefficients between the fusion results and the original MS images, all the fusion results are used the IHS and wavelet integration method except the indication cases. From those correlation coefficients, it can be found that fusion results are correlated with the original MS images, although the spatial information of the SAR data has been incorporated into it, unlike the correlation coefficients situation in Table 3.2. Because there exists such a large difference of spatial resolution between SAR data and MS data and the noncorrelation between SAR data and MS image, the correlation coefficients are not as high as for the optical images fusion which has small spatial resolution difference. For SNC SPOT data, the IHS method and the wavelet method have also been tested. The correlation coefficients of fusion results using the IHS fusion method and the wavelet fusion method are very low compared with the fusion result, which was applied by the proposed IHS and wavelet integration method. That means there exist higher color distortion in the fusion results processed by the IHS method and the wavelet method compared with the fusion result processed by the IHS and wavelet integration method.

Table 3.3. Correlation coefficients between individual bands of fusion results and original MS images

	Band R	**Band G**	**Band B**
ASTER	0.292	0.317	0.210
SPOT	0.313	0.205	0.068
SNC SPOT	0.127	0.226	0.246
SNC SPOT(IHS method)	-0.011	-0.020	-0.014
SNC SPOT(Wavelet method)	0.127	0.155	0.151
TM	0.176	0.054	-0.002

Table 3.4 shows the correlation coefficients between the fusion results and the original SAR data, all the fusion results are used the IHS and wavelet integration method except the indication cases. From those correlation coefficients, it can be found that fusion results are correlated with the original SAR, which means that the fusion

results have kept most of the spatial information of the original SAR (all correlation coefficients are greater than 0.70), unlike the bands of the original MS images which are not correlated with original SAR data (their correlation coefficients are almost 0). This fits with our fusion expectation: we want to integrate color information into high spatial resolution SAR data at the expense of the small loss of spatial detail. For SNC SPOT data, the IHS method and the wavelet method have also been tested. The correlation coefficients of the fusion results using the IHS fusion method and the wavelet fusion method are slightly high compared with the fusion result applied by the proposed wavelet and IHS integration method. Their results are very close to the high resolution SAR image, but they have very poor color information; while we want to integrate as much as possible color information into the SAR data; the image fusion method is used to find the balance between the spatial information and color information from the MS image. The fusion results of these two fusion methods could not achieve a good balance compared with the fusion results processed by the proposed the wavelet and IHS integration method.

Table 3.4. Correlation coefficients between original Star-3i SAR and individual bands of fusion results

	Band R	**Band G**	**Band B**
SAR (ASTER case)	0.828	0.811	0.847
SAR (SPOT case)	0.722	0.768	0.796
SAR (SNC SPOT case)	0.765	0.732	0.739
SAR (TM case)	0.769	0.803	0.795
SAR (SNC SPOT case) (IHS method)	0.989	0.987	0.995
SAR (SNC SPOT case) (wavelet method)	0.929	0.908	0.905

In the case of the Radarast image and the TM image fusion, Table 3.5 shows the correlation coefficients between the Radarsat image and the original Landsat TM data. From those correlation coefficients, it can be found that the original SAR data is slightly correlated with the Landsat TM because here TM band combination is band 7, band 4

and band 3. Compared with other TM bands, the band 7 wavelength is longer; it is very close to wavelength of SAR data, so there exists fairly high correlation coefficient between band 7 and SAR data.

Table 3.5. Correlation coefficients between Radarsat data and individual bands of Landsat TM

	Band R	**Band G**	**Band B**
Radarsat	0.104	0.155	0.004

Table 3.6 shows the correlation coefficients between the fusion result obtained by the proposed fusion method and the original Landsat TM data. We can see that the correlation coefficients between the fusion result and the original Landsat TM are much bigger than those between the original SAR data and the original Landsat TM data, although there is more high resolution spatial information of the SAR data incorporated into the fusion result. Those correlation coefficients are so high, it can also be judged from visual point: fusion result looks very similar to the original Landsat image.

Table 3.6. Correlation coefficients between the fusion result obtained by the proposed fusion method and TM data

	Band R	**Band G**	**Band B**
TM	0.527	0.620	0.549

Table 3.7 shows the correlation coefficients between the fusion result obtained by the proposed fusion method and the original Radarsat data. From those correlation coefficients, the fusion result is also correlated with the original Radarsat image; that means most of the high resolution information of the SAR has been retained (all of the correlation coefficients are greater than 0.6).

Table 3.7. Correlation coefficient between the fusion result obtained by the proposed fusion method and Radarsat data

	Band R	**Band G**	**Band B**
Radarsat	0.623	0.622	0.684

For statistical analysis, it is hard to define the term "sufficient correlation coefficients". We can not say a correlation coefficient of 0.70 is sufficient, while a coefficient of 0.65 is not sufficient, because this value could be different for different images. In this statistical analysis, we evaluate a fusion result by referring to the correlation coefficient between original SAR data and original MS data. The improvement caused by the fusion method could be inferred from those correlation coefficient comparisons. Also, there are few publications investigating the image fusion method related to the high resolution SAR image and the optical MS image; even there are few publications, they only list some fusion results, no further quantitative evaluation of the fusion result is undertaken. Thus, the quantitative evaluation of the fusion result of those data is very rare. This is also a good subject for further research.

3.5 Conclusion

This paper has proposed a new fusion method based on the integration of wavelet transform and IHS transform. The IHS method is good at preserving the spatial characteristics, but is strongly dependent on the resemblance between the panchromatic image and the intensity of the MS image (Svab and Ostir, 2006). Simply using the IHS method to fuse the SAR data and the MS image cannot get a good fusion result, because SAR image is low correlated with the optical MS images. When the wavelet transform is integrated into the IHS transform, the problem is to maintain the low frequency of the

intensity and low frequency of SAR data correlated. This integration makes fusion process simpler and faster. This integration can also better preserve color information. The fusion method can also fuse the MS image and the panchromatic image with arbitrary spatial resolutions.

This paper has also demonstrated the robustness of this method in fusing all kinds of multisource data with the SAR data: two data sets (10,000 by 10,000 pixels) of Star-3i, ASTER, SPOT, Landsat TM, and one data set (4096 by 4096 pixels) of Radarsat and TM have been used to evaluate this fusion method. The spectral range used in this evaluation has related to not only visible bands and infra bands but also microwave bands. The largest spatial resolution ratio between SAR data and MS data is 1:24. For those data that lack a blue band, a natural image is simulated by using a natural image as the reference image. Using color transformed data to fuse with high resolution SAR data, a fusion result, which has similar color to the color transformed MS image, can be obtained. This color transform fusion test has been applied to SPOT data and ASTER data, and the SPOT result has been listed in the Figure 3.3 (b). The ASTER result is also very good; because of space limitations, not all the fusion results are listed. The successful fusion results have been achieved for all those experimental data. Visual inspection and statistical analysis have been applied in evaluating the fusion results. Except for SAR data fusion with MS data, the fusion between optical images has also been tested; the good fusion results have been obtained and published in Hong and Zhang [2003]. To date, this fusion method has been applied to all available data sets, and satisfactory fusion results of all these data sets have been achieved.

ACKNOWLEDGEMENTS

The authors would like to thank the GEOIDE (GEOmatics for Informed DEcisions) Network of Centres of Excellence of Canada for their funding support to this research and Intermap Technologies Corp. for data support. We thank Dan Edwards and Joel Maduck of Intermap for preparing the Star-3i SAR and corresponding MS images.

REFERENCES

Aiazzi, B., L. Alparone, S. Baroni, and A. Garzelli (2002). "Context-Driven Fusion of Spatial and Spectral Resolution Images Based on Oversampled Multiresolution Analysis." *IEEE Transaction on Geoscience and Remote Sensing,* Vol. 40, No. 10, pp. 2300-2312.

Aiazzi, B., L. Alparone, S. Baronti, A. Garzelli, and M. Selva (2006). "MTF-tailored Multiscale Fusion of High-resolution MS and Pan Imagery". *Photogrametric Engineering and Remote Sensing*, Vol. 72, No. 5, pp. 591-596.

Chavez, P.S., S.C. Slides, and J.A. Anderson (1991). "Comparison of Three Different Methods to Merge Multiresolution and Multispectral Data: Landsat TM and SPOT panchromatic." *Photogrammetric Engineering and Remote Sensing,* Vol. 57, No. 3, pp. 295-303.

Crisp (2006). "What distinguishes SAR from hi-res optical imagery?" Available online at: www.crisp.nus.edu.sg/sar/sar.html (accessed on July 7, 2006).

Foody, G.M. (1988). "Crop classification from airborne synthetic aperture radar data." *International Journal of Remote Sensing*, Vol. 9, pp. 655–668.

Garguet-Duport, B., J. Girel, J.M. Chassery, and G. Pautou (1996). "The use of multiresolution analysis and wavelets transform for merging SPOT panchromatic and multispectral image data." *Photogrammetric Engineering and Remote Sensing*, Vol. 62, No. 9, pp. 1057-1066.

Hellwich, O., C. Heipke, and B. Wessel (2001). "Sensor and Data Fusion Contest: Information for mapping from airborne SAR and optical imagery." *Geoscience and Remote Sensing Symposium*, 2001. IGARSS '01. IEEE 2001. pp. 2793-2795

Hill, J., C. Diemer, O. Stöver, and Th. Udelhoven (1999). "A local correlation approach for the fusion of remote sensing data with different spatial resolutions in forestry applications." *International Archives of Photogrammetry and Remote Sensing*, Vol. 32, Part 7-4-3 W6, Valladolid, Spain, 1999.

Hong, G. and Y. Zhang (2003). "High resolution image fusion based on wavelet and IHS transformations." *Proceedings of the IEEE/ISPRS joint Workshop on "Remote Sensing and Data Fusion over Urban Areas",* Berlin, Germany, 22-23 May 2003, pp. 99 - 104.

Li, H., B.S. Manjunath, and S. K. Mitra (1995). "Multisensor image fusion using the wavelet transform." *Graph. Models Image Process*. Vol. 57, No. 3, pp. 235–245.

Mallat, S.G. (1989) "A theory for multiresolution signal decomposition: The wavelet representation." *IEEE Transactions on Pattern Analysis and Machine Intelligence,* Vol. 11, No. 7, pp. 674-693.

Mercer, J.B. and S. Schnick (1999) "Comparison of DEMs from STAR-3i Interferometric SAR and Scanning Laser." *Proceedings of the Joint Workshop of ISPRS III/5 and III/2*, La Jolla, November, 1999.

Mercer, B., D. Edwards, G. Hong, Y. Zhang, and J. Maduck. (2005). "Fusion of inSAR high resolution imagery and low resolution multi-spectral optical Imagery." *ISPRS Hannover Workshop, 2005*.

Nuñez, J., X. Otazu, O. Fors, A. Prades, V. Palà and R. Arbiol (1999). "Multiresolution-based image fusion with additive wavelet decomposition." *IEEE Transactions on Geosciences and Remote Sensing,* Vol. 37, No. 3, pp.1204-1211.

Piella, G. (2002). "A General Framework for Multiresolution Image Fusion: from Pixels to Regions". *Research Report PNA-R0211*, CWI, Amsterdam.

Pohl, C., J.L. Van Genderen (1998). "Multisensor image fusion in remote sensing: concepts, methods, and applications." *International Journal of Remote Sensing,* Vol. 19, No. 5, pp.823-854.

Pradhan, P. (2005). *Multiresolution based, multisenor, multispectral image fusion*. Ph.D dissertation, Department of Electrical and Computer Engineering, Mississippi State University, Mississippi, Mississippi State, USA, 191 pp.

Qiu, Z.C. (1990). "The study on the remote sensing data fusion." *Acta Geodaetica et Cartographica Sinica*, Vol. 19, No. 4, pp.290-296.

Ranchin, T., L. Wald, and M. Mangolini (1996). "The ARSIS method: A general solution for improving special resolution of images by the means of sensor fusion." *Proceedings of the First Conference Fusion of Earth Data: Merging Point Measurements, Raster Maps and Remotely Sensed Images*, Cannes, France, 06-08 February 1996, pp. 53-58.

Ranchin, T., L. Wald (2000) "Fusion of High Spatial and Spectral Resolution images: The ARSIS Concept and Its Implementation." *Photogrammetric Engineering and Remote Sensing,* Vol. 66, No. 1, pp. 49-61.

Shettigara, V.K. (1992). "A generalized component substitution technique for spatial enhancement of multispectral images using a higher resolution data set." *Photogrammetric Engineering and Remote Sensing,* Vol. 58, No. 5, pp. 561-567.

Svab, A and K. Ostir (2006). "High-resolution image fusion: methods to preserve spectral and spatial resolution." *Photogrammetric Engineering and Remote Sensing*, Vol. 72, No. 5, pp. 565-572.

Wald, L., T. Ranchin, and M. Mangolini (1997). "Fusion of satellite images of different spatial resolutions: assessing the quality of resulting images." *Photogrammetric Engineering and Remote Sensing,* Vol. 63, No. 6, pp. 691-699.

Yocky, D.A. (1995). "Image merging and data fusion using the discrete two-dimensional wavelet transform." *J. Opt. Soc. Am. A.,* Vol. 12, No. 9, pp. 1834-1841.

Yocky, D.A. (1996). "Multiresolution wavelet decomposition image merger of Landsat Thematic Mapper and SPOT panchromatic data." *Photogrammetric Engineering and Remote sensing*, Vol. 62, No. 3, pp. 295-303.

Zhang, Y. (1999). "A new merging method and its spectral and spatial effects." *International Journal of Remote Sensing*, Vol. 20, No. 10, pp. 2003-2014.

Zhang, Y. (2002). "Problems in the fusion of commercial high-resolution satellites images as well as LANDSAT 7 images and initial solutions." Proceedings of the ISPRS, CIG, and SDH Joint International Symposium on Geospatial Theory, Processing and Applications, 9-12 July 2002, Ottawa, Canada, unpaginated CD-ROM.

Zhou, J., D.L. Civco, and J.A. Silander (1998). "A wavelet transform method to merge Landsat TM and SPOT panchromatic data." *International Journal of Remote Sensing,* Vol. 19, No. 4, pp. 743-757.

Zhu, S.L., Z.M. Zhang (2000). *Remote Sensing Data Acquisition and Analysis*. Scientific Press, Beijing, China.

Chapter 4. COMPARISON AND IMPROVEMENT OF WAVELET-BASED IMAGE FUSION[♣]

ABSTRACT

The wavelets used in image fusion can be categorized into three general classes: orthogonal, biorthogonal, and nonorthogonal. Although these wavelets share some common properties, each wavelet also has a unique image decomposition and reconstruction characteristic that leads to different fusion results. This paper focuses on the comparison of the image fusion methods that utilize the wavelet of the above three general classes, and theoretically analyzes the factors that lead to different fusion results. Normally, when a wavelet transformation alone is used for image fusion, the fusion result is not good. However, if a wavelet transform and a traditional fusion method, such as an IHS transform or a PCA transform, are integrated, better fusion results may be achieved. Therefore, this paper also discusses methods to improve wavelet-based fusion by integrating an IHS or a PCA transform. Because the substitution in the IHS transform or the PCA transform is limited to only one component, the integration of the wavelet transform with the IHS or PCA to improve or modify the component, and the use of IHS or PCA transform to fuse the image can make the fusion process simpler and faster. This integration can also better preserve color information. IKONOS and QuickBird image data are used to evaluate the seven kinds of wavelet fusion methods (orthogonal wavelet

---

[♣] This chapter has been accepted for publication in the [*International Journal of Remote Sensing*]

Hong G., Y. Zhang (2007). "Comparison and improvement of wavelet-based image fusion." *Submitted to International Journal of Remote Sensing, in press, 2007.*

fusion with decimation, orthogonal wavelet fusion without decimation, biorthogonal wavelet fusion with decimation, biorthogonal wavelet fusion without decimation, wavelet fusion based on the "à trous", wavelet and IHS transformation integration, and wavelet and PCA transformation integration). The fusion results are compared graphically, visually, and statistically, and show that wavelet-integrated methods can improve the fusion result, reduce the ringing or aliasing effects to some extent, and make the whole image smoother. Comparisons of the final results also show that the final result is affected by the type of wavelets (orthogonal, birorthogonal, and nonorthogonal), decimation or undecimation, and wavelet decomposition levels.

Keywords: image fusion, wavelet, multispectral, panchromatic image, IKONOS

4.1 Introduction

Image fusion is a technique used to integrate a high-resolution panchromatic image with a low-resolution multispectral image to produce a high resolution multispectral image, which contains both the high-resolution spatial information of the panchromatic image and the color information of the multispectral image. Although an increasing number of high-resolution images are available along with sensor technology development, image fusion is still a popular and important method to interpret the image data for obtaining a more suitable image for a variety of applications, such as visual interpretation, digital classification, etc. From studying existing image fusion techniques and applications, Pohl and Genderen [1998] concluded that image fusion can provide the following functions:

(1) sharpen images;

(2) improve geometric corrections;

(3) provide stereo-viewing capabilities for stereophotogrammetry;

(4) enhance certain features not visible in either of the single data alone;

(5) complement data sets for improved classification;

(6) detect changes using multitemporal data;

(7) substitute missing information (e.g., clouds-VIR, shadows-SAR) in one image with signals from another sensor image;

(8) replace defective data.

Many research papers have reported problems of existing fusion techniques. The most significant problem is color distortion. To reduce the color distortion and improve the fusion quality, a wide variety of strategies has been developed, each specific to a particular fusion technique or image set [Zhang, 2004]. Compared with the traditional fusion methods, such as intensity, hue, and saturation (IHS), principal component analysis (PCA), brovey transform etc., wavelet is a new fusion method. It is a mathematical tool initially designed for signal processing. Since it provides multiresolution and multiscale analysis functions, image fusion can be implemented in the wavelet transform domain. This characteristic cannot be replaced by some traditional fusion methods. A number of papers that discuss image fusion based on wavelet transform have been published in recent years [Yocky, 1995; Li et al., 1995; Yocky, 1996; Garguet-Duport et al., 1996; Zhou et al., 1998; Ranchin and Wald., 2000]. There are also papers published about wavelet integration with other fusion methods. Nunez *et al.* [1999] presented a multiresolution-based image fusion method which integrated IHS

with additive wavelet decomposition. Tseng et al [2001] used a combination of PCA and wavelet based sharpening methods. King and Wang [2001] introduced a wavelet based sharpening method that uses IHS transformation and biorthogonal wavelet decomposition. Chibani and Houacine [2002] described the joint use of IHS transform and redundant wavelet decomposition for fusing the multispectral image and panchromatic image. Hong and Zhang [2003] integrated IHS and wavelet to fuse Quickbird images and IKONOS images, and obtained promising results. Gonzalez-Audicana et al. [2004] proposed the wavelet-based fusion method by integrating wavelet with IHS and PCA, respectively.

In recent years, several studies have compared different wavelet based fusion techniques. Aiazzi et al. [2002] compared undecimated discrete wavelet transform with a generalized Laplacian pyramid in fusing multispectral with high resolution panchromatic images. Chiabani and Amrane [2003] compared a redundant wavelet with an orthogonal wavelet decomposition. Gonzalez-Audicana et al. [2004] proposed IHS and PCA integrated with wavelet respectively and compared the results with a decimated and an undecimated wavelet-based fusion method by testing a SPOT 4 XI image. Pajares and De La Cruz [2004] introduced a wavelet-based image fusion tutorial based on three previous works [Li et al., 1995; Zhang and Blum, 1999; Ranchin and Wald, 2000]. Gonzalez-Audicana et al. [2005] compared Mallat's and "à trous" discrete wavelet transforms by testing a degraded IKONOS image.

From the above literature, the wavelets that are used in image fusion can generally be categorized into three different types: orthogonal, biorthogonal, and nonorthogonal. This paper focuses on these three wavelets and compares their fusion results; at the same

time, two improvement methods (wavelet-integrated methods) are also introduced. This paper also provides a clear overview of some important factors that need to be considered in the wavelet fusion process, namely, wavelet selection, decimation or undecimation, and the wavelet decomposition level selection.

The rest of this paper is organized as follows: a general description of wavelet theory used in the image fusion is given in section 4.2; section 4.3 introduces wavelet-based and wavelet-integrated fusion algorithms; section 4.4 contains experimental results; section 4.5 provides an accuracy analysis and comparison of the fusion results; and the conclusion is provided in the final section.

4.2 Wavelet used in the image fusion

4.2.1 Basic wavelet transform theory

In wavelet transformation, the basis functions are a set of dilated and translated scaling functions:

$$\varphi_{j,k}(n) = 2^{j/2}\varphi(2^j n - k) \tag{4.1}$$

and a set of dilated and translated wavelet functions:

$$\psi_{j,k}(n) = 2^{j/2}\psi(2^j n - k) \tag{4.2}$$

where $\varphi(n)$ and $\psi(n)$ are the scaling function and the mother wavelet function respectively.

One property that the basis function must satisfy is that both the scaling function and the wavelet function at level j can be expressed as a linear combination of the scaling functions at the next level j-1:

$$\varphi_{j,k}(n) = \sum_m h(m-2k)\varphi_{j-1,m}(n) \tag{4.3}$$

and

$$\psi_{j,k}(n) = \sum_m g(m-2k)\varphi_{j-1,m}(n) \tag{4.4}$$

where h(m) and g(m) are called the scaling filter and the wavelet filter respectively.

For any continuous function, it can be represented by the following expansion, defined as a given scaling function and its wavelet derivatives [Burrus et al., 1998]:

$$f(n) = \sum_k c_{j_0}(k)\varphi_{j_0,k}(n) + \sum_{j=j0}^{\infty}\sum_k d_j(k)\psi_{j,k}(n) \tag{4.5}$$

The Discrete Wavelet Transform (DWT) can be expressed as follows:

$$c_j(k) = \sum_n c_{j-1}(n)h^*(n-2k) \tag{4.6}$$

$$d_j(k) = \sum_n c_{j-1}(n)g^*(n-2k) \tag{4.7}$$

the scaling filter $h^*(n)$ is a low pass filter extracting the approximation coefficients, $c_j(k)$ with $c_0(n) = f(n)$, while the wavelet filter $g^*(n)$ is a high-pass filter extracting the detail coefficients $d_j(k)$. The coefficients are downsampled (i.e. only every other coefficient is taken).

The reconstruction formula is given by:

$$c_j(k) = \sum_n (c_{j-1}(n)h^*(n-2k) + d_{j-1}(n)g^*(n-2k)) \tag{4.8}$$

Generally, discrete wavelet is introduced using the method of multi-resolution analysis. Let $L^2(R)$ be the Hilbert space of functions, a multiresolution analysis (MRA) of $L^2(R)$ is a sequence of closed subspaces V_j, $j \in Z$ (Z is the set of integers), of $L^2(R)$ satisfying the following six properties [Mallat, 1989]:

(1) The subspace are nested: $V_j \subset V_{j-1} \quad \forall j \in Z$

(2) Separation: $\cap_{j \in Z} V_j = \{0\}$

(3) The union of the subspace generate $L^2(R)$: $\overline{\cup_{j \in Z} V_j} = L^2(R)$

(4) Scale invariance: $f(t) \in V_j \Leftrightarrow f(2t) \in V_{j-1} \quad \forall j \in Z$

(5) Shift invariance: $f(t) \in V_0 \Leftrightarrow f(t-k) \in V_0 \quad \forall k \in Z$

(6) $\exists \varphi \in V_0$, the scaling function, so that $\{\varphi(2^{-j/2} - k) | k \in Z\}$ is a Riesz basis of V_0.

There is also a related sequence of wavelet subspaces W_j of $L^2(R)$, $\forall j \in Z$, W_j is the orthogonal complement of V_j in V_{j-1}. Then, $V_{j-1} = V_j \oplus W_j$, where $\oplus$ is the direct sum.

The situation discussed above concerns a one-dimension situation; for two-dimension, the scaling function is defined as:

$$\Phi(x, y) = \varphi(x)\varphi(y) \tag{4.9}$$

vertical wavelet:

$$\Psi^1(x, y) = \varphi(x)\psi(y) \tag{4.10}$$

horizontal wavelet:

$$\Psi^2(x,y) = \psi(x)\varphi(y) \tag{4.11}$$

diagonal wavelet:

$$\Psi^3(x,y) = \psi(x)\psi(y) \tag{4.12}$$

$\Phi(x,\ y)$ can be thought as 2-D scaling function, $\Psi^1(x,\ y)$, $\Psi^2(x,\ y)$, $\Psi^3(x,\ y)$ are the three 2-D wavelet functions.

4.2.2 Different wavelets used in image fusion

4.2.2.1 Orthogonal wavelet

The dilations and translations of the scaling function $\{\varphi_{j,k}(x)\}$ constitute a basis for V_j and, similarly, $\{\psi_{j,k}(x)\}$ for W_j, if the $\varphi_{j,k}(x)$ and $\psi_{j,k}(x)$ are orthonormal, they include the following properties [Starck et al., 1998]:

$$V_j \perp W_j \tag{4.13}$$

$$\left\langle \varphi_{j,l}, \varphi_{j,l'} \right\rangle = \delta_{l,l'}, \quad \left\langle \psi_{j,l}, \psi_{j',l'} \right\rangle = \delta_{j,j'}\delta_{l,l'}, \quad \left\langle \varphi_{j,l}, \psi_{j,l'} \right\rangle = 0 \tag{4.14}$$

The orthogonal property puts a strong limitation on the construction of wavelets. For example, it is hard to find any wavelets that are compactly supported, symmetric and orthogonal.

4.2.2.2 Biorthogonal wavelet

If the orthogonal condition is relaxed to biorthogonal conditions, wavelets with some special properties that are not possible with orthogonal wavelets can be obtained. In the biorthogonal transform, there are two multiresolution analyses, a primal and a dual [Strang and Nguyen, 1996]:

Primal: $V_j, W_j, \varphi_{j,k}, \psi_{j,k}$

Dual: $\widetilde{V}_j, \widetilde{W}_j, \widetilde{\varphi}_{j,k}, \widetilde{\psi}_{j,k}$

The dilations and translations of the scaling function $\{\widetilde{\varphi}_{j,k}(x)\}$ constitute a basis for $\widetilde{V}_j$ and similarly, $\{\widetilde{\psi}_{j,k}(x)\}$ for $\widetilde{W}_j$, the biorthogonality conditions imply:

$$\widetilde{V}_j \perp W_j \quad , V_j \perp \widetilde{W}_j, \quad W_j \perp \widetilde{W}_{j'} \qquad j \neq j' \tag{4.15}$$

$$\left\langle \widetilde{\varphi}_{j,l}, \varphi_{j,l'} \right\rangle = \delta_{l,l'}, \left\langle \widetilde{\psi}_{j,l}, \psi_{j',l'} \right\rangle = \delta_{j,j'}\delta_{l,l'}, \left\langle \widetilde{\psi}_{j,l}, \varphi_{j\ ,l'} \right\rangle = 0, \left\langle \widetilde{\varphi}_{j,l}, \psi_{j\ ,l'} \right\rangle = 0 \tag{4.16}$$

For biorthogonal transform, perfect reconstruction is available. Orthogonal wavelets give orthogonal matrices and unitary transforms; biorthogonal wavelets give invertible matrices and perfect reconstruction. For the biorthogonal wavelet filter, the low pass and the high pass filters do not have the same length. The low pass filter is always symmetric, while the high pass filter could be either symmetric or anti-symmetric.

4.2.2.3 à trous (nonorthogonal wavelet)

"à trous" (with holes) is a kind of nonorthogonal wavelet that is different from orthogonal and biorthogonal. It is a "stationary" or redundant transform, i.e., decimation is not implemented during the process of wavelet transform, while orthogonal or biothorgonal wavelet can be carried out using either decimation or undecimation mode. Compared with other wavelet-based fusion methods, this method is relatively easy to implement. The limitation is that it uses a large amount of computer memory.

4.3 Wavelet based image fusion method

4.3.1 Additive wavelet-based image fusion method

Figure 4.1 shows the work flow of the wavelet-based fusion method. In the figure, the different numbers refers to different processes: (1) histogram match, (2) wavelet decomposition, (3) details combination from different image by adding, and (4) inverse wavelet transform.

The whole process can be divided into four steps:

(1) Assuming the panchromatic image and multispectral image has been registered, apply histogram match process between panchromatic image and different bands of the multispectral image respectively, and obtain three new panchromatic images (PAN_R, PAN_G, and PAN_B).

(2) Use the wavelet transform to decompose new panchromatic images and different bands of multispectral image twice, respectively.

(3) Add the detail images of the decomposed panchromatic images at different levels to the corresponding details of different bands in the multispectral image and get the new details component in the different bands of multispectral image.

(4) Perform an inverse wavelet transform on the bands of multispectral images, respectively, and obtain the fused image.

Additive wavelet-based method using "à trous" algorithm is similar to the above steps. The only difference is that "à trous" has only one detail plane while the above has three details.

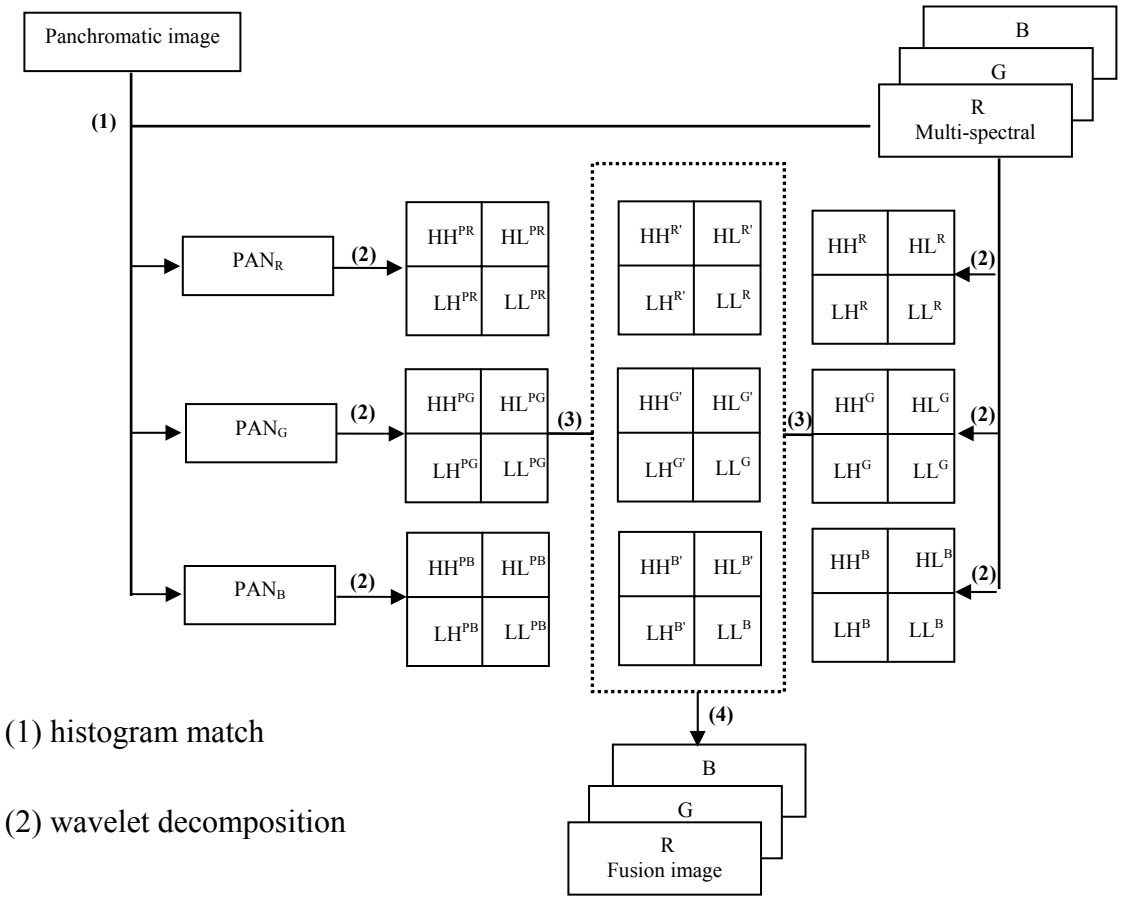

Figure 4.1. Work flow of the wavelet-based fusion method

4.3.2 Integration of substitution method with wavelet method

Figure 4.2 shows the work flow of the integration of wavelet-based and substitution method. Numbers 1 and 2 are used to divide the whole process into two parts: 1 refers to substitution fusion method, 2 refers to the wavelet-based fusion method.

The whole process consists of the following steps:

(1) Transform the multispectral image into the IHS or PCA components.

(2) Apply a histogram match between panchromatic image and Intensity component or PC1, and obtain new panchromatic image (New Pan).

(3) Decompose the histogram-matched panchromatic image and Intensity component or PC1 to wavelet planes respectively.

(4) Replace the LL^{P} in the panchromatic decomposition with the LL^{I} of the intensity or PC1 decomposition, add the detail images in the panchromatic decomposition to the corresponding detail image of the intensity or PC1 decomposition and obtain LL^{I}, $LH^{P'}$, $HH^{P'}$ and $HL^{P'}$. Perform an inverse wavelet transform, and generate a new intensity or new PC1 component.

(5) Transform the new intensity together with the hue, saturation components, or new PC1 with PC2, PC3, back into RGB space.

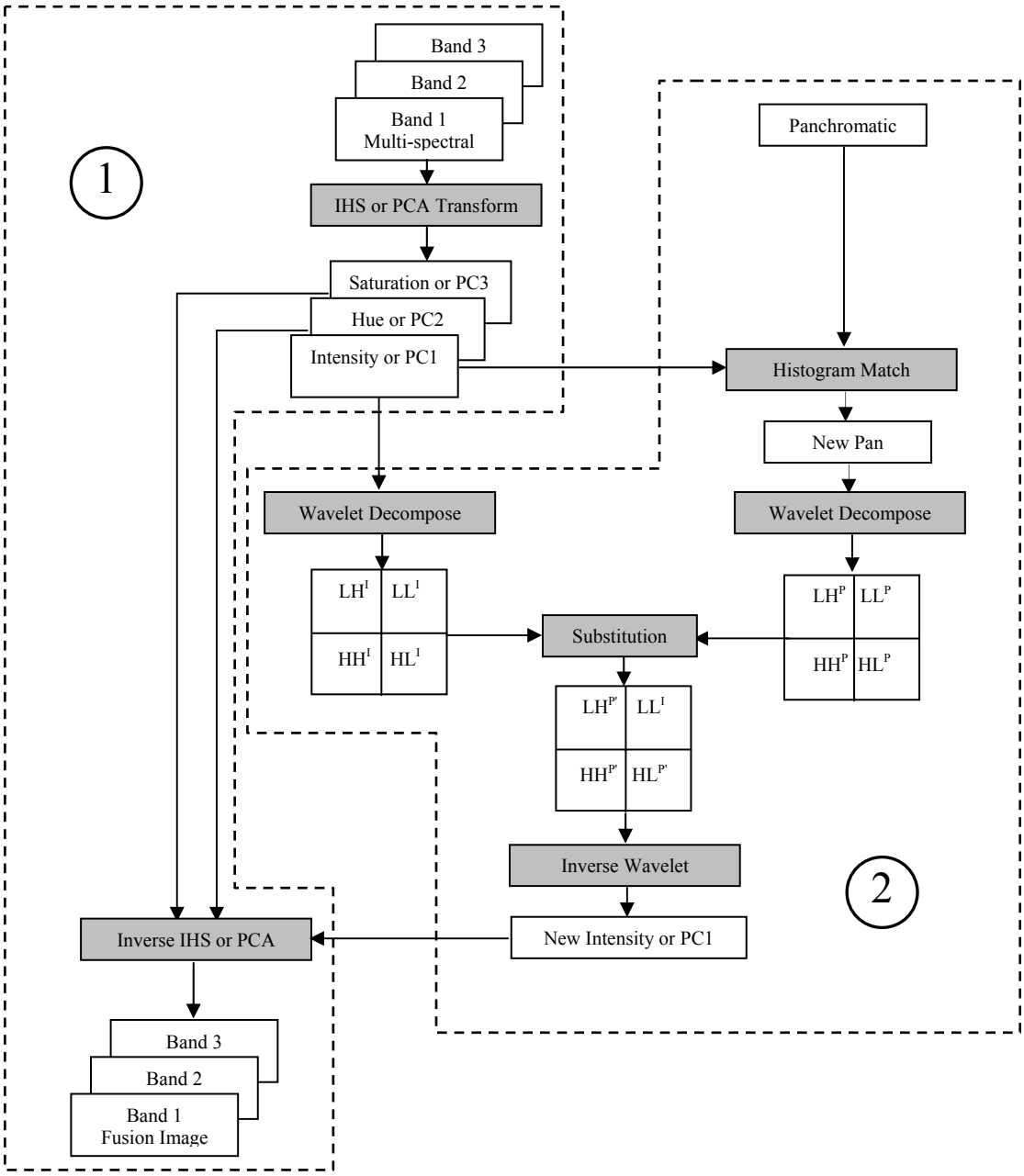

Figure 4.2. Flow of the fusion based on wavelet and substitution integration

4.4 Experimental results

In this research, five kinds of wavelet-based fusion methods and two kinds of wavelet-based integration methods are implemented to test and compare their fusion results. Decimation and undecimation cases are considered in the orthogonal and biorthorgonal wavelet, respectively. These fusion methods are orthogonal wavelet fusion with decimation (simply called ORTH), orthogonal wavelet fusion without decimation (simply called UORTH), biorthogonal wavelet fusion with decimation (simply called BIOR), biorthogonal wavelet fusion without decimation (simply called UBIOR), wavelet fusion based on the "à trous" wavelet (simply called ATRO), wavelet and IHS transformation integration (simply called WIHS) and wavelet and PCA transformation integration (simply called WPCA). The undecimation orthogonal wavelet is used in the WIHS and WPCA fusion method.

A subset of IKONOS data (320 by 320) and QuickBird data (320 by 320) are used to evaluate the different fusion methods. The IKONOS multispectral image (Figure 4.4(b) is more colorful than the QuickBird multispectral image (Figure 4.3(b)) since the IKONOS image was acquired in the autumn and the QuickBird image in the summer, the vegetation is almost all green in the QuickBird image while it appears in a variety of colors in the IKONOS image. Two data set fusion results are shown in Figure 4.3 and Figure 4.4, respectively. Figure 4.3 (a) is the original QuickBird panchromatic image, Figure 4.3 (b) is the original QuickBird multispectral image, Figure 4.3 (c) is the fusion result of orthogonal wavelet fusion with decimation, Figure 4.3 (d) is the fusion result of biorthogonal wavelet fusion with decimation, Figure 4.3 (e) is the fusion result of orthogonal wavelet without decimation, Figure 4.3 (f) is the fusion result of

biorthogonal wavelet without decimation, Figure 4.3 (g) is the fusion result of "à trous" wavelet, Figure 4.3 (h) is the fusion result of PCA transformation combined with wavelet, and Figure 4.3 (i) is the fusion result of IHS transformation combined with wavelet. The sequence of the different fusion results of IKONOS in Figure 4.4 is the same as that in Figure 4.3.

(a) Panchromatic image (b) Multispectral image

(c) ORTHO (d) BIOR

Figure 4.3. Fusion results of different fusion algorithms using QuickBird data

(e) UORTHO

(f) UBIOR

(g) ATROU

(h) WPCA

Figure 4.3. Fusion results of different fusion algorithms using QuickBird data

(Continued)

(i) WIHS

Figure 4.3. Fusion results of different fusion algorithms using QuickBird data (Continued)

(a) panchromatic image

(b) Multispectral image

(c) ORTHO

(d) BIOR

Figure 4.4. Fusion results of different fusion algorithms using IKONOS data

(e) UORTHO

(f) UBIOR

(g) ATROU

(h) WPCA

Figure 4.4. Fusion results of different fusion algorithms using IKONOS data (Continued)

(i) WIHS

Figure 4.4. Fusion results of different fusion algorithms using IKONOS data (Continued)

4.5 Accuracy analyses and comparison of the fusion results

4.5.1 Visual analysis

From the fusion results (Figure 4.3 and Figure 4.4), it is easy to see that the fusion methods improve spatial resolution and preserve the color of the original multispectral image. This phenomenon is consistent with the characteristic of wavelet-based fusion result which can preserve the color information very well compared with the other fusion methods. From the original multispectral images in Figure 4.3 (b) and Figure 4.4 (b), some houses appears as bright spots in the original multispectral image, and cars are too blurry to see clearly on the road. After fusion, we can easily see that the buildings and cars are better characterized, and as such, are more easily identifiable in the images.

To be precise, when we compare the orthogonal wavelet with the biorthogonal wavelet, the fusion results of ORTH have more aliasing effects than the biorthogonal wavelet fusion result because of the shift-invariant property of the biorthogonal wavelet.

If the fusion results are overlaid with a reference image, it can be found the fusion results of the orthogonal flicking is heavier than the fusion results of the biorthogonal. When the decimation is compared with the undecimation method, the fusion results of UORTH (Figure 4.3 (e) and Figure 4.4 (e)), UBIOR (Figure 4.3 (f) and Figure 4.4 (f)), ATRO (Figure 4.3 (g) and Figure 4.4 (g)) are smoother than the fusion results of ORTH (Figure 4.3 (c) and Figure 4.4 (c)) and BIOR (Figure 4.3 (d) and Figure 4.4 (d)). Although the rendering of road feature in fusion results of ORTH and BIOR is superior to that in the original mutispectral image, there are discontinuities in these fusion results. This situation is in contrast to the continuous rendering (or smooth appearance) of these features in the fusion results of UBIOR, UORTH and Atrous. From the fusion results of the wavelet-based methods (ORTH, BIOR, UORTH, UBIOR, ATRO), the fused images exhibit similar characteristics to images processed using a high pass filter (e.g., features appear more discrete, the color is not smoothly integrated into the spatial features). In the fusion results of WIHS and WPCA, the above phenomena is reduced to some extent-that is, the fused images are smoother than the wavelet-based results (ORTH, BIOR, UORTH, UBIOR, and ATRO), because in this wavelet-based fusion method, panchromatic information is added in the same amount to all three bands, biasing the color of the pixel toward the gray, while in wavelet-integration method (WIHS, WPCA), the high-resolution information modifies only the intensity or first component, which preserves multispectral information in a better way.

4.5.2 Statistical analysis

All the fusion results are analyzed statistically by using correlation coefficients. The higher the value of the correlation coefficients, the more similar the fused image is to the corresponding original multispectral image. In other words, its spectral information is preserved in the fusion result. Figure 4.5 shows the correlation coefficients between the original multispectral image and fusion results of QuickBird and Figure 4.6 shows the correlation coefficients between the original multispectral image and fusion results of IKONOS. Because the correlation coefficients in the graphic representation are so similar, the detail values are also included in the figures 4.5-4.6. In Figure 4.5, the original panchromatic image of Quickbird has a low correlation with the original multispectral image. This is the same for the IKONOS image (Figure 4.6). The correlation between the fusion result and multispectral image are much greater than the correlation between the panchromatic image and multispectral image. In the QuickBird case, the highest correlation coefficients are WPCA and WIHS (they indeed are very close). The lowest are ORTH and BIOR, UORTH, UBIOR and ATRO are in the middle. According to this quantitative analysis, ORTH and BIOR are the worst and WPCA and WIHS are the best. The IKONOS case is similar to the Quickbird case, WIHS is the best , WPCA is the second best, the worst are ORTH and BIOR, UORTH , UBIOR and ATRO are similar and in the middle.

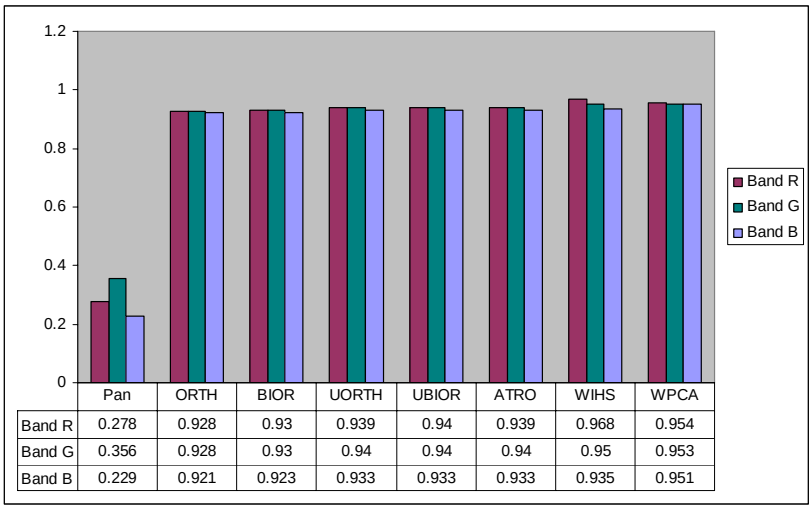

	Pan	ORTH	BIOR	UORTH	UBIOR	ATRO	WIHS	WPCA
Band R	0.278	0.928	0.93	0.939	0.94	0.939	0.968	0.954
Band G	0.356	0.928	0.93	0.94	0.94	0.94	0.95	0.953
Band B	0.229	0.921	0.923	0.933	0.933	0.933	0.935	0.951

Figure 4.5. Correlation coefficients between the original multispetral image and fusion results (QuickBird)

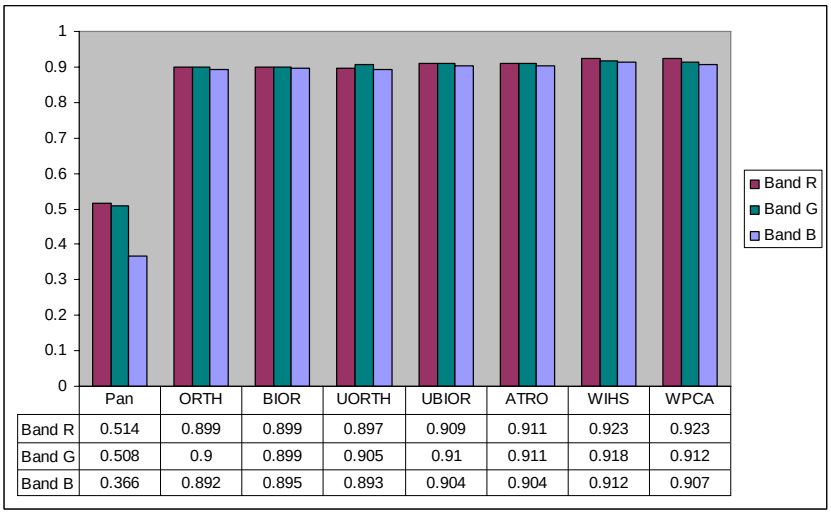

	Pan	ORTH	BIOR	UORTH	UBIOR	ATRO	WIHS	WPCA
Band R	0.514	0.899	0.899	0.897	0.909	0.911	0.923	0.923
Band G	0.508	0.9	0.899	0.905	0.91	0.911	0.918	0.912
Band B	0.366	0.892	0.895	0.893	0.904	0.904	0.912	0.907

Figure 4.6. Correlation coefficient between the original multispectral image and fusion results (IKONOS)

A visual examination can provide us with an appreciation for the spatial information that has been injected into the fusion result, while it can not provide quantitative information. The spatial quality analysis method in Zhou et al. [1998] was employed to evaluate the spatial quality of the fused result. The correlation coefficients between the high-pass filtered fusion results and the high-pass filtered panchromatic image is used as an index of the spatial quality. The principle is that the spatial

information unique in panchromatic image is mostly concentrated in the high frequency domain. The higher correlation between the high frequency components of fusion result and the high frequency component of panchromatic image indicates that more spatial information from panchromatic image has been injected into the fusion result. For the QuickBird case(Figure 4.7), in terms of the correlation coefficients between high pass filtered results and high pass filtered panchromatic image, WPCA is the highest, WIHS is the second, followed by ATRO, UBIOR, UORTH, BIOR,and ORTH is the lowest. That means the WPCA fusion result is injected into the most spatial information, while the ORTH fusion result is injected into the least spatial information. The IKONOS case (Figure 4.8) is similar to the QuickBird case.

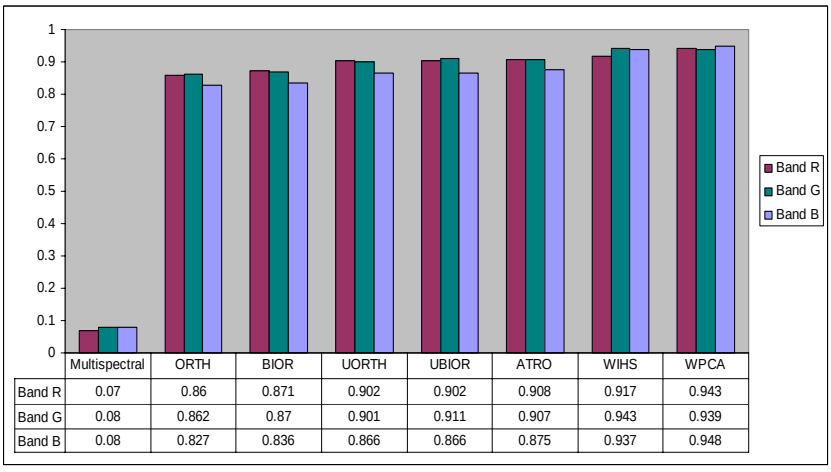

	Multispectral	ORTH	BIOR	UORTH	UBIOR	ATRO	WIHS	WPCA
Band R	0.07	0.86	0.871	0.902	0.902	0.908	0.917	0.943
Band G	0.08	0.862	0.87	0.901	0.911	0.907	0.943	0.939
Band B	0.08	0.827	0.836	0.866	0.866	0.875	0.937	0.948

Figure 4.7. Correlation coefficients between the high pass filtered panchromatic image and high pass filtered fusion results (QuickBird)

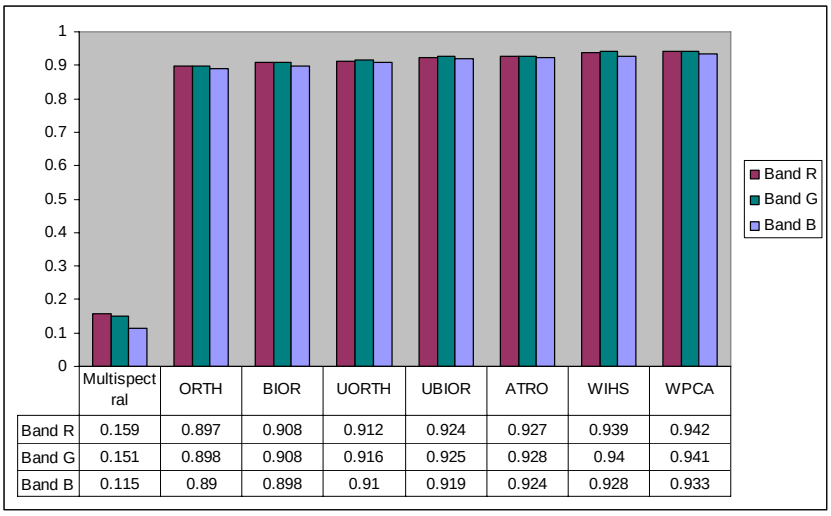

	Multispectral	ORTH	BIOR	UORTH	UBIOR	ATRO	WIHS	WPCA
Band R	0.159	0.897	0.908	0.912	0.924	0.927	0.939	0.942
Band G	0.151	0.898	0.908	0.916	0.925	0.928	0.94	0.941
Band B	0.115	0.89	0.898	0.91	0.919	0.924	0.928	0.933

Figure 4.8. Correlation coefficients between the high pass filtered panchromatic image and high pass filtered fusion results (IKONOS)

In conclusion, from the above statistical analysis results, we can see that the WIHS or WPCA method is the best fusion method from a spatial and spectral information perspective, the worst is ORTH or BIOR, UORTH, while UBIOR and ATRO are in the middle.

The fusion results of the degraded panchromatic and multispectral images (four times degraded in resolution) were also compared with original multispectral images using the approach outlined in Wald et al. [1997] and the same statistical analysis results as above were obtained. Owing to space restrictions, the results of this analysis are not listed in the paper.

4.6 Factors affecting the fusion result

4.6.1 Comparison between orthogonal wavelet and biorthogonal wavelet in terms of fusion purpose

Figure 4.9 shows the approximation images at 4 different levels produced using the orthogonal and biorthogonal wavelet transform under the decimation situation. It compares the shift property between the orthogonal wavelet and the biorthogonal wavelet in the decimation case. From Figure 4.9, in the orthogonal wavelet case, it is easy to see that the approximation image at the higher level is shifted to the lower right corner. This is because the orthogonal wavelet is not symmetric; while the biorthogonal wavelet used in this research is symmetric, shifting phenomenon does not happen in this case.

Aliasing is a common phenomenon in the wavelet-based image fusion process. Theoretically, aliasing introduced by the discrete wavelet transform (DWT) can be removed when the inverse DWT is performed using all of the original wavelet coefficients. However, the original coefficients have been changed to some extent in the image fusion process. Although we try to keep the changed wavelet coefficients as the same as the original wavelet coefficients, there are still some differences between those coefficients. The orthogonal wavelet can make this phenomenon more pronounced, while the biorthogonal wavelet can reduce this phenomenon to some extent because of the shift-invariant property.

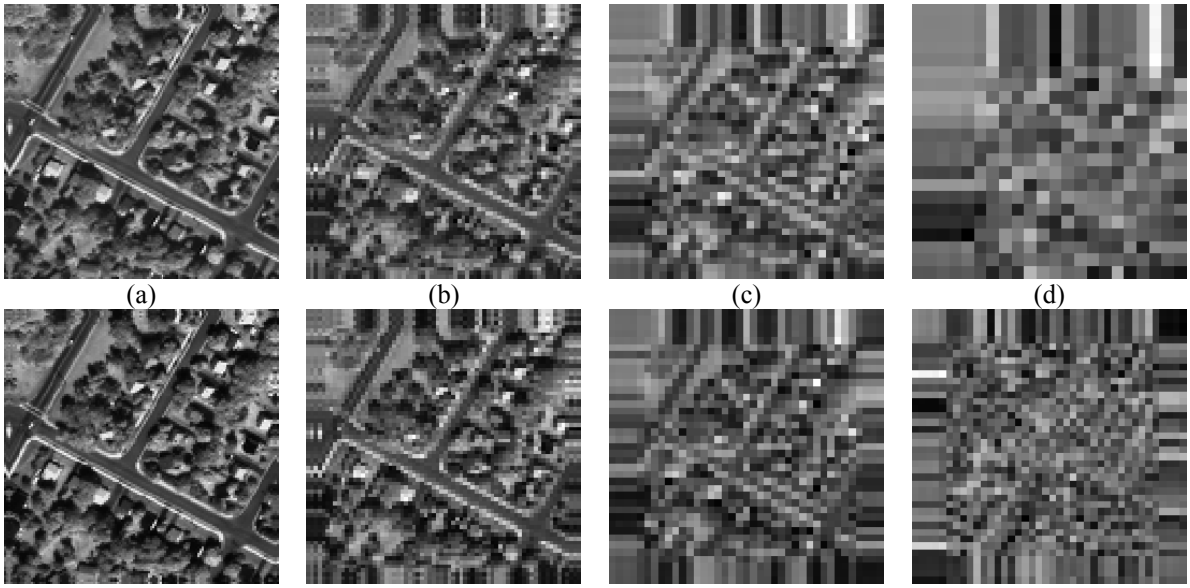

Figure 4.9. Shifting comparison between the orthogonal and biorthogonal wavelets (decimation case)

(a-d) are the approximation images by using the orthogonal wavelet at levels 1 to 4 respectively.
(e-h) are the approximation images by using the biorthogonal wavelet at levels 1 to 4 respectively.

Figure 4.10 shows the approximation images at four different levels produced using the orthogonal and biorthogonal wavelet transform under the undecimation situation. It compares the shift property between the orthogonal and the biorthogonal wavelet in the undecimation case. Because no subsampling is applied to the wavelet decomposition process, no shifting phenomenon is found in both the Orthogonal and Biorthogonal case. These two kinds of wavelet transform will not cause aliasing in the fusion result.

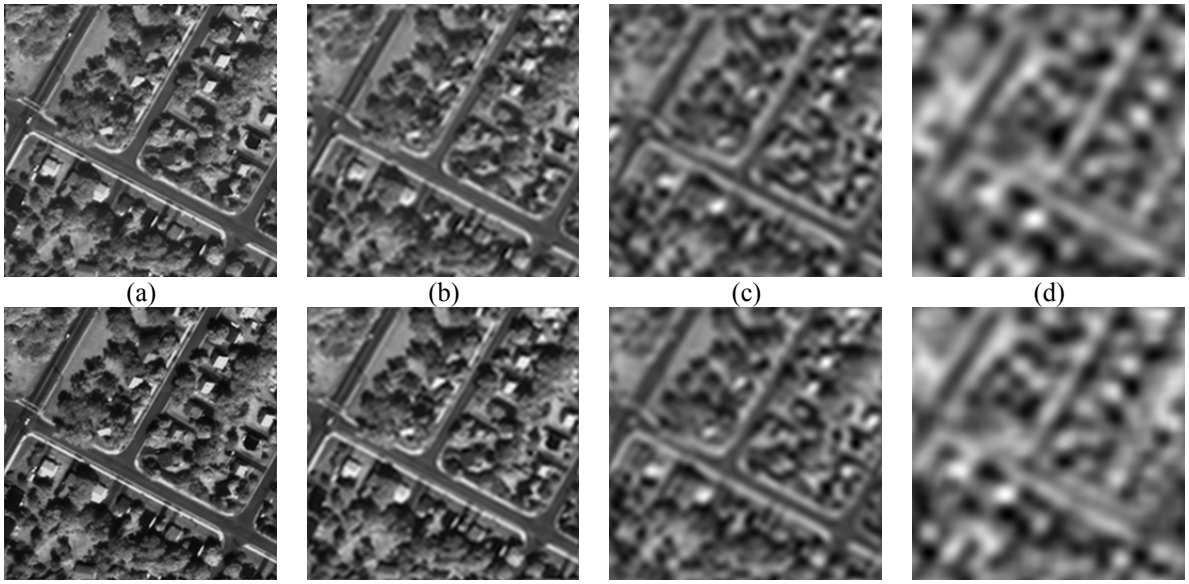

Figure 4.10. Shifting comparison between the orthogonal and biorthogonal wavelets (undecimation case)
(a-d) are the approximation images by using the orthogonal wavelet at levels 1 to 4 respectively.
(e-h) are the approximation images by using the biorthogonal wavelet at levels 1 to 4 respectively.

4.6.2 Comparison between decimation and undecimation

Figure 4.11 shows the detail images for the second level of the wavelet transform for both decimation (Figure 4.11 (a-c)) and undecimation (Figure 4.11 (d-f)) respectively. From Figure 4.11 (a-c), we can see that linear features are disjointed (i.e. not continuous) in the detail image of the decimation case. In contrast, linear features in the undecimated cases appear continuous. The discontinuities existing in the decimation case will introduce artifacts into image fusion process and thus, will affect the final fusion result. While continuity existing in the undecimation case does not have this problem during the image fusion process.

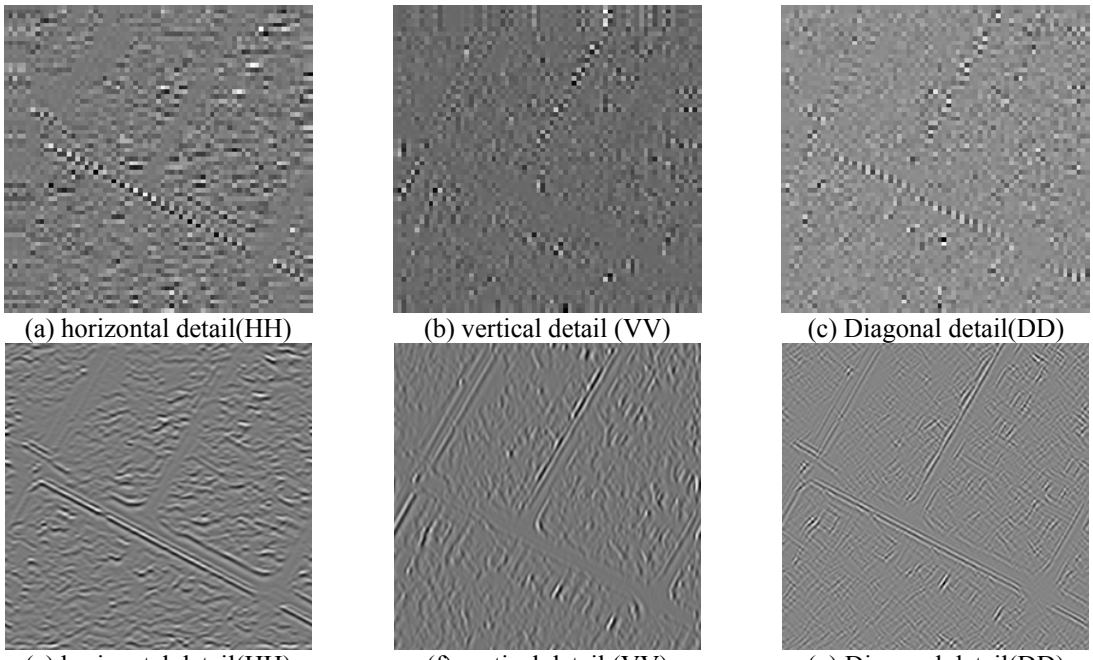

(a) horizontal detail(HH) (b) vertical detail (VV) (c) Diagonal detail(DD)

(e) horizontal detail(HH) (f) vertical detail (VV) (g) Diagonal detail(DD)

Figure 4.11. Detail comparisons between the decimation and undecimation process

(a-c) are the HH, VV, DD details by using the decimation process at level 2 respectively.
(e-g) are the HH, VV, DD details by using the undecimation process at level 2 respectively.

4.6.3 Comparison of wavelet decomposition levels

Figure 4.12 (a) and (b) shows the fusion results produced using three wavelet decomposition levels by using the orthogonal wavelet and biorthogonal wavelet, respectively. From Figure 4.12, we see that the fusion images created with three decomposition levels is clearer than the fusion images created with two decomposition levels (Figure 4.4), also the spatial quality of the fusion images created with three decomposition levels is superior to the fusion images created with two decomposition levels as measured by their spatial quality metric according to the method mentioned in Section 5.2. However, the fusion image shown in Figure 4.12 exhibit a greater spatial distortion (i.e., ringing effect, aliasing) and a higher spectral distortion compared with the fusion results created with two decomposition levels (see the results in Figure 4.4),

we can see that the color of the fusion images created with two decomposition levels is closer to the original multisepctral image (Figure 4.4 (b)) than that of the fusion images created with three decomposition levels. Zhou et al. [1998] merged a SPOT PAN with LANDSAT TM images using two and three decomposition levels and obtained similar observations. In general, it may be stated that increasing decomposition level will improve spatial quality but degrade spectral quality. Taking this inverse relationship and the results of the above experiments into account, two decomposition levels is the optimum level in the wavelet decomposition process of image fusion.

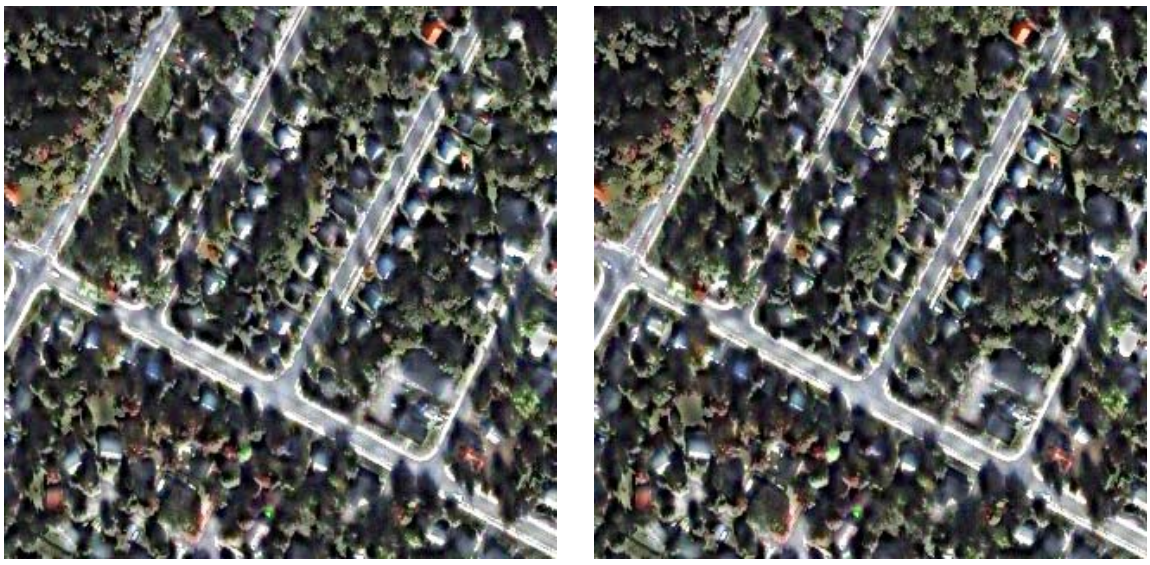

(a)Wavelet decompose 3 levels(orthogonal) (b) wavelet decompose 3 levels (biorthogonal)

Figure 4.12. Wavelet decomposition level comparison

4.6.4 The mother wavelet selection

The choice of an appropriate wavelet transform plays an important role in the image fusion process [Zhang and Blum, 1999; Chibani and Houacine, 2003]. In this paper, we have not compared the results with the selection of the mother wavelets but

relied on the recommendations of other researchers [King and Wang, 2001; Garzelli 2002; Du et al., 2003].

DB4, a family of Daubechies Wavelets, is used as an orthogonal wavelet. Daubechies Wavelets are compactly supported wavelets with extremal phase and the highest number of vanishing moments for a given support width. Associated scaling filters are minimum-phase filters [Misiti et al., 2006]. In DB4, the number of the vanishing moments for the analysis wavelet is four. The coefficients for the analysis and the synthesis filters are all eight. Garzelli [2002] reported that Daubechies filters with eight or ten coefficients have provided good results for image merging of multiresolution data. Du et al. [2003] proposed a fusion method that uses DB4, and claimed that the method can preserve spatial information and minimize artifacts.

Biorthogonal Spline 4.4 is used as a biorthogonal wavelet. Biorthogonal Spline Wavelets are compactly supported and symmetric, and thus exact reconstruction is possible with finite impulse response filters, while it is impossible except for DB1 in the orthogonal case. The number of the vanishing moments of this kind of wavelet for the analysis wavelet is four. The numbers of coefficients for the analysis filter and synthesis filter are nine and seven, respectively. Because of symmetry, Biorthogonal Spline 4.4 is shift-invariant. King and Wang [2001] proposed a method which uses the Biorthogonal Spline 4.4 with the decimation mode, and won the IGARSS 2000 Data Fusion Committee contest.

“à trous” wavelet is used as a nonorthogonal wavelet. Some researchers used it in the image fusion process successfully [Núñez et al., 1999; Chibani and Houacine, 2002].

4.7 Conclusion

This paper has studied and compared wavelet-based and wavelet-integrated fusion methods. All fusion methods were tested on two data sets, IKONOS and Quickbird images. The fusion results were compared both visually and statistically. Wavelet-based fusion extracts spatial details from high-resolution bands. In this manner, the color distortion can be reduced to a certain extent, but the fused image appears similar to a high-pass filtered image, e.g., the color appears not to be smoothly integrated into the spatial features. The wavelet-integrated method can improve the fusion result, reduce the ringing or aliasing effects to some extent, and make the whole image smoother.

This paper has also elucidated following factors: wavelets (orthogonal, biorthogonal, non-orthogonal), decimation or undecimation, and wavelet decomposition levels, which could affect the final fusion result. In the wavelet decomposition process, the wavelet selection affects the final fusion: the orthogonal wavelet used in this research cause aliasing in the decimation case, but does not cause aliasing in the undecimation case; the biorthogonal wavelet used in this research does not cause aliasing in either the decimation or the undecimation cases; “à trous” (nonorthogonal) does not cause aliasing. Also decimation introduces discontinuities into the image fusion process, thus producing many artifacts in the fusion result; since undecimation does not cause a discontinuity in the image fusion process, fewer artifacts are present in the fusion result. Wavelet decomposition levels also affect the fusion result. Theoretically, increases in wavelet decomposition level produce more detailed information in the fusion result, but at the same time, also increase the amount of spatial distortion present in the fusion result, i.e. more artifacts, and spectral or color distortion.

Thus, the appropriate selection wavelet decomposition level is also important for the fusion result.

ACKNOWLEDGMENTS

This research was supported by the GEOIDE Network (Geomatics for Informed Decisions) of Canada under the project MNG#TAO. The authors would like to thank Mr. Rob Lunn, GIS supervisor of the City of Fredericton, NB, Canada, for providing the IKONOS and QuickBird multispectral and panchromatic images.

REFERENCES

Aiazzi, B., L. Alparone, S. Baronti, and A. Garzelli (2002). "Context driven fusion of high spatial and spectral resolution images based on oversampled multiresolution analysis." *IEEE Transactions on Geoscience and Remote Sensing*, Vol. 40, No. 10, pp.2300-2312.

Burrus, C.S., R.A. Gopinath, and H. Guo (1998). *Introduction to Wavelets and Wavelet Transforms*. Prentice-Hall. Inc. New Jersey.

Chibani, Y., and A. Houacine (2002). "The joint use of IHS transform and redundant wavelet decomposition, for fusing multispectral and panchromatic images." *International Journal of Remote Sensing*, Vol. 23, No. 18, pp. 3821–3833.

Chibani, Y., and A. Houacine (2003). "Redundant versus orthogonal wavelet decomposition for multisensor image fusion." *Pattern Recognition*, Vol. 36, No. 4, pp. 879-887.

Du, Y., P.W. Vachon, and J.J. Van der Sanden (2003). "Satellite image fusion with multiscale analysis for marine applications: preserving spatial information and minimizing artifacts (PSIMA)." *Canadian Journal of Remote Sensing*, Vol. 29, No. 1, pp.14-23.

King, R.L., and J.W. Wang (2001). "A wavelet based algorithm for pan sharpening Landsat 7 imagery." *Geoscience and Remote Sensing Symposium, IGARSS '01.* IEEE 2001 International Volume 2, 9-13 July 2001, pp.849 – 851.

Li, H., B.S. Manjunath, and S.K. Mitra (1995). "Multisensor image fusion using the wavelet transform." *Graph. Models Image Process*. Vol. 57, No. 3, pp. 235–245.

Hong, G., and Y. Zhang (2003). "High resolution image fusion based on Wavelet and IHS transformations." In: *Proceedings of the IEEE/ISPRS joint Workshop on "Remote Sensing and Data Fusion over Urban Areas*", Berlin, 2003; pp. 99 - 104.

Garguet-Duport, B., J. Girel, J.M. Chasseny, and G. Pautou (1996). "The use of multiresolution analysis and wavelet transform for merging SPOT panchromatic and multispectral image data." *Photogrammetric Engineering and Remote Sensing*, Vol. 62, pp. 1057–1066.

Garzelli, A. (2002). "Possibilities and limitations of the use of wavelets in image fusion." *Procedings of the International Geoscience and Remote Sensing Symposium, 2002*, IGARSS '02, Vol. 1, pp. 66-68.

Gonzalez-Audicana, M., J.L. Saleta, and R.G. Catalan (2004). "Fusion of multispectral and panchromatic images using improved IHS and PCA mergers based on wavelet decomposition." *IEEE Transactions on Geoscience and Remote Sensing*, Vol. 42, No. 6, pp. 1204–1211.

Gonzalez-Audicana, M., X. Otazu, O.Fors, and A. Seco (2005). "Comparison between Mallat's and the 'à trous' discrete wavelet transform based algorithms for the fusion of multispectral and panchromatic images." *International Journal of Remote Sensing,* Vol. 26, No. 3, pp. 595-614.

Mallat, G.S. (1989). "A theory for multiresolution signal decomposition: The wavelet representation." *IEEE Transactions of Pattern Analysis and Machine Intelligence*, Vol. 11, No. 7, pp: 674--693.

Misiti, M., Y. Misiti, G. Oppenheim, and J.-M. Poggi (2006). *Wavelet Toolbox User's Guide (For Use with Matlab)*, The MathWorks Inc.

Núñez, J., X. Otazu, O. Fors, A. Prades, V. Palà, and R. Arbiol (1999). "Multiresolution-based image fusion with additive wavelet decomposition." *IEEE Transactions on Geoscience and Remote Sensing*, Vol. 37, No. 3, pp. 1204–1211.

Pajares, G. and J.M. De La Cruz (2004). "A wavelet-based image fusion tutorial." *Pattern Recognition*, Vol. 37, pp.1855-1872.

Pohl, C., and J.L. Van Genderen (1998). "Multisensor image fusion in remote sensing: concepts, methods, and applications." *International Journal of Remote Sensing*, Vol. 19, pp 823-854.

Ranchin, T., and L. Wald (2000). "Fusion of high spatial and spectral resolution images: The ARSIS concept and its implementation." *Photogrammetric Engineering and Remote Sensing*, Vol. 66, pp. 49-61.

Starck, J.L., F. Murtagh, and A. Bijaoui (1998). *Image Processing and Data Analysis: The Multiscale Approach.* Cambridge Univ. Press, Cambridge, U.K.

Strang, G., and T.Q. Nguyen (1996). *Wavelets and Filter Banks.* Cambridge, MA: Wellesley-Cambridge.

Tseng, D.C., Y-L. Chen, and S.C. Liu (2001). "Wavelet-based multispectral image fusion." *Proceedings of the International Geoscience and Remote Sensing Symposium*, Vol. 4, pp. 1956-1958.

Wald, L., T. Ranchin, and M. Mangolini (1997). "Fusion of satellite images of different spatial resolutions: assessing the quality of resulting images." *Photogrammetric Engineering and Remote Sensing,* Vol. 63, No. 6, pp.691–699.

Yocky, D.A. (1995). "Image merging and data fusion using the discrete two-dimensional wavelet transform." *J. Opt. Soc. Am. A.*, Vol. 12, No. 9, pp. 1834-1841.

Yocky, D.A. (1996). "Multiresolution wavelet decomposition image merger of Landsat Thematic Mapper and SPOT panchromatic data." *Photogrammetric Engineering and Remote Sensing,* Vol. 62, No. 3, pp. 295-303.

Zhang, Y. (2004). "Understanding Image Fusion." *Photogrammetric Engineering and Remote Sensing,* Vol. 70, No. 6, pp. 657-661.

Zhang, Z., and R.S. Blum (1999). "A categorization of multiscale decomposition-based image fusion schemes with a performance study for a digital camera application." *Proc. IEEE 87 (8)*, pp. 1315–1326.

Zhou, J., D.L. Civco, and J.A. Silander (1998). "A wavelet transform method to merge Landsat TM and SPOT panchromatic data." *International Journal of Remote Sensing*, Vol. 19, No. 4, pp. 743-757.

Chapter 5. Wavelet-Based Image Registration Technique for High Resolution Remote Sensing Images[♣]

ABSTRACT

Image registration is the process of geometrically aligning one image to another image of the same scene taken from different viewpoints at different times or by different sensors. It is an important image processing procedure in remote sensing and has been studied by remote sensing image processing professionals for several decades. Nevertheless, it is still difficult to find an accurate, robust, and automatic image registration method, and most existing image registration methods are designed for a particular application. High resolution remote sensing images have made it more convenient for professionals to study the Earth; however, they also create new challenges when traditional processing methods are used. In terms of image registration, a number of problems exist in the registration of high resolution images: (1) the increased relief displacements, introduced by increasing the spatial resolution and lowering the altitude of the sensors, cause obvious geometric distortion in local areas where elevation variation exists; (2) precisely locating control points in high resolution images is not as simple as in moderate resolution images; (3) a large number of control points are required for a precise registration, which is a tedious and time consuming process; and (4) high data volume often affects the processing speed in the image

[♣] This chapter has been submitted.
Hong G., Y. Zhang (2006). "Wavelet-based image registration technique for high resolution remote sensing images." *Submitted to Computers & Geosciences, November, 2006.*

registration. Thus, the demand for an image registration approach that can reduce the above problems is growing. This study proposes a new image registration technique, which is based on the combination of feature-based matching (FBM) and area-based matching (ABM). A wavelet-based feature extraction technique and a normalized cross-correlation matching and relaxation-based image matching techniques are employed in this new method. Two pairs of data sets, one pair of IKONOS panchromatic images from different times and the other pair images consisting of an IKONOS panchromatic image and a QuickBird multispectral image, are used to evaluate the proposed image registration algorithm. The experimental results show that the proposed algorithm can select sufficient control points semi-automatically to reduce the local distortions caused by local height variation, resulting in improved image registration results.

Keywords: wavelet transform, image registration, image matching, high resolution

5.1 Introduction

Image registration is the process of geometrically aligning one image to another image of the same scene taken from different viewpoints at different times or by different sensors. It is a fundamental image processing technique and is important for integrating information from different sensors, finding changes in images taken at different times, inferring three-dimensional information from stereo images, and recognizing model-based objects [Rosenfeld and Kak, 1982]. It has been a research topic of three major research areas [Brown, 1992]: computer vision and pattern

recognition, medical image analysis, and remotely sensed data processing. In this study, image registration of remote sensing images is discussed.

Generally, the image registration process consists of the following steps [Rignot et al., 1991]:

(1) Feature extraction, which identifies the relevant features in the two images (reference image, sensed image), such as edges, intersection of lines, and regions.

(2) Feature matching, which establishes relationship between the features in the two images.

(3) Mapping function building, which determines transformation parameters of the mapping functions using the features being matched.

(4) Image registration, which geometrically transforms and resamples the sensed image according to the mapping function established in step (3).

Image registration algorithms can be broadly classified into two categories according to matching method [Fonseca and Manjunath, 1996]: area based methods (ABM) and feature based methods (FBM). In ABM algorithms, a small window of pixels in the sensed image is compared statistically with windows of the same size in the reference image. The most commonly used methods are cross-correlation matching and least-squares matching. The centers of the matched windows are treated as control points, which can be used to solve for mapping function parameters between the reference and sensed images [Li et al., 1995]. ABM is a classical matching method. Cideciyan et al. [1992] used Fourier transformation and cross-correlation for image

registration. Zheng and Chellappa [1993] used the area correlation in the spatial domain to match the feature points that are extracted by the Gabor wavelet decomposition.

On the other hand, feature-based matching techniques do not use the gray values to describe matching entities, but use image features derived by a feature extraction algorithm. These features include edges, contours, surfaces, other salient features such as corners, line intersections, and points of high curvature, statistical features such as moment invariants or centroids, and higher level structural and syntactic descriptions [Brown, 1992]. The form of the description as well as the type of feature used for matching depends on the task to be solved. Different methods have been developed for FBM, including region-based method [Goshtasby et al., 1986], contour-based method [Li et al., 1995], structure matching method [Ventura et al., 1990], invariant moment method [Flusser and Suk, 1994; Dai and Khorram, 1999], linear feature based method [Medioni and Nevatia, 1984; Habib et al., 2003; Shi and Shaker, 2006], and wavelet-based feature extraction method [Djamdji et al., 1993; Zheng and Chellappa, 1993; Simhadri et al., 1998; Moigne et al., 2002; Zavorin and Moigene, 2005].

The prerequisite of ABM is that the gray level distribution of the sensed image and reference image must be similar. Very good initial approximations are required to assure convergence. Since gray values contain little explicit information about the object space, area-based matching methods are not reliable enough. Therefore, ABM methods are not well adapted to the problem of multisensor image registration since the gray-level characteristics of images to be matched can vary from sensor to sensor. Compared with ABM, FBM is more robust and reliable for the following reasons [Schenk, 1999]: first, features are derived properties of the original gray level images and are inherently

unique; second, similarity is based on the attributes and /or relations, and is thus more invariant to illumination, reflectance, and geometry; third, features are sufficient for describing image content. However, FBM often requires sophisticated image processing for feature extraction and depends on the robustness of feature detection for reliable matching. As a result, the image matching precision is not as high as that of ABM.

Image registration techniques have been studied and developed for decades. Manual registration remains by far the most common way to accurately align the imaging data, although it is often time consuming and inaccurate [Zavorin and Moigene, 2005]. At present, increasingly high-resolution remote sensing images have made it more convenient for professionals to study the Earth. However, the high resolution images also introduce new challenges for traditional processing methods, including current image registration techniques, for the following reasons:

(1) Very high spatial resolution data introduces a new image geometry problem. In order for spatial resolution to become smaller than 1 m, the altitude of the sensors is being decreased, which increases the relief displacement and causes localized distortion related to landscape height.

(2) Precisely locating control points in high resolution images is not as simple as with moderate resolution images; moreover, it is more error-prone.

(3) To get precise registration, a large number of control points must be manually selected across the whole image, which is a tedious and time consuming job.

(4) High data volume often affects the processing speed in the image registration.

The objective of this study is to develop a new image registration technique in order to reduce the above problems that high resolution images bring. As known, the polynomial-model image registration is often used to register different images, because it is included in the commercial software and easy to operate. However, for those high resolution images with terrain relief, the registration accuracy produced by the polynomial-model registration method is poor. While the accurate DEM data of those areas are not always available, the orthorectification cannot be implemented; thus, there exist necessities to resolve this problem under the situation of no DEM data. The proposed method is expected to reduce the problems in registering high resolution images with terrain relief and see the improvement compared with the commonly used polynomial-based image registration method.

5.2 Methodology

Finding control points for IKONOS and QuickBird images for an operator may not be as easy as it would be for moderate resolution images because of those images' high spatial resolution. For example, a road intersection appearing as a point in a SPOT or TM image but as an area in an IKONOS or QuickBird image, making it difficult to locate the precise position of the road intersection, and a large number of control points must be selected across the whole image in order to obtain the precise registration. This is a very tedious and repetitive task for the operator to select them manually. Furthermore, this approach requires someone who is knowledgeable in the application domain, and is not feasible in cases where there is a large amount of data. Thus, there is a need for automated techniques that require little or no operator supervision [Fonseca

and Manjunath, 1996; Zavorin and Le Moigne, 2005]. However, until now, there still exist a number of scenarios where automatic image registration is not well developed for multitemporal and/or multisensor image registration [Bentoutou et al., 2005]; automatica image registration still remains an open problems, for example, local distortion belongs to the most challenging tasks [Zitova and Flusser, 2003]. For the high resolution, there is another problem, namely, the high data volume will affect the processing speed for image registration. The proposed method to solve these problems is introduced below.

5.2.1 Proposed wavelet-based image registration method

An innovative image registration algorithm that combines the ABM with FBM techniques is proposed. The registration process can be divided into three major steps, as illustrated in Figure 5.1: (1) finding the feature points, (2) refining the control points and obtaining accurate control point pairs, and (3) building a mapping function according to the accurate control point pairs and then resampling the sensed image.

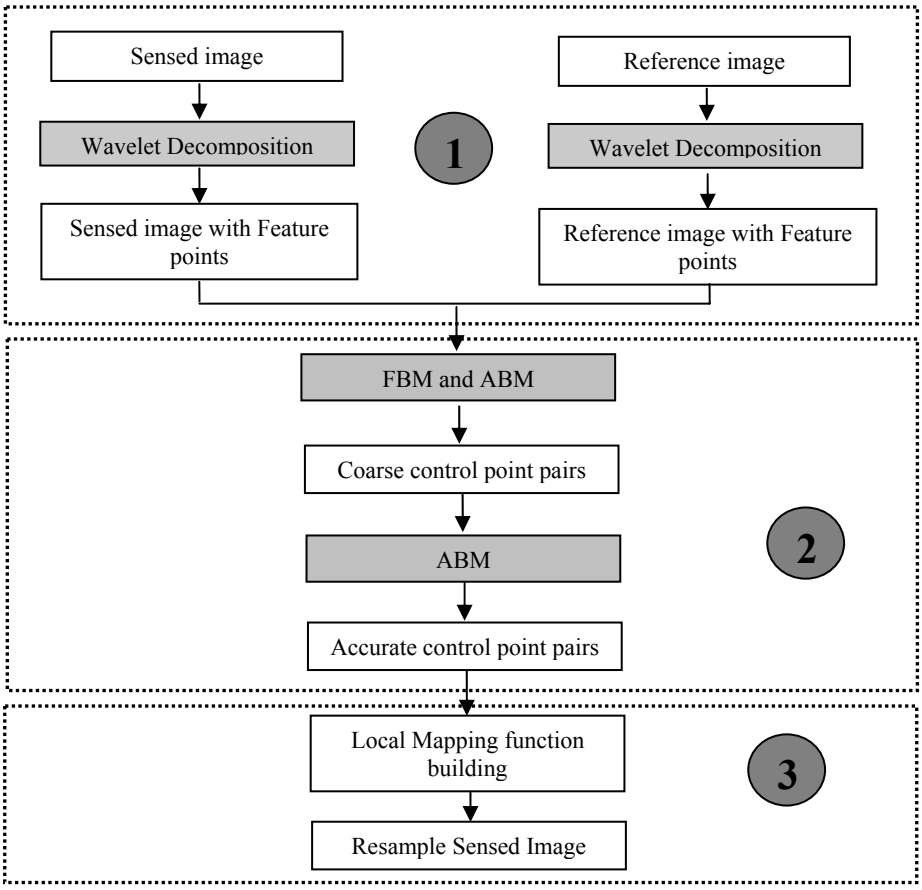

Figure 5.1. The work flow of the proposed image registration method

In the first step, feature points detection, the wavelet multi-resolution property [Mallat, 1989] is used to produce pyramid images from fine to coarse resolution to represent the sensed and reference images. A number of distinct feature points can be obtained through finding the local maxima of the modulus wavelet coefficients. The pyramidal structure can accelerate the processing speed and is helpful in processing high volume data.

In the second step, matching the feature points, the relationship of feature points between the reference image and the sensed image is initially established using the normalized cross-correlation method, and then the probability relaxation method is used to remove false matching control pairs. As thousands of feature points are selected to

find the true control matching pairs, it is very difficult for the probability relaxation method (FBM) because of the computation speed limitation; however, the normalized cross-correlation (ABM) is fast enough to process many feature points compared with the probability relaxation based image matching method, but it also has its limitation since it only considers the gray value of the feature points. The matched feature points can provide the initial value for the next level of point matching, and the threshold value is adjusted to get more feature points varying with the image levels. The next task is to obtain the accurate control point pairs according to these initial values. In order to achieve a highly accurate registered image, normalized cross-correlation matching is employed to refine the control points and to correct for minor control point errors.

The third step is to build the mapping function for every triangle and to rectify the image. Traditionally, one set of polynomial transformation coefficients is used for the entire image. The shortcoming of this kind of transformation is that it cannot resolve the problem of local distortion. The high resolution satellites, such as IKONOS and QuickBird, are close to the Earth relative to the other satellites, so the terrain relief affects the geometric distortion seriously. Especially in moderate relief or mountainous areas, the distortion is common and cannot be resolved with only one set of transformation coefficients for the entire image. In order to resolve this problem, the proposed algorithm uses several sets of mapping function coefficients to rectify the sensed image.

5.2.2 Wavelet-based feature extraction

Wavelet-based feature extraction applies the principle of finding the modulus maxima of wavelet transform locally to detect feature points. Mallat and Hwang [2002] used this method to detect edge points, where the magnitude of the gradient is the local maximum in the direction of the gradient. Fonseca and Costa [1997] used this method to find feature points with the remote sensing data. The basic principle is listed as follows.

Let $\phi(x,y)$ be a smoothing function. Two wavelets, $\psi^1(x,y)$ and $\psi^2(x,y)$ are obtained by taking the first order derivative of $\phi(x,y)$ decomposed in two components along the x and y directions respectively [Fonseca and Costa, 1997], where

$$\begin{aligned}\psi^1(x,y) &= \frac{\partial\phi(x,y)}{\partial x} \\ \psi^2(x,y) &= \frac{\partial\phi(x,y)}{\partial y}\end{aligned} \tag{5.1}$$

For an image *I*, the wavelet transform at scale $a = 2^j$ (i.e. level *j*) applied with the above two wavelets, has two components:

$$\begin{aligned}W_{2^j}^1\left[I(x,y)\right] &= I * \psi_{2^j}^1(x,y) \\ W_{2^j}^2\left[I(x,y)\right] &= I * \psi_{2^j}^2(x,y)\end{aligned} \tag{5.2}$$

These two components of the wavelet transform are proportional to the two components of the gradient vector. At each level, the modulus of the wavelet transform at the scale 2^j is defined as follows:

$$M\left[I(2^j,x,y)\right] = \left(\left|W_{2^j}^1\left[I(x,y)\right]\right|^2 + \left|W_{2^j}^2\left[I(x,y)\right]\right|^2\right)^{1/2} \tag{5.3}$$

The local maxima of $M\left[I(2^j,x,y)\right]$ can be located by thresholding the wavelet transform modulus image at a given value; accordingly, the feature points at scale 2^j can be obtained.

The wavelet transform decomposes the original image into several sub-images. Four sub-images (LL, LH, HL, and HH) are obtained at each level of decomposition [Zitova and Flusser, 2003]. LL contains low frequency components in the horizontal and vertical directions. LH contains low frequency components in the horizontal direction and high frequency components in the vertical direction. HL contains high frequency components in the horizontal direction and low frequency components in the vertical direction. HH contains high frequency components in both the horizontal and vertical directions. The LH and HL sub-bands at each level of the wavelet transform are used to form the image gradient. The modulus maxima of the wavelet transform are used to detect edge points in the images. Figure 5.2 illustrates the process.

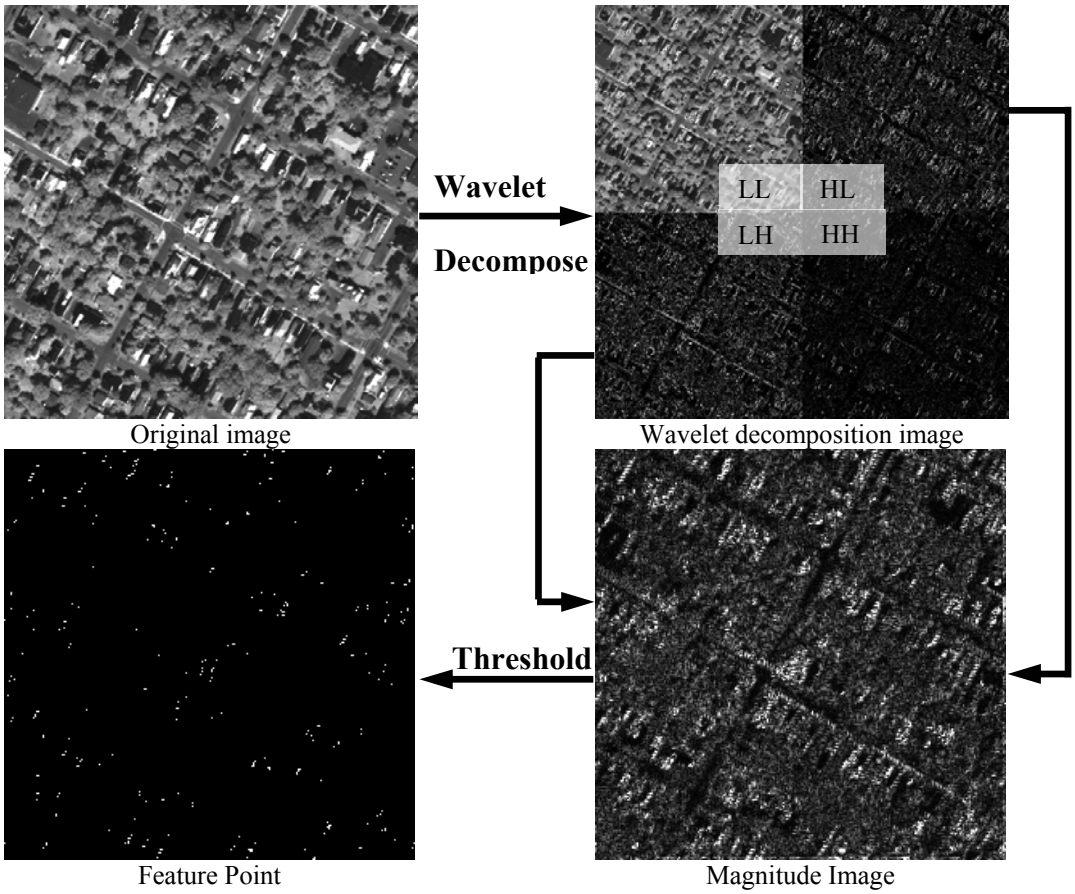

Figure 5.2. Work flow of the feature point extraction based on wavelet decomposition

The “à trous” wavelet is used to overcome the problem of the shift-variance that occurs with general discrete wavelet transforms. The “à trous” wavelet is applied once to the original image to obtain the highest level feature points, and can keep the shift-invariance of these feature points because it does not subsample (decimate) the original image during the wavelet decomposition process. The shift-variance is very important in image registration, since it affects the geometric accuracy of the registered image. Moigne et al. [2002] also reported the problem of shift-variance existing in discrete wavelet transforms. The discrete wavelet transform decomposes the original image into several sub-levels with decimation mode, and the feature points can be obtained in the next levels; however, feature points for the highest level cannot be obtained by using the discrete wavelet decomposition method.

5.2.3 Normalized cross-correlation matching

Normalized cross-correlation matching is used to find similarity between the feature points in the reference image and the sensed image. The normalized cross-correlation coefficient, r_{AB}, is calculated below.

$$r_{AB} = \frac{\sum_{i=1}^{M}\sum_{j=1}^{N}(I_A(i,j)-\bar{I}_A)(I_B(i,j)-\bar{I}_B)}{\left(\sum_{i=1}^{M}\sum_{j=1}^{N}(I_A(i,j)-\bar{I}_A)^2\sum_{i=1}^{M}\sum_{j=1}^{N}(I_B(i,j)-\bar{I}_B)^2\right)^{1/2}} \tag{5.4}$$

where $I_A(i, j)$ and $I_B(i, j)$ mean the grey value of a subset A in a image and a subset B in the other image respectively, $\bar{I}_A$ and $\bar{I}_B$ represent the mean grey value of the two subset

images respectively, and M and N are the number of rows and columns in the subset images.

A coarse-to-fine matching technique is employed in the proposed image registration algorithm. For the lowest level, the number of feature points is not large, one feature in the reference image is compared with all the feature points in the sensed image, the point in the sensed image that has the maximum correlation coefficient with the point in the reference is the corresponding point. A threshold can be set to determine the number of matched feature points in the level. After obtaining the initial matched feature points, the relaxation based matching method is used to remove the wrongly matched feature points. This step is important because the matched feature points will be used to determine the approximate position in the next level of the matching procedure. If some wrongly matched feature points were transferred to the next level, it would definitely affect the matching accuracy at next level. For each level, the number of feature points is larger than at the previous level, and the matched feature points from the previous level are used to determine the approximate position of every feature point in the reference image. For every feature point in the reference image, it is matched with the feature points in the sense image which are close to the approximate position determined by the matched feature points in the previous level. After obtaining matched points, the probability relaxation based matching is used to remove the wrongly matched feature points. The same procedure is iterated until the highest level matching.

5.2.4 Discrete probability relaxation

The reason used discrete probability relaxation in image matching is that image matching based on hierarchical probabilistic relaxation should be useful for utilizing contextual information to reduce local ambiguity and achieve global consistency. If it is applied in gray-level-based image matching, it can take advantage of spatial relationships, and global consistency can be improved greatly. While in the area-based matching process, the cross correlation function may not reach its maximum value at the true corresponding points because of the threshold value, some matching results may be incorrect. The correct results of the nearest neighbor matching should be used to correct the incorrect matching [Zhang et al., 2000]. There are some publications about using the probability relaxation in the image matching [Liao et al., 2004; Zhang and Fraser, 2005].

Consider a set of feature points $A = \{A_1, A_2, \cdots, A_m\}$ in an image A, and a set of feature points $B = \{B_1, B_2, \cdots, B_n\}$ in an image B. The principle of the relaxation-based matching method is based on the following assumption: if (A_i, B_j) is a true control point pair between the image A and the image B, then for any other point A_h in the image A there may exist a corresponding point B_r in the image B such that the distance (A_i, A_h) is equal to the distance (B_j, B_r) when (A_h, B_r) is also a correct match. If (A_i, B_j) is a true control pair, then the remaining (m-1) point pairs (A_h, B_r) are expected to provide support to (A_i, B_j) [Ton and Jain, 1989; Fang, 2000].

The compatible coefficient, $C\ (i, j; h, r)$, is used to describe the relationship between two events: (A_i, B_j) is a true pair, and (A_h, B_r) is a true pair. A positive value means that the two events are compatible, a value of zero means that they are not correlated, and a negative value means that the two events are not compatible. The initial probability that

(A_i, B_j) is a true control points is defined as $p_{ij}^0 \quad (1 \le i \le m, 1 \le j \le n)$, and $0 \le p_{ij}^0 \le 1, \quad \sum_{j=1}^{n} p_{ij}^0 = 1$. The probability of the event after *s* iterations is denoted p_{ij}^s, with $0 \le p_{ij}^s \le 1, \quad \sum_{j=1}^{n} p_{ij}^s = 1$. Figure 5.3 shows the relationship between P_{ij} and P_{hr}.

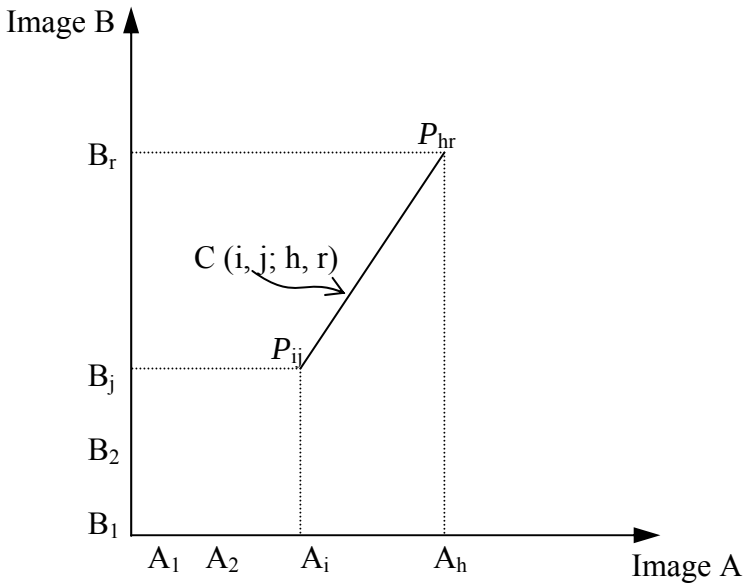

Figure 5.3. The illustration of the relationship between the parameters in the relaxation process

The compatible coefficient is defined as equation 5.5 and the updating value is given by equation 5.6. Equation 5.7 is used to update the matching probability after every iteration. It is expected that the final matching probability p_{ij} will be close to 1 if the pair (A_i, B_j) is a true pair; otherwise it will be close to 0.

$$C\ (i, j; h, r) = \min\left(\frac{d_{ih}}{d_{jr}}, \frac{d_{jr}}{d_{ih}}\right) \tag{5.5}$$

where d_{ih} is the Euclidean distance between A_i and A_h, and d_{jr} is the Euclidean distance between B_j and B_r.

$$q_{ij}^{l} = \frac{1}{m-1} \sum_{\substack{h=1 \\ h \neq i}}^{m} [\max_{\substack{1 \le r \le n \\ r \neq j}} (C(i, j; h, r)\, p_{hr}^{l})] \tag{5.6}$$

where q_{ij}^{l} is the support in the l^{th} iteration of all other pairs to the pair (A_i, B_j). Relative distance instead of absolute distance in the support function, which is more tolerate of geometric distortion was reported by Ton and Jain [1989].

$$p_{ij}^{l+1} = p_{ij}^{l} q_{ij}^{l} \tag{5.7}$$

An example of the probability relaxation process in the image matching is given in the following figures and tables: Figure 5.4 shows several control points detected in the reference image and the sensed image. Table 5.1 gives the coordinate values of the points in Figure 5.4. Table 5.2 shows the matching probability for different iterations. The initial probability is uniform that is 1/N (N is the number of feature points). From the iteration results, it can be found that the matching probability is close to 1 after 8 iterations.

(a) Reference image (b) Sensed image

Figure 5.4. The control points on the reference image and the sensed image

Table 5.1. The control points in the reference image and the sensed image

Reference Image		Sensed Image	
Point No.	**Coordinate(x, y)**	**Point No.**	**Coordinate(x, y)**
1	(648,1943)	1	(685,1939)
2	(1310,1801)	2	(1339,1795)
3	(757,1582)	3	(786,1578)
4	(665,2088)	4	(703,2085)
5	(716,2154)	5	(757,2153)
6	(800,2042)	6	(838,2039)
7	(939,1814)	7	(971,1810)

Table 5.2. The matching probability of several iterations (as percentage)

First iteration

	1	2	3	4	5	6	7
1	14	14	14	14	14	14	14
2	14	14	14	14	14	14	14
3	14	14	14	14	14	14	14
4	14	14	14	14	14	14	14
5	14	14	14	14	14	14	14
6	14	14	14	14	14	14	14
7	14	14	14	14	14	14	14

Second iteration

	1	2	3	4	5	6	7
1	27	6	8	14	16	17	9
2	10	29	18	12	13	8	7
3	10	16	27	10	10	11	14
4	15	6	6	29	23	16	5
5	15	7	7	21	28	15	6
6	19	5	8	16	16	28	7
7	14	9	17	8	10	9	31

Fifth iteration

	1	2	3	4	5	6	7
1	44	2	4	12	14	17	5
2	4	59	19	5	6	3	4
3	6	16	52	4	5	6	11
4	12	2	2	43	27	12	2
5	12	2	3	25	43	11	2
6	19	1	4	14	13	45	3
7	10	4	14	3	5	5	60

Eighth iteration

	1	2	3	4	5	6	7
1	100	0	0	0	0	0	0
2	0	100	0	0	0	0	0
3	0	0	100	0	0	0	0
4	0	0	0	100	0	0	0
5	0	0	0	0	100	0	0
6	0	0	0	0	0	100	0
7	0	0	0	0	0	0	100

5.2.5 Transformation function determination

A global polynomial mapping function cannot properly deal with images that have varying local distortions. The high resolution sensors often use the off-nadir mode to capture images, unlike moderate resolution sensors, which normally use a nadir mode. Figure 5.5 illustrates the local distortion caused by terrain relief. In Figure 5.5, P represents a point on the ground, A represents the location of P on an image captured in nadir mode, and B represents the location of P on an image captured in off-nadir mode

with angle θ. Assuming the height of P is h, the displacement can be calculated using equation 5.8.

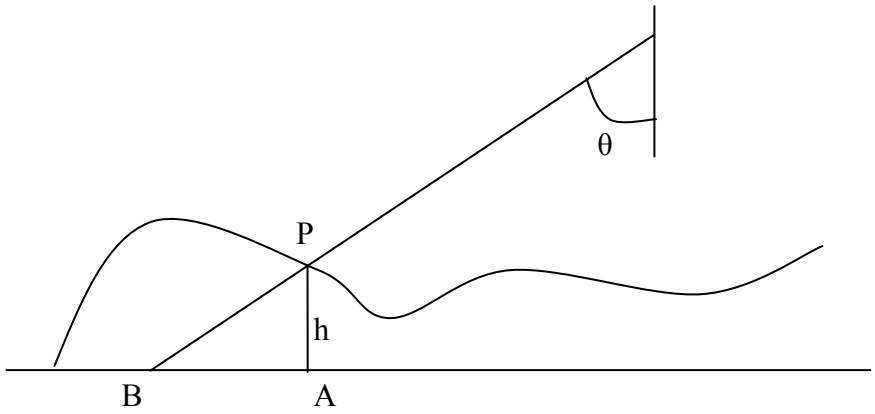

Figure 5.5. The displacement caused by the terrain relief

$$disp_{AB} = htg\theta \tag{5.8}$$

From equation 5.8, for an angle θ of 45^0, if h is 30 m (relief area), then $disp_{AB}$ is 30 m; while if h is 0 m (flat area), then $disp_{AB}$ is 0 m. That means for flat area there is no displacement, but in a relief area, there is a displacement; thus, in an image with both types of terrain areas, the relief area will have a local distortion, while the flat area will not. The elevation error also affects the geometric accuracy when elevation is used to correct the displacement caused by the terrain relief; one meter of elevation error is equal to one meter horizontal error, which is equal to an error of one pixel for IKONOS image or an error of 1.6 pixels for QuickBird images. The local distortion caused by the off-nadir angle cannot therefore be neglected in high resolution image.

A triangle-based local transformation is employed in the mapping function to reduce the local geometric distortion caused by the terrain relief. Every three neighbour

control points form a triangle in both the reference image and sensed image. Once the triangle mesh has been constructed for all the control points, the resample process can be performed on a triangle-by-triangle basis [ERDAS, 2002]; for every triangle, there is a set of transformation coefficients, unlike with the global polynomial transformation, which has only one set of transformation coefficients for the entire image. Linear transformation within a triangle is a fast and easy method. The equation is listed as follows.

$$\begin{aligned} x' &= a_0 + a_1 x + a_2 y \\ y' &= b_0 + b_1 x + b_2 y \end{aligned} \tag{5.9}$$

where (x', y') are the coordinates in the sensed image and (x, y) are coordinates in the reference image.

In Figure 5.6, the vertices represent matched control points in the sensed image and reference image. For a pixel (x, y) in a triangle of the reference image, the equation 5. 9 is used to find its corresponding position (x', y') in the sensed image and then the gray value of this position is used to fill the corresponding pixel (x, y) of resampled sensed image.

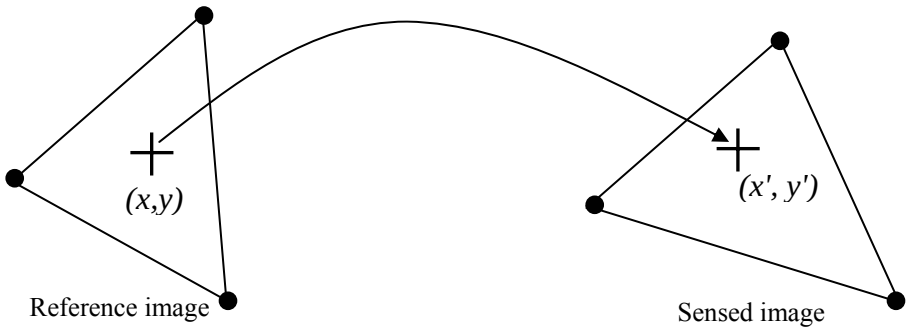

Figure 5.6. Illustration of the triangle-based resampling process

5.3 Experiment and results

In order to evaluate the proposed image registration algorithm, two data sets (Fredericton city, NB, Canada) are used to test the algorithm: one set consists of images from the same sensor but acquired at different times (two years difference, multitemporal data), while the other set consists of images from different sensors acquired in the same year (multisenor data). Details of the data sets are described in Table 5.3. These two data sets are especially selected to increase the degree of difficulty that the image registration algorithm will deal with. As known, multitemporal or multisensor data has radiometric differences because of time differences or sensor differences, these kinds of data are more difficult to process compared with the data acquired by the same sensor at same time [Bentoutou et al., 2005]. The terrain characteristic of the data is of moderate relief with buildings on a slope (Figure 5.7). For urban and sub-area areas, this study terrain has a certain representative, because most of the urban and sub-urban areas lie in the flat or moderate relief areas in order to be easy for people living, although there may be some urban areas lie in mountainous areas.

Table 5.3. Data used in this experiment

No.	Reference image	Sensed image	Resolution	Size
1 (IKONOS-IKONOS)	IKONOS panchromatic image (2002)	IKONOS panchromatic image (2000)	1m	2048X2048
2 (IKONOS-QuickBird)	IKONOS resampled panchromatic image (2002)	QuickBird multispectral image (2002)	2.8m	1024X1024

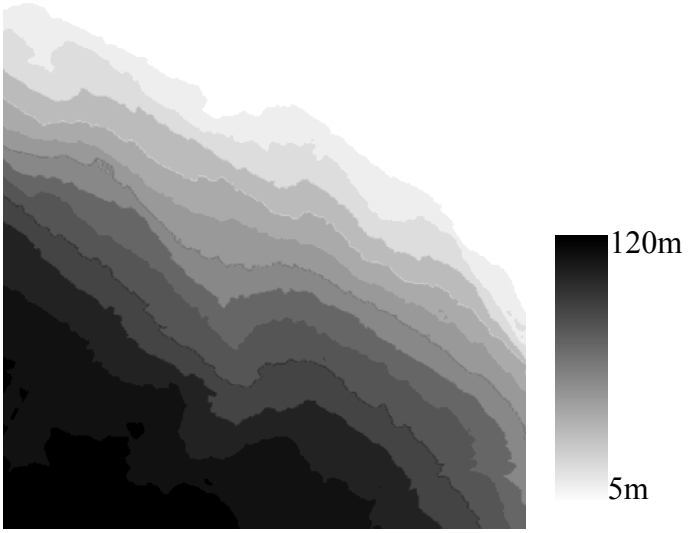

Figure 5.7. Terrain characteristic of the study area

A three level pyramid structure is employed in this experiment. For the second and third levels, a discrete wavelet transform with decimation mode is used to get the approximation image and a feature points' image; the feature points of first level are obtained by applying an "à trous" wavelet decomposition once. The normalized cross-correlation matching method is used to get initial matched feature points and the probability relaxation matching method is applied to refine the initially matched feature points. During the matching process, three thresholds can be set to control the number and accuracy of the feature points: the first is the value of acceptable maximum correlation coefficients, the second is for the window size for the normalized cross-correlation matching, and the third is the number of iterations for the probability relaxation matching. For the IKONOS-QuickBird case, the IKONOS panchromatic image is resampled to 2.8m to keep the same resolution as the QuickBird multispectral image. The details for the feature points for every pyramid level are listed in Table 5.4 and Table 5.5. A total of 101 feature pairs have been obtained in the IKONOS-IKONOS case, and 80 feature pairs in the IKONOS-QuickBird case.

Table 5.4. Feature point information (IKONOS-IKONOS case)

Level no.	File size (pixels)	Number of feature points		Number of initial matched pairs	Number of refined matched pairs
		Sensed image	Reference image		
3	512X512	1153	1142	79	25
2	1024X1024	1547	1495	159	35
1	2048X2048	6325	6251	290	101

Table 5.5. Feature point information (IKONOS-QuickBird case)

Level No.	File Size (pixels)	Number of feature points		Number of initial matched pairs	Number of refined matched pairs
		Sensed image	Reference image		
3	256X256	755	784	68	28
2	512X512	1156	1289	135	34
1	1024X1024	5986	6083	263	80

The registered results of these data sets are shown in Figure 5.8 (IKONOS-IKONOS) and Figure 5.9 (IKONOS-QuickBird). In Figure 5.8, (a) is the IKONOS image captured in 2000 (sensed image), (b) is the IKONOS image captured in 2002 year (reference image), (c) is the distribution of feature points and (d) is the final registered IKONOS image. In Figure 5.9, (a) is the multispectral QuickBird image captured in 2002 (sensed image), (b) is the IKONOS image captured in 2002 (reference image), (c) is the distribution of feature points and (d) is the final registered QuickBird multispectral image.

(a) IKONOS panchromatic image(2000)

(b) IKONOS panchromatic image(2002)

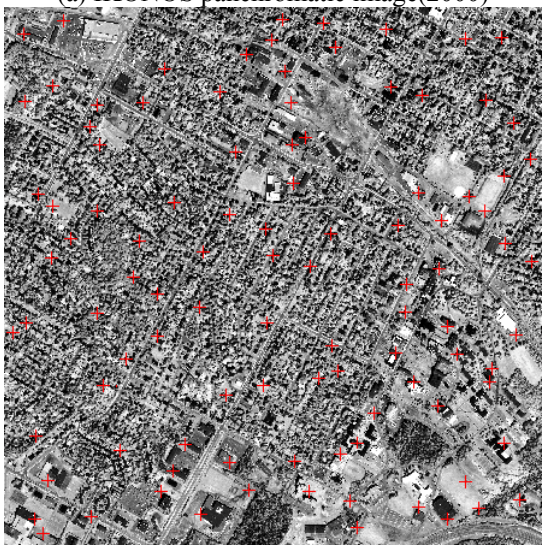

(c) feature points distribution

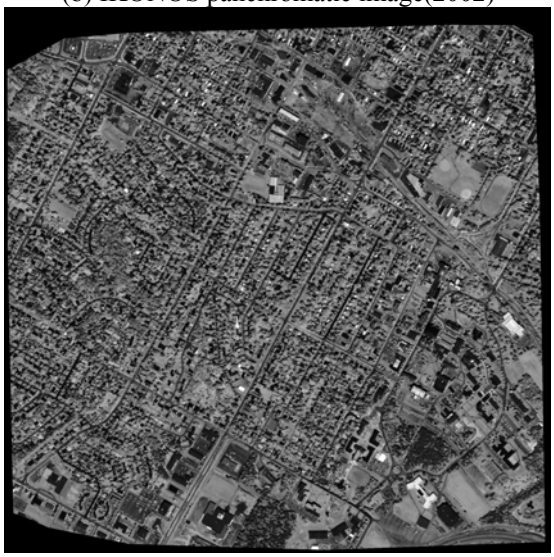

(d) registered image (2000)

Figure 5.8. The sensed image (a), the reference image (b), and the registered image (d) (IKONOS-IKONOS case)

(a) QuickBird multispectral image (2002)

(b) IKONOS image (2002)

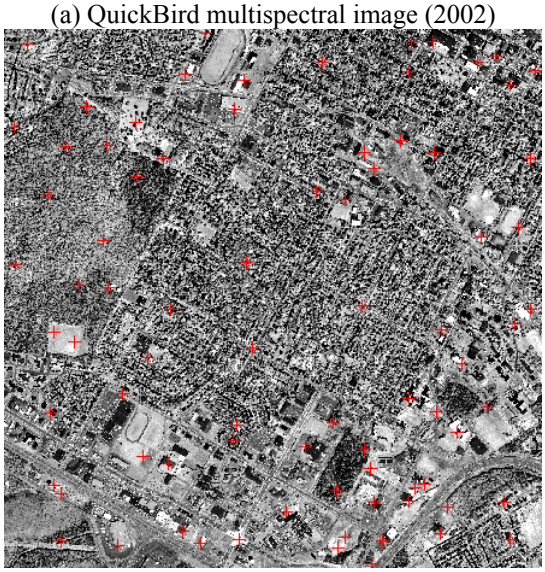

(c) feature points distribution

(d) registered QuickBird multispectral image

Figure 5.9. The original reference image, the sensed image and registered image (IKONOS-QuickBird case)

Two methods have been used to check the accuracy of final registered image. The first method is the visual analysis, to check the overlaid image between the reference image and the registered image. This is a fast and commonly used method. The second method is to measure manually selected check points across the image.

The results using triangle-based mapping function (TMF) are compared with those of a third order polynomial mapping function (PMF). Figure 5.10 shows the registered result analysis: (a) is the overlaid image between the registered image and the reference image, (b) is a subset of TMF at location I, (c) is a subset of PMF at location I, (d) is a subset of TMF at location II and (e) is a subset of PMF at location II. In the overlaid image (Figure 5.10 (a)), red area shows objects that exist in the reference image but not in the registered image, and green areas show objects that exist in the registered image but not in the reference image. Generally speaking, the registered image fits very well with the reference image; we cannot find the special red or green color across the overlaid image except for some small areas due to the temporal changes. In Figure 5.10 (c), it can be found that one road appears as red and green two colors, because these roads are not registered very well with PMF, while in Figure 5.10 (b) the same roads in the triangle-based registered result do not show any red or green, which means that the roads in the reference image and the registered image fit very well. The same difference can be seen when comparing for the location II (Figure 5.10 (d) and (e)).

However, it needs to be noted that on the top of buildings and trees, for example, at the location III, there are still some parallaxes in green around the building in the overlaid image due to the relief displacement of the buildings. This is a typical problem for the registration of high resolution images, which cannot be solved by an image to image registration algorithm, unless a true ortho-rectificaiton is applied. But the same problem does not occur in the moderate resolution image.

Figure 5.11 shows the result analysis for IKONOS-QuickBird case. In this analysis, the red band of the QuickBird multispectral image is overlaid with the reference image. In Figure 5.11 (a), red shows objects that exist in the reference image but not in the registered image; green shows objects that exist in the registered image but not in the reference image. The color of the overlaid image is different from the previous case, because these images are from two different sensors. There is a great difference between the spectral ranges of the two bands resulting in color difference in vegetation. Thus, when the images are overlaid, it appears to have a large change in vegetation. To analyze the result, vegetation should be disregarded; the color of terrain objects is still similar to previous case. From Figure 5.11 (a), it can be seen that there is no more red or green around terrain features, such as roads, open areas and parking lots, which means that the two images are very well registered. Figure 5.11 (c) is a subset of location I in the registered image, it can be seen that the roads appear red and green two colors, and they seem to be two different roads in the overlaid image, due to the registration errors of the PMF. In Figure 5.11 (b), however, we cannot see red and green roads, because the roads they register very well with TMF. The same to the location II when we compare Figure 5.11 (d) and (e).

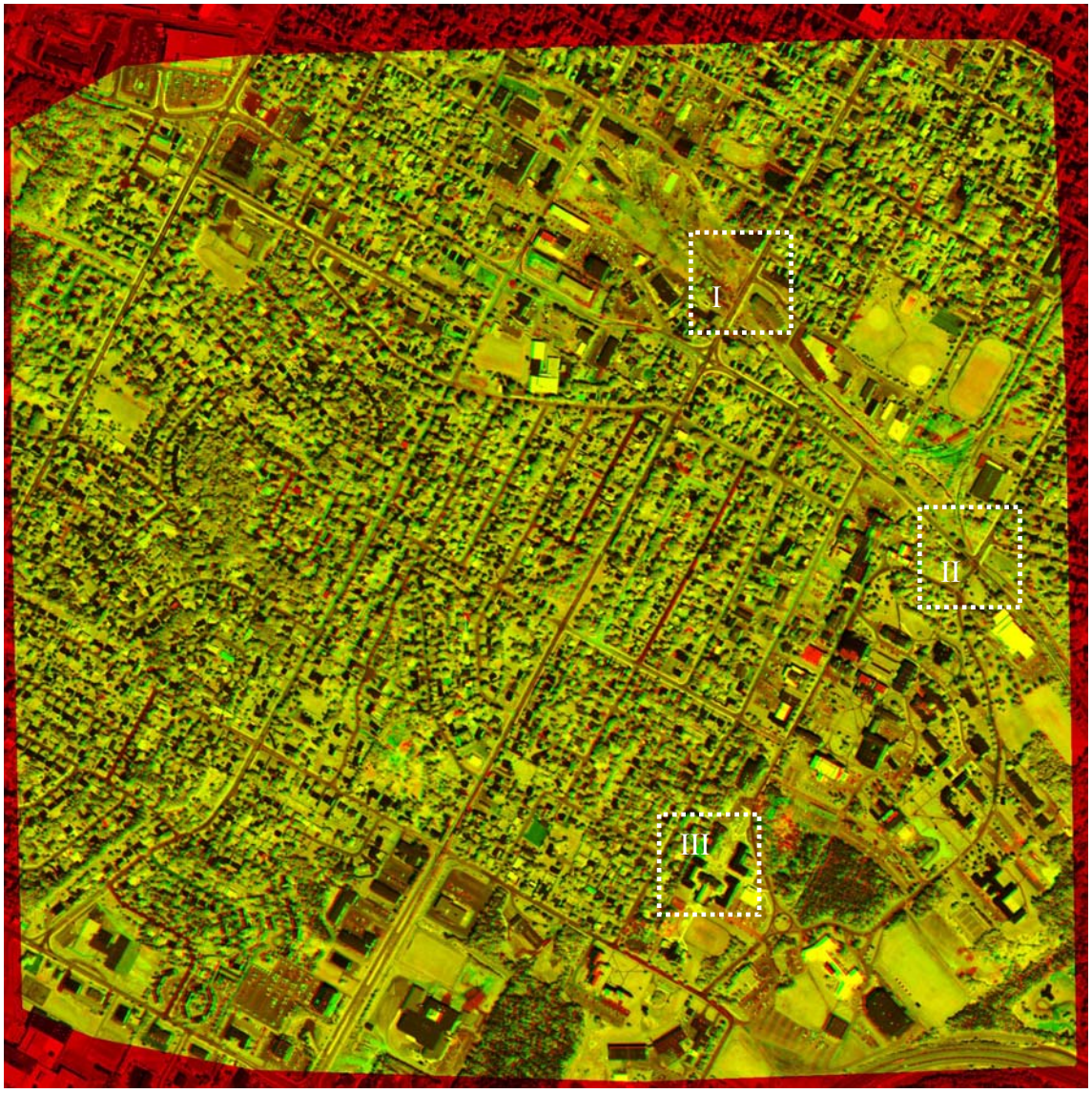

(a) Overlay of the reference image and the registered image

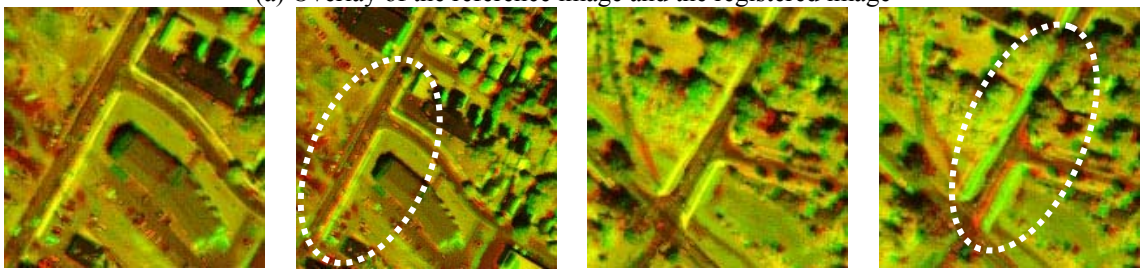

(b)TMF(I) (c) PMF (I) (d) TMF (II) (e) PMF(II)

Figure 5.10. Comparison of registered results (IKONOS-IKONOS case)

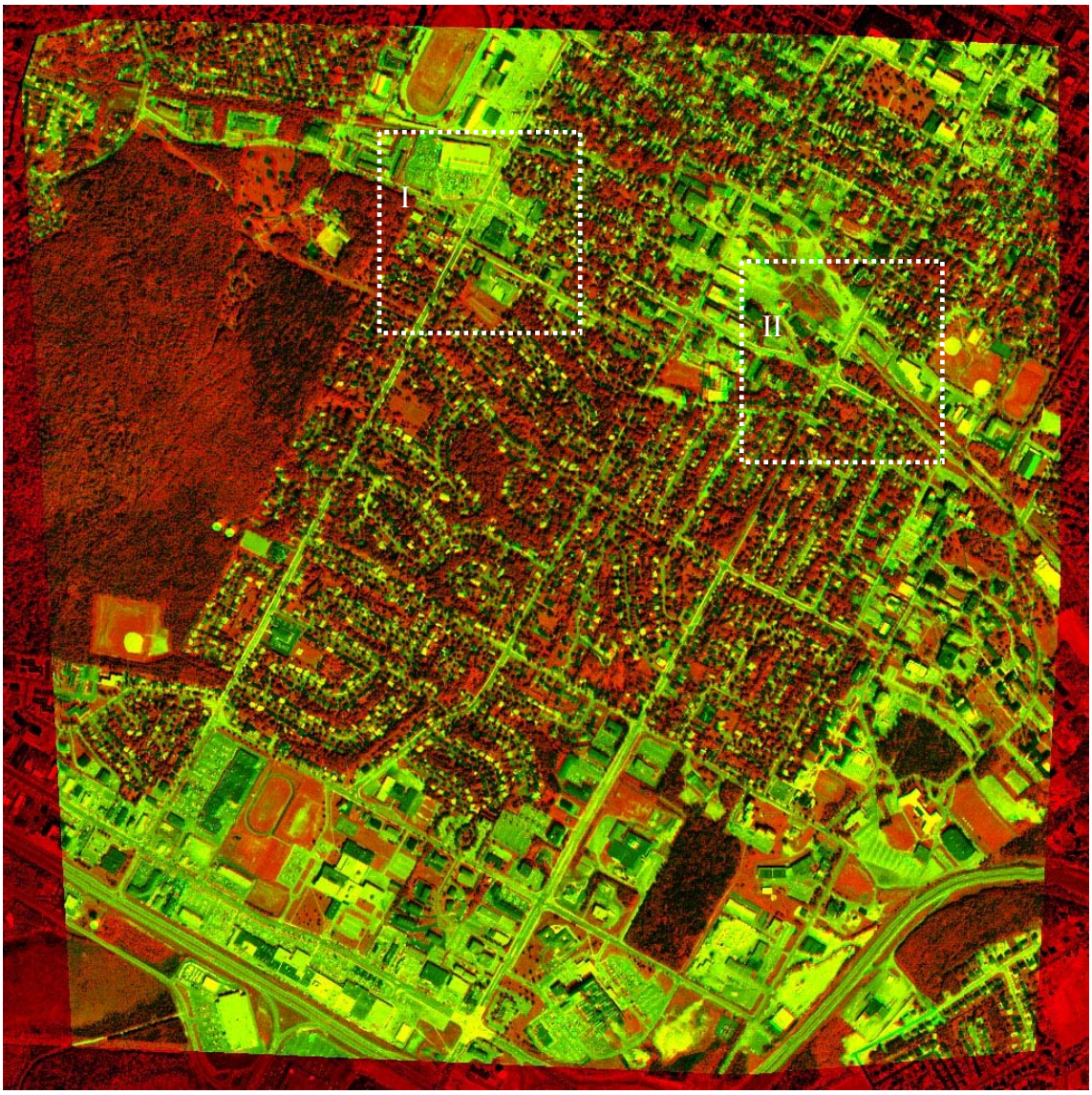

(a) Overlay of the reference image with one band of the registered image

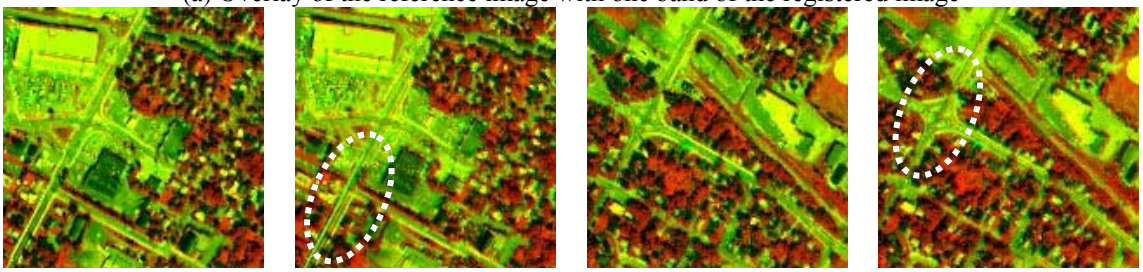

(b)TMF(I) (c) PMF (I) (d) TMF (II) (e) PMF(II)

Figure 5.11. Comparison of registered results (IKONOS-QuickBird case)

The registered results have also been analyzed by manually selecting checking points evenly distributed across the images. Figure 5.12 shows the Root Mean Square (RMS) error of the registered images for two cases. The triangle-based registration results also are compared with those of first order, second order and third order polynomial transformation results. For the IKONOS-QuickBird case, the RMS error of the result using triangle-based method is 0.95 pixels, which is the lowest RMS error, and the highest error, 2.47 pixels, is associated with first order polynomial transformation. For the IKONOS-IKONOS error, the smallest RMS error is 3.21 pixels (for the triangle-based mapping method), and the highest is 5.13 pixels (for first order polynomial transformation).

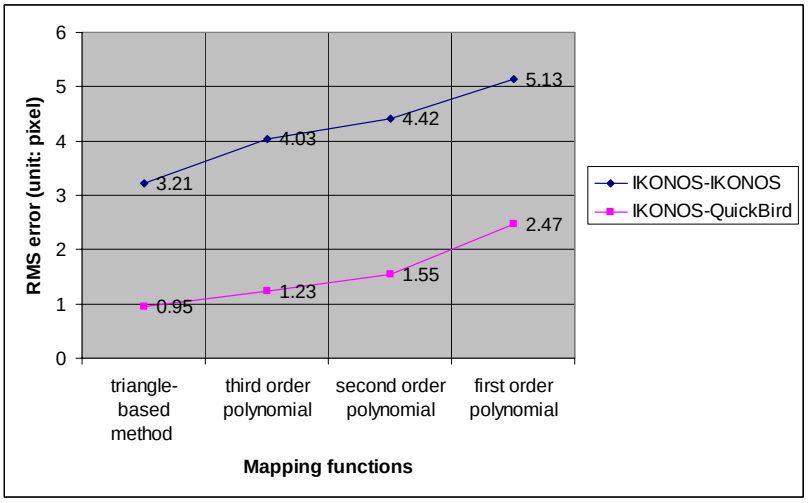

Figure 5.12. RMS error comparison of the registered images
(The spatial resolution for IKONOS-QuickBird case : 4m; for IKONOS-IKONOS case: 1m)

5.4 Conclusion

This study has proposed a new image registration algorithm based on the wavelet multiresolution feature extraction techniques. It integrates a discrete wavelet transform (decimate mode) and a redundant wavelet transform ("à trous") into one image registration process. The discrete wavelet transform with decimate mode is used to generate a pyramid structure and locate feature points in each level; the "à trous" wavelet is used to obtain the feature points at highest level, and to keep the shift-invariant property of the feature points, which is however a problem when discrete wavelet transform with decimate mode is used. Normalized cross-correlation and probability relaxation matching techniques are used to find similarity between feature points in the reference image and sensed image.

Two data sets are used to evaluate this method: one set is from the same sensor but captured in different years (two years difference), and the other set is from different sensors captured in the same year. The results of the proposed method are compared with results generated by using first order, second order, and third order polynomial transformations; in both cases of comparison, the RMS errors of the triangle-based resigtration are the smallest. The experiments demonstrated that the proposed method can provide improved registration results and resolve the following problems existing in the registration of high resolution images using traditional image registration techniques: (1) manually selecting a large number of control point pairs, (2) high volume data, and (3) local distortion existing in different sensors and different temporal images. However, it has also been noticed that the relief displacement of individual above-ground objects,

such as buildings and trees, cannot be solved by the proposed method. To solve this problem, a true ortho-rectification technique may have to be used.

ACKNOWLEDGMENTS

This research was supported by the GEOIDE Network (Geomatics for Informed Decisions) of Canada under the project MNG#TAO. The authors would like to thank Mr. Rob Lunn, GIS supervisor of the City of Fredericton, NB, Canada, for providing the IKONOS and QuickBird multispectral and panchromatic images.

REFERENCES

Bentoutou Y., N.Taleb, K.Kpalama and J. Ronsin (2005) "An automatic image registration for applications in remote sensing." *IEEE Trans. on Geoscience and Remote Sensing*, Vol.43, No.9, pp.2127-2137.

Brown, L.G. (1992). "A survey of image registration techniques." *ACM Computing Surveys*, Vol. 24, No. 4, pp. 325-376.

Cideciyan, A.V., S.G. Jacobson, C.M. Kemp, R.W. Knighton and J.H. Nagel (1992). "Registration of high resolution images of the retina." *Proceedings of the SPIE-The International Society for Optical Engineering, Medical Imaging VI. Image processing*, 1652. pp.310-322.

Dai, X.L., and S. Khorram (1999). "A feature-based image registration algorithm using improved chain code representation combined with moment invariants." *IEEE Trans. on Geoscience and Remote Sensing*, Vol.37, No.5, pp. 2351-2362.

Djamdji, J.P., A. Bijaoui, and R. Maniere (1993). "Geometrical registration of images, the multiresolution approach." *Photogrammetric Engineering and Remote Sensing*, Vol.59, No.5, pp.645-653.

ERDAS. (2002). *"ERDAS Field Guide™."* Fifth Edition, ERDAS Inc, Atlanta, Georgia, pp. 251.

Fang, Y.H. (2000). *The study of stereo image matching and DTM automatic generation.* PH.D dissertation, Institute of Zhengzhou Surveying and Mapping.

Flusser, J., and T. Suk (1994). "A moment-based approach to registration of images with affine geometric distortion." *IEEE Trans. Geoscience and Remote Sensing*, Vol.32, No.2, pp.382–387.

Fonseca, L., and B.S. Manjunath (1996). "Registration techniques for multisensor remotely sensed imagery." *Photogrammetric Engineering and Remote Sensing*, Vol. 62, No. 9, 1996.

Fonseca, L.M.G., and M.H. Costa, (1997) "Automatic Registration of Satellite Images." *Brazilian Symposium on Graphic Computation and Image Processing, 10, Campos de Jordão, 1997.Proceedings*. Los Alamitos: IEEE Computer Society, 1997. pp. 219-226.

Goshtasby, A., G. Stockman, and C. Page (1986). "A region-based approach to digital image registration with subpixel accuracy." *IEEE Transactions on Geoscience and Remote Sensing*, Vol.24, No.3, pp. 390-399.

Habib, A., Y. Lee and M. Morgan (2003). "Automatic matching and three-dimensional reconstruction of free-form linear features from stereo images." *Photogrammetric Engineering and Remote Sensing*, Vol. 69, No. 2, pp.189-197.

Inglada, J. and A. Giros (2004). "On the possibility of automatic multisensor image registration". *IEEE Transaction on Geoscience and Remote Sensing*, Vol. 42, No.10, pp.2104-2120.

Li, H, B.S. Manjunath, and S.K. Mitra (1995). "A contour-based approach to multisensor image registration." *IEEE Trans. Image Processing*, Vol.4, pp. 320-334.

Liao, M., H. Lin and Z. Zhang (2004). "Automatic registration of InSAR data based on least-squares matching and multi-step strategy." *Photogrammetric Engineering and Remote Sensing,* Vol.70, No.10, pp.1139-1144.

Mallat, S.G. (1989). "A theory for multi-resolution signal decomposition. The wavelet representation." *IEEE Transactions on Pattern Analysis and Machine Intelligence,* Vol.2, No.7, pp. 674-693.

Mallat, S.G. and W.H. Hwang (1992). "Singularity detection and processing with wavelets." *IEEE Transactions on Information Theory*, Vol.38, No.2, pp. 617–643.

Medioni, G. and R. Nevatia (1984). "Matching images using linear features." *IEEE Trans. on Pattern Analysis and Machine Intelligence*, Vol.6, No.6, pp. 675-685.

Moigne, J.Le., W.J. Campbell, and R.F. Cromp (2002). "An automated parallel image registration technique of multiple source remote sensing data." *IEEE Trans. on Geoscience and Remote Sensing*, Vol.40, No.8, pp.1849-1864.

Rignot, E.J.M., R. Kowk, J.C. Curlander, and S. Pang (1991). "Automated multisensor registration, requirements and techniques." *Photogrammetric Engineering and Remote Sensing*, Vol.57, pp. 1029-1038.

Rosenfeld, A. and A.C. Kak (1982). *Digital Picture Processing*, Vol. I and II, Academic Press, Orlando, FL.

Schenk, T. (1999). *Digital Photogrammetry (volume I).* Ed. TerraScience, Laurelville, Ohio, pp. 232-295.

Shi, W.Z and A. Shaker (2006). "The Line-Based Transformation Model (LBTM) for image-to-image registration of high-resolution satellite image data." *International Journal of Remote Sensing,* Vol. 27, No. 14, pp. 3001–3012.

Simhadri, K.K., S.S. Iyengar and R.J. Holyer (1998). "Wavelet-based feature extraction from oceanographic images." *IEEE Transactions on Geoscience and Remote Sensing*, Vol.36, No.3, pp.767-778.

Ton, J. and A.K. Jain (1989). "Registering Landsat images by point matching." *IEEE Trans. Geoscience and Remote Sensing*, Vol. 27, No. 5, pp. 642-651.

Townshend, J.R.G., C.O. Justice, C. Gurney, and J. McManus (1992). "The impact of misregistration on change detection." *IEEE Transaction on Geosience and Remote Sensing*, Vol. 30, No.5, pp.1054-1060.

Ventura, A.D., A. Rampini, and R. Schettini (1990). "Image registration by recognition of corresponding structures." *IEEE Trans. Geoscience and Remote Sensing*, Vol. 28, No. 3, pp. 305-314.

Zavorin, I., and J. Le Moigne (2005). "Use of multiresolution wavelet feature pyramids for automatic registration of multisensor imagery." *IEEE Transactions on Image Processing*, Vol. 14, No. 6, pp. 770-782.

Zhang, C. and C.S. Fraser (2005). "Automated registration of high resolution satellite imagery for change detection." *ISPRS Hannover Workshop 2005 -High- Resolution Earth Imaging for Geospatial Information*, Hannover, Germany,May 17-20, 2005.

Zhang, Z., J. Zhang, M. Liao and L. Zhang (2000). "Automatic registration of multi-source imagery based on global image matching." *Photogrammetric Engineering and Remote Sensing,* Vol.66, No.5, pp.625-629.

Zheng, Q. and R. Chellappa (1993). "A computational vision approach to image registration." *IEEE Transaction on Image Processing*, Vol. 2, No. 3, pp. 311–326.

Zitova, B., and J. Flusser (2003). "Image registration methods: a survey." *Image and Vision Computing*, Vol. 21, No. 11, pp. 977-1000.

Chapter 6. A COMPARATIVE STUDY ON RADIOMETRIC NORMALIZATION USING HIGH RESOLUTION SATELLITE IMAGES[♣]

ABSTRACT

Remotely sensed multitemporal, multisensor data are often required in Earth observation applications. A common problem associated with the use of multisource image data is the grey value differences caused by non-surface factors such as different illumination, atmospheric, or sensor conditions. Such differences make it difficult to compare images using same color metric system. Image normalization is required to reduce the radiometric influences caused by non-surface factors and to ensure that the grey value differences between temporal images reflect actual changes on the surface of the Earth.

A variety of image normalization methods, such as pseudoinvariant features (PIF), dark and bright set (DB), simple regression (SR), no-change set determined from scattergrams (NC), and histogram matching (HM), have been published in scientific journals. These methods have been tested with either Landsat TM data, MSS data or both, and test results differ from author to author. However, whether or not existing methods could be adopted for normalizing high resolution multispectral satellite images,

[♣] This chapter has been accepted for publication in the [*International Journal of Remote Sensing*]

Hong G., Y. Zhang (2006). "A comparative study on radiometric normalization using high resolution satellite images." *International Journal of Remote Sensing*, in press, 2006.

such as IKONOS and QuickBird, is still open for discussion because of the dramatic change in spatial resolution and the difference of available multispectral bands. In this research, the existing methods are introduced and employed to normalize the radiometric difference between IKONOS and QuickBird multispectral images taken in different years. Some improvements are introduced to the existing methods to overcome problems caused by band difference and to achieve more stable and better results. The normalized results are compared in terms of visual inspection and statistical analysis. This paper examined whether or not existing methods can be directly adopted for image normalization with high resolution satellite images, and showed how these methods can be modified for use with such images.

Keywords: multitemporal, multisensor, image normalization, high-resolution

6.1 Introduction

Remotely sensed data is an effective source of information for monitoring changes in land use and land cover. With the advent of increasingly higher resolution remote sensing images, it is possible to precisely monitor changes in an urban area. In automatic change detection process, radiometric normalization and geometric registration of the temporal images are the first two operations that must be performed on the images. Both these operations affect the final accuracy of change detection. Geometric registration transforms the different temporal or sensor images into a common geometric coordinate system, while radiometric normalization unifies the color information into the same metric system. After image normalization, the images have the same color metric system;

thus, they have the same comparability metric. It can be more difficult to quantify and interpret changes on multitemporal images under different illumination, atmospheric, or sensor conditions without radiometric calibration. Although many changes can be detected without applying a radiometric calibration, in order to identify automatically what the detected changes are, even in a general sense, image normalization is required [Chavez and Mackinnon, 1994].

There are two kinds of image radiometric normalization: absolute and relative. Absolute normalization needs sensor parameters, atmospheric refraction parameters and other data that are difficult to obtain after satellite data acquisition. Absolute normalization is generally performed at the satellite data receiving ground station before satellite data is released.

The relative approach to radiometric correction, known as relative radiometric normalization, is preferred because no *in situ* atmospheric data at the time of satellite overpasses are required [Yang and Lo, 2000]. Relative radiometric normalization is a method of correction that applies one image as a reference and adjusts the radiometric properties of subject images to match the reference [Hall et al., 1991; Yuan and Elvidge, 1996]. Thus, normalized images appear to have been acquired with the reference image sensor under atmospheric and illumination conditions equal to those in the reference scene [Hall et al., 1991]. From the above descriptions, a key difference between the methods is that absolute normalization removes atmospheric errors that exist in both images, while relative normalization does not actually remove atmospheric errors. The subject image keeps the same atmospheric errors as the reference image. A variety of papers are available on image normalization methods [Schott et al., 1988; Eckhard et al.,

1990; Hall et al., 1991; Elvidge et al., 1995; Yuan and Elvidge, 1996; Heo and FitzHugh, 2000]. Yang and Lo [2000] and Yuan and Elvidge [1996] reviewed existing image normalization methods.

IKONOS and QuickBird are two popular types of high resolution satellite images. They are often used in monitoring land use and land cover and are often used together. In such cases, the matter of comparability and continuity between QuickBird and IKONOS is important for many monitoring-related applications. A drawback in combining QuickBird and IKONOS for monitoring applications is that most published papers on image normalization are based on Landsat TM or MSS data. Also, there exists other problems because of satellite sensor difference: first, most of publications were discussing the same sensor data, in this study, we discuss image normalization between different sensors; second, the high resolution causes problem in the PIF methods which didn't happen in Landsat TM or MSS cases; third, there is no publication coefficients for Tasseled Cap Transformation which is required in the DB method; and fourth, the NC method requires two near-infrared bands, while for IKONOS or QuickBird, there is only one near-infrared band. The purpose of this study is to find strategies and methods that can resolve these problems and can be effective in normalizing IKONOS images using QuickBird as a reference. The strategies employed in this study used existing image normalization methods based on spectral comparability and continuity between the IKONOS and QuickBird images. This paper examines if existing methods can be directly used for normalizing high resolution satellite images. This paper also describes how these existing methods can be modified so that they are suitable for use with such images.

6.2 Existing radiometric normalization methods

Image normalization methods can be classified into three general categories: statistical methods (i.e. standard deviation method); the histogram matching method; linear regression methods (i.e. PIF, DB, NC, etc.). Most existing normalization methods are based on simple linear regression. In order to clarify use of the term "image normalization" in this paper (except it relates to histogram matching method), the term "image normalization" means normalization based on linear regression methods.

6.2.1 The mathematical equation for image normalization

Casseles and Garcia [1989] verified the linear relationship between reference image and subject image. The linear relationship can be described using the following equation:

$$Y\_m = a_m X\_m + b_m \quad (6.1)$$

where Y_m is the band m of the reference image Y, X_m is the band m of the subject image, a and b are normalization coefficients, m is the band number of the image. In this equation, the subject image X is normalized by the reference image Y.

Image normalization can be divided into two steps: (1) selecting normalization targets; and (2) determining normalization coefficients.

6.2.2 Normalization target selection

Several methods have been introduced by different authors showing how to select ideal targets for estimating the normalization transformation coefficients [Schott et al., 1988; Eckhard et al., 1990; Hall et al., 1991; Elvidge et al., 1995]. In general, for all normalization methods, the targets that meet the following criteria are selected as ideal targets for normalization [Eckhardt et al., 1990]:

(1) The targets should be approximately at the same elevation so that the thickness of the atmosphere over each target is approximately the same;

(2) The targets should contain only minimal amounts of vegetation because vegetation spectral reflectance is subject to change over time;

(3) The targets must be in relatively flat areas so that changes in the sun angle between images will produce the same proportional increase or decrease in insolation to all normalization targets;

(4) When viewed on the image display screen, the patterns on the normalization targets should not change over time; and

(5) A set of targets must have a wide range of grey values for the regression model to be reliable.

6.2.3 Typical normalization methods

(1) Simple Regression (SR) method

Simple regression normalization [Jensen, 1983] uses least-squares to derive the normalization coefficients, which can be acquired using the following equation:

$$a_m = \frac{v_{X\_mY\_m}}{v_{X\_mX\_m}}, \qquad b_m = \overline{Y}\_m - a_m \overline{X}\_m \tag{6.2}$$

where $\overline{Y}\_m$ and $\overline{X}\_m$ are the means of band m in reference image Y and subject image X, $v_{X\_mY\_m}$ is the covariance of band m in the reference image Y and subject image X, and $v_{X\_mX\_m}$ is the variance of band m in the subject image X.

(2) Histogram Matching (HM) method

Histogram matching is a common image processing procedure for radiometric enhancement. It uses the reference image histogram to modify the subject image histogram in order to make the subject image histogram distribution similar to reference image histogram distribution. Histogram match is a process of determining a look up table that will convert the histogram of one image to resemble that of another. It is a useful technique for matching image data of the same scene acquired at different dates with slightly different sun angles or atmospheric effects [Yang and Lo, 2000]. Chavez and Mackinnon [1994] applied the histograms of the reference to normalize the subject images for automatic detection of vegetation changes in the southwestern United States.

(3) Pseudoinvariant Feature (PIF) method

Scott et al. [1988] presented pseudoinvariant feature normalization, which analyzed the elements whose reflection distribution is statistically invariant, such as concrete, asphalt and rooftops. These elements are assumed not to have any significant change between two acquisition dates. Differences in the gray-level distributions of

these invariant objects are assumed to be linear and are corrected statistically to perform the normalization.

The equation for solving the normalization coefficients is as follows:

$$a_m = \frac{\delta^{PIF}_{X\_m}}{\delta^{PIF}_{Y\_m}}, \qquad b_m = \overline{Y}^{PIF}_{\_m} - a_m \overline{X}^{PIF}_{\_m} \tag{6.3}$$

where $\delta^{PIF}_{X\_m}$ and $\delta^{PIF}_{Y\_m}$ are standard deviations of the selected pseudoinvariant feature set in band m of the reference image Y and subject image X, and $\overline{Y}^{PIF}_{\_m}$ and $\overline{X}^{PIF}_{\_m}$ are their corresponding means.

(4) Dark-Bright (DB) method

Hall et al. [1991] used the average of a set of dark and bright pixels (dark-bright set-simply called DB), which are extracted from the subject and reference image through Kauth-Thomas greenness-brightness transformation, to derive the normalization coefficients. It is assumed that an image always contains at least some pixels that have the same average surface reflectance among images acquired at different dates.

The normalization coefficients can be solved using the follow equation:

$$a_m = \frac{\overline{Y}^{(b)}_{\_m} - \overline{Y}^{(d)}_{\_m}}{\overline{X}^{(b)}_{\_m} - \overline{X}^{(d)}_{\_m}}, \qquad b_m = \overline{Y}^{(d)}_{\_m} - a_m \overline{X}^{(d)}_{\_m} \tag{6.4}$$

$\overline{Y}^{(b)}_{\_m}, \overline{Y}^{(d)}_{\_m}, \overline{X}^{(b)}_{\_m}$ and $\overline{X}^{(d)}_{\_m}$ are the means of the dark set (d) and bright set (b) of band m in the reference and subject images respectively.

(5) No Change Set (NC) method

Elvidge et al. [1995] developed a radiometric normalization method, which locates the statistical centers for stable land and stable water data clusters using the near-infrared date 1 versus date 2 scattergrams to establish an initial regression line. The near-infrared data were used because at these wavelengths the spectral clusters for water and land are clearly separated, and a distinct axis of "no change" can be observed. A no-change set is determined by placing thresholds about the initial line. Pixels falling within the no-change region will be used in the regression analysis of each band to compute normalization coefficients for them.

The normalization coefficients are derived from the following equations:

$$a_m = \frac{v^{NC}_{X\_m Y\_m}}{v^{NC}_{X\_m X\_m}}, \qquad b_m = \overline{Y}^{NC}_{\_m} - a_m \overline{X}^{NC}_{\_m} \tag{6.5}$$

where $\overline{Y}^{NC}_{\_m}$ and $\overline{X}^{NC}_{\_m}$ are the means of NC sets in band m of reference image Y and subject image X; $v^{NC}_{X\_m Y\_m}$ is the covariance of NC sets in band m of reference image Y and subject Image X, $v^{NC}_{X\_m X\_m}$ is the variance of NC sets in band m of subject X.

6.2.4 Pros and Cons of existing methods for Landsat TM or MSS

The SR method uses all pixels in both images to calculate the normalization coefficients. It works well if there are no big changes between the two satellite data acquisition dates. For this method, the accuracy of geometric registration will affect the normalized image accuracy.

Similar to the SR method, the HM method uses all pixels in every band of both images in calculating the normalization coefficients. It is useful for matching data for the same scenes acquired on different dates that have small differences in grey values. The final normalized image accuracy will be affected by the geometric registration accuracy.

The PIF method can overcome limitations of the SR method and the HM method. Normalized objects are not limited to the grey value differences caused by small changes in the sun angle and atmosphere. Accuracy of geometric registration will not affect the normalized image accuracy. The PIF method needs human intervention to extract the pseudoinvariant feature set.

The DB method was proposed to improve the PIF method. Similar to the PIF method, the DB method also does not require the subject and reference pixels to be exactly geometrically registered. In implementing this method, appropriate threshold values are required to obtain the dark and bright pixel sets. However, it is difficult to obtain them automatically.

According to Elvidge et al. [1995], the NC method can:

(1) reduce cloud, shadow, and snow effects compared with the SR method;

(2) use a large percentage of the total number of image pixels;

(3) distribute normalization error among different land-cover types;

(4) eliminate the necessity of identifying bright and dark radiometric control pixels;

(5) accelerate the speed of the normalization procedure.

The limitations of this method are:

(1) it requires the presence of both land and water areas in the satellite images;

(2) imagery is acquired under similar solar illumination geometries and similar phenological conditions;

(3) no changes take place in land cover for a large portion of the land between the subject image and the reference image.

Using the mean square error calculation as the statistical measure of the goodness of fit between the reference image and subject image, Yuan and Evlidge [1996) evaluated some methods and ranked the methods in descending order of NC, DB, SR, and PIF. From visual inspection, the NC method is the best and PIF is the worst compared with the reference image. No single approach has universal application because solutions are independent of location, application and image. Analysts must, therefore, be aware of existing procedures and be prepared to use or adapt these, or develop alternative procedures, as appropriate [Heo and Fitzhugh, 2000].

6.3 Normalization of the IKONOS image with the QuickBird image

6.3.1 Image data

Two datasets were used in this study: IKONOS data which was acquired on July 21, 2000; and QuickBird data which was acquired on Aug 2, 2002. All images were scaled to 16 bits. The resolution of multispectral IKONOS images and QuickBird images are 4m and 2.8m respectively.

6.3.2 Image registration

Multispectral IKONOS images and multispectral QuickBird images do not cover the same geographic area completely. IKONOS covers a larger area than does QuickBird. In the change detection process, the higher is the resolution, the better is the result. Therefore, the QuickBird image was used as the reference image, and the IKONOS image was used as the subject image. The final registered IKONOS image was resampled to 2.8m. Forty- two control points were selected. Those control points are distributed evenly throughout the whole image (listed in figure 6.1). Second order polynomial equation was used as the mathematical model in the image registration process (the equation is listed in Equation (6.6)). Both RMS errors, one of which is in the X direction and the other of which is in the Y direction, were less than 1 pixel. Nearest neighbour resampling method was used to resample the subject image in order to maintain the original spectral characteristic of the images.

$$\begin{aligned} x' &= b_0 + b_1 x + b_2 y + b_3 xy + b_4 x^2 + b_5 y^2 \\ y' &= g_0 + g_1 x + g_2 y + g_3 xy + g_4 x^2 + g_5 y^2 \end{aligned} \tag{6.6}$$

x' and y' are the coordinates in the uncorrected image generated from the referenced matrix system (x, y) coordinates.

Figure 6.1. The distribution of control points in reference image-QuickBird

6.3.3 Image normalization - difficulties and new solutions

The Landsat TM, MSS, IKONOS and QuickBird image wavelength and spatial resolution are listed in Table 6.1, Table 6.2, Table 6.3 and Table 6.4 respectively. From these tables, it can be easy to find that there exist differences between these satellite images.

Table 6.1. Landsat TM image wavelength and resolution

Band	Wavelength Region (μm)	Resolution (m)
1	0.45-0.52 (blue)	30
2	0.52-0.60 (green)	30
3	0.63-0.69 (red)	30
4	0.76-0.90 (near-IR)	30
5	1.55-1.75 (mid-IR)	30
6	10.4-12.5 (thermal-IR)	120
7	2.08-2.35 (mid-IR)	30

Table 6.2. MSS image wavelength and resolution

Band	Wavelength Region (μm)	Resolution (m)
1	0.5-0.6 (green)	80
2	0.6-0.7 (red)	80
3	0.7-0.8 (red - near-IR)	80
4	0.8-1.0 (near-IR)	80

Table 6.3. IKONOS image wavelength and resolution

Band	Wavelength Region (μm)	Resolution (m)
1	0.445–0.516(Blue)	3.2 m (nadir), 4 m (26^0 off-nadir)
2	0.506–0.595(green)	3.2 m (nadir), 4 m (26^0 off-nadir)
3	0.632–0.698(red)	3.2 m (nadir), 4 m (26^0 off-nadir)
4	0.757–0.853(near infrared)	3.2 m (nadir), 4 m (26^0 off-nadir)
Pan	0.526–0.929	0.82 m (nadir), 1m (26^0 off-nadir)

Table 6.4. Quickbird image wavelength and resolution

Band	Wavelength Region (μm)	Resolution (m)
1	0.450–0.520(Blue)	2.44 m (nadir), 2.88 m (25^0 off-nadir)
2	0.520–0.600(green)	2.44 m (nadir), 2.88 m (25^0 off-nadir)
3	0.630–0.690(red)	2.44 m (nadir), 2.88 m (25^0 off-nadir)
4	0.760–0.900(near infrared)	2.44 m (nadir), 2.88 m (25^0 off-nadir)
Pan	0.450–0.900	61 cm (nadir), 72 cm (25^0 off-nadir)

Due to differences in spatial resolution, spectral band and radiometric resolution between Landsat and IKONOS/QuickBird images, not all the existing methods can be directly applied to the normalization of IKONOS or QuickBird images. For example, high resolution images, (i.e. IKONOS, QuickBird) can reflect more detailed information of objects on the ground compared with low spatial resolution images. For instance, water bodies are generally used as pseudoinvariant objects in selecting normalization targets. Small objects floating on the water cannot not be recognized by Landsat or MSS, while these objects would most likely be detected by high resolution images such as IKONOS or QuickBird. Since these floating objects would be still counted as pseudoinvariant objects in low resolution images, but could not be counted as pseudoinvariant objects in high resolution images, more procedures are required to remove them, the detail descriptions have been given in the following PIF method

implementation. Also, the NC method requires two near-infrared bands to determine normalization coefficients in previous publication case [Elvidge et al., 1995]. However, only one near-infrared band is available in the new high resolution multispectral data sets, such as IKONOS and QuickBird. There also exist some problems for the DB method, because it requires Tasseled Cap Transformation step before collecting Dark set and Bright set, but there is only publication paper about experimental coefficients for IKONOS [Horne, 2003], and there is no publication paper about experimental coefficients for QuickBird. Therefore, difficulties were incurred during the testing of normalization methods. Some modifications were made to the existing methods so that they would be suitable for use with IKONOS/QuickBird data. The detailed implementation of each method for normalizing IKONOS and QuickBird data are described below:

(1) The SR method and the HM method

The SR method and the HM method both use all pixels of the reference image and subject image in the normalizing image process. No complicated normalized target selection is involved in both methods. There is no significant difference in implementing these methods between different satellite data. The normalization coefficients of the SR method was derived using Equation (6.2) and are listed in Table 6.5.

Table 6.5. The normalized coefficients for different normalized methods

Method	**Band 1**		**Band 2**		**Band 3**		**Band4**	
	a	**b**	**a**	**b**	**a**	**b**	**a**	**b**
SR	0.485	32.242	0.601	44.882	0.518	20.507	0.575	88.142
PIF	0.867	-88.605	1.062	-107.218	0.912	-80.272	0.925	-80.608
DB	0.623	-0.679	0.760	12.766	0.638	6.921	0.747	-3.085
NC	0.554	14.766	0.671	28.856	0.579	12.832	0.719	2.913

(2) The PIF method

The normalization coefficients were calculated using Equation (6.3) and are listed in Table 6.5.

For the IKONOS image and Quick Bird image, the pseudoinvariant feature set for the PIF method is defined by the following equations:

$$\text{PIF set}=\left\{\frac{\text{band4}}{\text{band3}} < t_1 \quad \text{and} \quad \text{band4} > t_2\right\} \tag{6.7}$$

where t_1 and t_2 are the threshold values. For IKONOS case, t_1 is set to 2 and t_2 is set to 80; for QuickBird case, t_1 is set to 2 and t_2 is set to 140. The threshold was set by comparing the different normalization results. The results of this method tested by Yuan and Elvidge [1996] and Yang and Lo [2000] were not good. Because the data set was different from previous research published by other authors [Schott et al., 1988; Eckhard et al., 1990; Hall et al., 1991; Elvidge et al., 1995; Yuan and Elvidge, 1996; Yang and Lo, 2000], the empirical values supported by those authors were not used in this study.

In this study, the normalized image and the reference image appear very different when directly using these pseudoinvariant feature sets derived from Equation (6.7). After analyzing the pseudoinvariant feature sets, the problem was that some floating objects in the river with reflectance similar to roof tops, roads and others were included in the pseudoinvariant feature sets. Those objects cannot be included into invariant change objects in the pseudoinvariant feature set because of its conflict with the assumption, wherein the selected normalization targets are assumed not to have any significant change between two acquisition dates. In such a case, a mask excluding all water area was required to refine the pseudoinvariant feature sets. After it was refined, the number of these pseudoinvariant feature sets was changed from 1629789 to 1543225

in the Quickbird image and from 1703930 to 1690168 in the IKONOS image. The normalized image was very similar to the reference image using refined pseudoinvariant feature sets, although it is not as good as other methods.

(3)The DB method

The greenness and brightness transformation formula differs between Landsat TM image/MSS image pairs and QuickBird image/IKONOS image pairs because of differences in the satellite sensors. Horne [2003] developed a set of translation coefficients for IKONOS images:

$$\text{brightness} = 0.326x_{blue} + 0.509x_{green} + 0.560x_{red} + 0.567x_{nir}$$

$$\text{greeness} = -0.311x_{blue} - 0.356x_{green} - 0.325x_{red} + 0.819x_{nir} \quad (6.8)$$

There is no special transformation formula in recent publications for QuickBird images. Since it is similar to the IKONOS image in both spectral range and radiometric resolution, Equation (6.8) was also applied to the QuickBird image for this study.

Both the dark set and bright set were defined using Equation (6.9), which was applied to the IKONOS image and the QuickBird Image:

$$\text{Dark set} = \{ \textit{greeness} \le t_1 \quad \textit{and} \quad \textit{brightness} \le t_2 \}$$

$$\text{and Bright set} = \{ \textit{greeness} \le t_1 \quad \textit{and} \quad \textit{brightness} \ge t_2 \} \quad (6.9)$$

where t_1 and t_2 are the threshold values. For IKONOS case, dark set, t_1 is set to 1 and t_2 is set to 300; bright set, t_1 is set to 1 and t_2 is set to 300.For QuickBird case, dark set, t_1 is set to 1 and t_2 is set to 190; bright set, t_1 is set to 1 and t_2 is set to 220. The threshold values in Equation (6.9) were obtained by comparing different results. All the empirical values that appeared in previous publications had no reference value for this study. The

normalization coefficients were calculated using Equation (6.4) and were listed in Table 6.5.

(4) The NC method

IKONOS and QuickBird only have one Near-IR band, unlike MSS satellite data which has two Near-IR bands. Thus, there is only one limited condition for determining the no-change pixels in the scattergram between Near-Infrared bands for IKONOS and QuickBird. In this study, good results were also obtained using the single Near-IR band. The NC set was defined by the following equation:

$$\text{NC set}=\{\left|Y\_4 - a_{40}X\_4 - b_{40}\right| \le \text{HVW}\} \tag{6.10}$$

where a_{40} and b_{40} are initial normalization coefficients for the Near-Infrared band normalization coefficients (a_4 and b_4) obtained through locating the centers of water and land-surface data clusters from Near-Infrared band—band 4 scattergram, the HVW was the corresponding half vertical width of the no-change regions in the scattergrams. The relationship of HVW and HPW was:

$$\text{HVW} = \sqrt{1 + a_{40}{}^2}\,(\text{HPW}) \tag{6.11}$$

where a_{40} is the initial normalization coefficient of band 4, HPW is the half perpendicular width which is set as 10 in this study.

In this study, the water cluster center coordinate in the scattergram is (53, 45), the land cluster center coordinate in the scattergram is (707,511). From these two coordinates, the initial normalization coefficients were acquired: a_{40}=0.7125, b_{40}=7.235. The HVW is 12.278, which was obtained with known a_{40} value by using Equation (6.11).

The normalization coefficients were calculated using Equation (6.5) and are listed in Table 6.5.

6.4 Results

The original QuickBird, IKONOS images, and the results of the normalized image are shown in figure 6.2. In terms of visual inspection, the HM is closest to the reference image, that is, the original QuickBird image. The SR, NC and DB look similar and it is difficult to determine which of these three normalized images is the best. To the naked eye, they all appear similar to the reference image. Compared with the other results, the PIF normalized image is most dissimilar to the reference image but it was still considered to be acceptable by the authors.

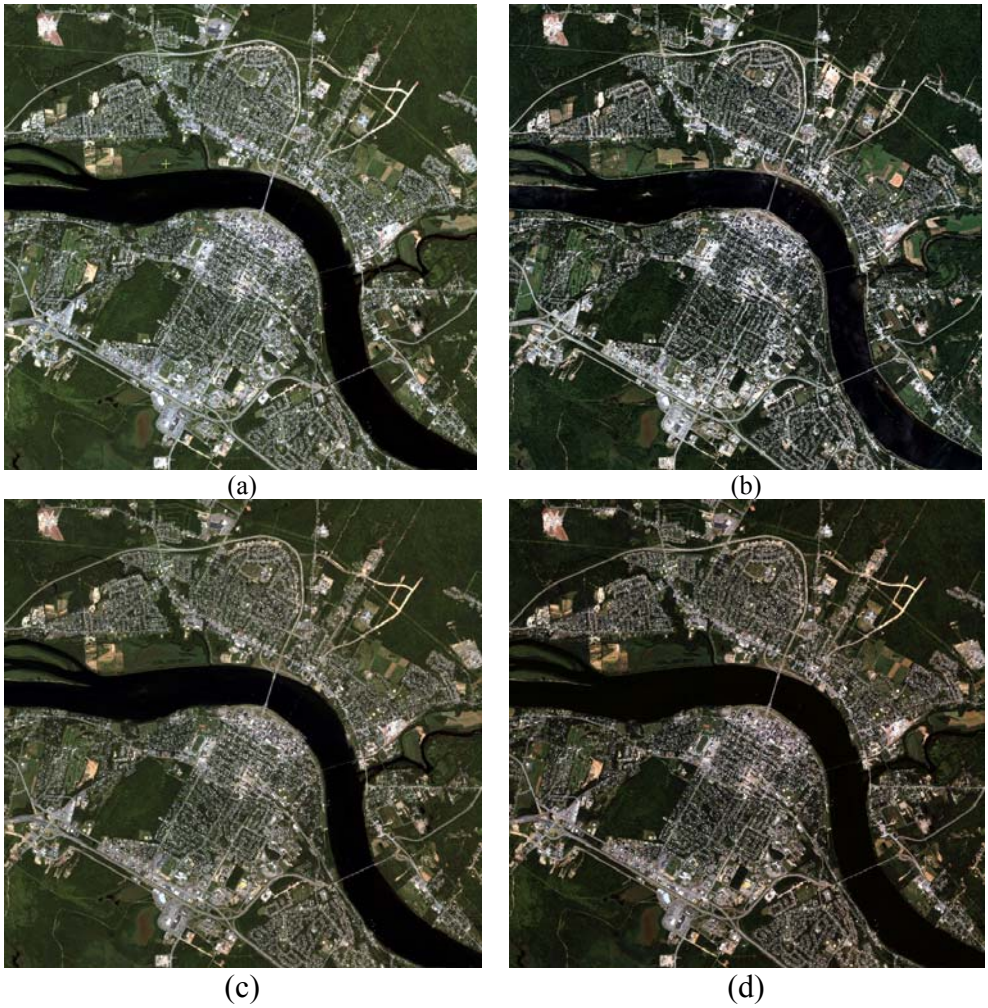

(a) (b)

(c) (d)

Figure 6.2. The reference image, the subject image and normalized images

(a) Original IKONOS image as the subject image; (b) Original QuickBird image as the reference image; (c) SR normalized IKONOS image; (d) HM normalized IKONOS image.

(e)

(f)

(g)

Figure 6.2. The reference image, the subject image and normalized images (continued)
(e) PIF normalized image; (f) DB normalized IKONOS image; (g) NC normalized IKONOS image.

Because the visual inspection is prone to subjectivity, the root mean square error (RMSE) is also used to evaluate the normalized images statistically. The root mean square error and sample sizes are listed in Table 6.6. In this table, the average RMSE of the original data is 118.98, all the normalized images average RMSE are less than this value. This implies that the normalized images are radiometrically more similar to the reference image. Different methods can be ranked according to their average RMSE value in descending order of HM, SR, NC, DB, PIF. The average RMSE difference is not significant among SM, NC and DB methods. These small differences underscore that visually distinguishing between them is difficult.

Table 6.6. Sample size and root mean square error of different normalization methods

Method	Radiometric control sets in IKONOS		Radiometric control sets in QuickBird		Root Mean Square Error				
	Number	%	Number	%	Band1	Band2	Band3	Band4	Average
RAW*	7639212	100	7639212	100	115.18	90.82	96.57	173.35	118.98
SR	7639212	100	7639212	100	30.39	53.41	48.06	125.34	64.3
HM	7639212	100	7639212	100	20.12	45.34	39.16	98.67	50.82
PIF	1690168	22.12	1543225	20.20	42.36	70.04	65.55	138.92	79.21
DB	895445(**D***) 1226286(**B***)		710399(**D***) 1133372(**B***)						
	2121731(**T***)	27.74	1843771(**T***)	24.13	32.77	57.47	53.25	128.03	67.88
NC	1240017	16.23	1240017	16.23	31.67	54.88	51.58	127.32	66.36

*** D: dark set; B: bright set; T: total pixel number; RAW means between the subject image and the reference image.**

6.5 Conclusion

This study investigated applying typical methods of image normalization for normalizing an IKONOS image with a QuickBird image. In this study, the color differences between the QuickBird image and the IKONOS image was not very significant, there was not much change between the two acquisition dates (2 years), and there exists a large water area (water is required in NC method). These characteristics satisfy the implementation requirements for all tested image normalization methods. This means that the image characteristics do not favor one method over another. Under these equitable conditions, the findings or contributions of this research are:

(1) Refining the PIF set yields a reasonable result, which differs from the negative results of previous published studies [Elvidge et al., 1996; Yang and Lo, 2000];

(2) The DB method provides a good result for the IKONOS image through introducing the empirical brightness and greenness transformation formula. In addition, it also works well on the QuickBird image, even though there is no special brightness and greenness transformation formula for the QuickBird image;

(3) In the NC method, using only one Near-IR band, it is possible to define no change area sets and obtain a good result.

From visually and statistically analyzing the normalized Quickbird and IKONOS images, HM produced the best results. That is, HM is the closest to the reference image, and is followed by SR, NC, DB and PIF. The differences among SR, NC, and DB are negligible. The PIF method ranks the lowest among all the tested normalization methods.

In terms of level of automation for each method, DB and PIF methods require more operator experience to set the threshold values, while other methods are relatively operator independent. Considering the combined effect of normalization and the degree of automatic implementation, this study concludes that HM is the most suitable method for normalizing QuickBird and IKONOS.

ACKNOWLEDGEMENTS

We would like to thank the GEOIDE (GEOmatics for Informed DEcisions) Network of Centres of Excellence of Canada for their financial support of this research and David Fraser (University of New Brunswick) for his suggestive comments.

REFERENCES

Caselles, V., and M.J.L. Garcia (1989). "An alternative simple approach to estimate atmospheric correction in multispectral studies." *International Journal of Remote Sensing*, Vol. 10, pp. 1127-1134.

Chavez, P.S., and D.J. Mackinnon (1994). "Automatic detection of vegetation changes in the Southwestern United States using remotely sensed images." *Photogrammetric Engineering and Remote Sensing*, Vol. 60, No. 5, pp. 571-583.

Eckhardt, D.W., J.P. Verdin, and G.R. Lyford (1990). "Automated update of an irrigated lands GIS using SOPT HRV imagery." *Photogrammetric Engineering and Remote Sensing*, Vol. 56, No. 11, pp. 1515-1522.

Elvidge, C.D., D. Yuan, R.D. Werackoon, and R.S. Lunetta (1995). "Relative radiometric normalization of Landsat Multispectral Scanner (MSS) data using an automated scattergram controlled regression." *Photogrammetric Engineering and Remote Sensing*, Vol. 61, No. 10, pp. 1255-1260.

Hall, F.G., D.E. Strebel, J.E. Nickeson, and S.J. Goetz (1991). "Radiometric rectification toward a common radiometric response among multidate, multisensor images." *Remote Sensing of Environment*, Vol. 35, No. 1, pp. 11-27.

Heo, J. and T.W. FitzHugh (2000). "A standardized radiometric normalization method for change detection using remotely sensed imagery." *Photogrammetric Engineering and Remote Sensing,* Vol. 66, No. 2, pp. 173-181.

Horne, H.J. (2003). "A tasseled cap transformation for IKONOS image." *ASPRS 2003 Annual conference proceedings,* Anchorage, Alaska.

Jensen, J.R. (1983). "Urban/suburban land use analysis." In. R. N. Colwell (Ed.), *Manual of Remote Sensing*, 2nd ed., American Society of Photogrammetry, Falls Church, VA, pp. 1571-1666.

Schott, J.R., C. Salvaggio, and W.J. Volchok (1988). "Radiometric scene normalization using pseudoinvariant features." *Remote Sensing of Environment*, Vol. 26, No. 1, pp. 1-16.

Yuan, D., and C.D. Elvidge (1996). "Comparison of relative radiometric normalization techniques." *ISPRS Journal of Photogrammetry and Remote Sensing*, Vol. 51, No. 3, pp. 117-126.

Yang, X.J., and C.P. Lo (2000). "Relative radiometric normalization performance for change detection from multi-date satellite images." *Photogrammetric Engineering and Remote Sensing*, Vol. 66, No. 8, pp. 967-980.

Chapter 7. CONCLUSION

7.1 Summary of major work

This research has developed several techniques and methods to resolve the problems encountered in processing high resolution remote sensing data. Three topics that have been studied are image fusion, image registration, and image normalization.

For **image fusion**, a novel image fusion method based on wavelet transform and IHS transform integration has been proposed. The method applies the IHS transform to fuse spatial information of the high-resolution image into the low-resolution multispectral image, through using the wavelet transform to generate a new high-resolution component that highly correlates to the intensity component of the IHS transform. Then, the new component is used to replace the intensity image for a reverse IHS transform. The fused image is obtained after the reverse IHS transform. While proposing the new image fusion method, the conventional IHS fusion methods (the cylinder model and the triangular model) and the conventional wavelet fusion have also been analyzed, and their fusion results have been compared by visual and statistical analysis. Initially, the optical images IKONOS and QuickBird, were used to evaluate the method. Later, three microwave data sets are used to evaluate the proposed fusion method in order to test the robustness of the proposed method. Two of the data sets consist of airborne SAR data and multispectral data (ASTER, Landsat, and SPOT) at different resolutions. The third data set is a Radarsat image and a Landsat TM image. Promising results were achieved in all the fusions of SAR images and multispectral

images from a variety of sensors with significant spatial and spectral variations. The ratios of resolution are different for the cases of SAR to Landsat TM, SPOT and ASTER: 1:24, 1:16, and 1:12 respectively. In addition, the spectral variations of the test images range from visible to infrared and microwave. Promising results were also achieved in the fusion of SAR and simulated natural colour SPOT images. To date, this method has been able to process any input data. In all fusion results, the color information of the multispectral image is preserved as well as the spatial information of the high resolution image.

As the proposed image fusion method is related to wavelet, some problems and factors related to wavelet-based image fusion methods have also been discussed. First, the limitations of the standard wavelet-based image fusion method have been analyzed. Second, two improvement methods, wavelet-IHS integration and wavelet-PCA integration, have been described. Third, factors that affect the wavelet-based image fusion have been discussed, such as wavelet selection (orthogonal, biorthogonal or nonorthogonal), decimation or undecimation, and wavelet decomposition level. Seven types of wavelet fusion methods (orthogonal wavelet fusion with decimation, orthogonal wavelet fusion without decimation, biorthogonal wavelet fusion with decimation, biorthogonal wavelet fusion without decimation, wavelet fusion based on the "à trous" wavelet and IHS transformation integration, and wavelet and PCA transformation integration) have been tested and compared. IKONOS and QuickBird have been used to evaluate these fusion methods.

For **image registration**, a new image registration technique, which is based on a combination of feature-based and area-based matching, has been proposed. A wavelet-

based feature extraction technique is used to extract the feature points and produce the pyramidal structure. Normalized cross-correlation matching is used to build the initial correspondence of feature points between the reference image and the sensed image. The accurate correspondent feature points can be obtained by using probability relaxation-based image matching, which is based on feature information, unlike the normalized cross-correlation matching technique, which is based on gray information. A coarse-to-fine matching strategy has been used in this registration process. A triangle-based model (a local transformation) has been used to resample the sensed image. Two pairs of data sets, panchromatic images of IKONOS and a panchromatic image of IKONOS with a multispectral image of QuickBird, were used to evaluate the proposed image registration algorithm.

For **image normalization**, current image normalization methods were proposed based on the Landsat images; due to differences in spatial resolution, spectral band and radiometric resolution between Landsat and IKONOS/QuickBird images, not all the existing methods can be directly applied to normalize IKONOS or QuickBird images. This research has examined whether or not existing methods can be directly adopted for image normalization with high resolution satellite images, and has shown how these methods can be modified for use with such images. Some improvements are introduced to the existing methods to overcome problems caused by differences of the spatial resolution, spectral band, and radiometric resolution. IKONOS and QuickBird multispectral images taken in different years have been used to evaluate the improved image normalization methods. The normalized results are compared using visual inspection and statistical analysis.

7.2 Conclusion and recommendation

The author has proposed a new image fusion method based on wavelet transform and IHS integration. The method has been evaluated using the optical image (IKONOS and QucikBird) and microwave images (airborne SAR and Radarsat with commonly used multispectral images, ASTER, Landsat, and SPOT). Successful results have been achieved for those images. This technique has also been evaluated by the industry and has attracted corporate interest. Further industrial commercialization will be considered.

This research has also discussed wavelet-based fusion problems, improvement approaches, and the factors that should be considered in the fusion process. For standard wavelet-based fusion, color distortion can be reduced to a certain extent, but the fused image appears similar to a high-pass filtered image. Wavelet-integrated methods, such as wavelet-IHS and wavelet-PCA, can improve the fusion result, reduce ringing or aliasing effects to some extent, and make the whole image smoother. The research has also elucidated the following factors: wavelets (orthogonal, birorthogonal, non-orthogonal), decimation or undecimation, and wavelet decomposition levels, which can affect the final fusion result.

The author has proposed a new image registration method, which uses a wavelet-based feature extraction technique, normalized cross-correlation and relaxation-based probability matching techniques, and a triangle-based local transformation model to resample the sensed image. The method has been tested on two pairs of data sets: panchromatic IKONOS images and a panchromatic IKONOS image with a multispectral QuickBird image. It can semi-automatically select enough control points for registration and can reduce the local distortions caused by terrain relief.

The research has also given improved strategies to normalize the high resolution images by using existing image normalization methods which were designed for the Landsat TM/MSS image. Due to differences in spatial resolution, spectral band and radiometric resolution between Landsat and IKONOS/QuickBird images, not all the existing methods can be directly applied to the normalization of IKONOS or QuickBird images. From this research, the following findings have been achieved. Refining the Pseudoinvariant Feature Set method yields a reasonable result; this differs from the negative results of previous published studies. The Dark-Bright method provides a good result for the IKONOS image through introducing an empirical brightness and greenness transformation formula; in addition, it works well with the QuickBird image, even though there is no special brightness and greenness transformation formula for QuickBird imagery. In the No Change Set method, using only one Near-IR band, it is possible to define no change area sets and obtain a good result.

Four contributions have been achieved in this research:

(1) This research has proposed a new image fusion algorithm to reduce the color distortion met in using current image fusion methods to process high resolution images. The new image fusion algorithm based on integration of wavelet transform and IHS transform, can process many different types of data and does not have data-specific limitations; to date, it has not been unable to process any available input data.

(2) This research has examined the problems of wavelet-based image fusion and provided the improvement methods. The factors that affect the wavelet-based

fusion have also been analyzed. The analysis can help researchers understand and control the wavelet-based fusion process.

(3) This research has proposed a new image registration algorithm to reduce the local distortion existing in high resolution images with terrain relief, which cannot be resolved by traditional image registration methods. The new image registration algorithm uses: the wavelet multiresolution property to extract feature points; a combination of normalized cross-correlation and probability relaxation matching techniques to find similarity between feature points in the reference and sensed images; and a triangle-based local transformation model to reduce the local distortion caused by terrain relief. The method can select a number of feature points semi-automatically, and reduce the local distortion existing in high resolution images with relief areas.

(4) This research has provided improved strategies to resolve the problems encountered by using the traditional image normalization methods for moderate resolution images. The strategies are used for normalizing the high resolution images through modifications to the existing image normalization methods.

7.3 Suggestions for further research

For **image fusion**, suggestions include further testing the proposed method, evaluation of SAR fusion results, and research on factors affecting wavelet-based fusion results. Because of data availability, the author could not use all of the existing types of data to evaluate the proposed method; it would be worthwhile to test the proposed

method by using as many data as possible. Also, quantitative evaluation of the fusion results of a high resolution SAR image and an optical MS image is very rare. The most commonly used method is the correlation coefficient. The fusion results should be evaluated by more quantitative evaluation methods. Good topics for further research on wavelet-based fusion are factors that could affect the fusion result, such as selection of mother wavelet, selection of the number of vanishing moments, and different fusion rules.

For **image registration**, suggestions include further refining the control points automatically and integrating more matching entities to improve the robustness of the proposed method. The proposed method is designed for high resolution images; some control points located in trees or buildings have to be removed manually in this research. Further research about removing those kinds of control point automatically would be beneficial. The control points are used in the proposed image registration method; if other matching entities, such as line or area based features, could be integrated into the image registration process, the proposed image registration would be more robust when applied to different data sources.

For **image normalization**, suggestions include objective selection of target objects and evaluation of nonlinear mathematical models in image normalization. The target selection of most of the image normalization methods is based on human visual inspection, and it is prone to subjectivity. The objective selection of normalization targets will be explored in further research. The mathematical model used currently is mostly based on the linear model, and the nonlinear model is also worth discussing in further research.

Appendix I

An Email from the Elsevier Ltd. regarding the permission to include articles published in Information Fusion in the dissertation

Dear Gang Hong

We hereby grant you permission to reproduce the material detailed below at no charge in your thesis subject to the following conditions:

1. If any part of the material to be used (for example, figures) has appeared in our publication with credit or acknowledgement to another source, permission must also be sought from that source. If such permission is not obtained then that material may not be included in your publication/copies.
2. Suitable acknowledgement to the source must be made, either as a footnote or in a reference list at the end of your publication, as follows:

"Reprinted from Publication title, Vol number, Author(s), Title of article, Pages No., Copyright (Year), with permission from Elsevier".

3. Reproduction of this material is confined to the purpose for which permission is hereby given.
4. This permission is granted for non-exclusive English rights only. For other languages please reapply separately for each one required. Permission excludes use in an electronic form. Should you have a specific electronic project in mind please reapply for permission.

5. This includes permission for UMI to supply single copies, on demand, of the complete thesis. Should your thesis be published commercially, please reapply for permission.

Yours sincerely
Marion Moss
Senior Rights Assistant
Elsevier Ltd
The Boulevard
Langford Lane
Kidlington
Oxford
OX5 1GB

Tel : +44 1865 843280
Fax : +44 1865 853333
E-mail: m.moss@elsevier.com

Appendix II

An Email from the Taylor & Francis regarding the permission to include articles published in International Journal of Remote Sensing in the dissertation

Dear Gang Hong,

'A Comparative Study on Radiometric Normalization Using High Resolution Satellite Images' by Hong G. and Y. Zhang *International Journal of Remote Sensing*

Thank you for your correspondence requesting permission to reproduce the above material from our journal in your forthcoming publication.

We will be pleased to grant you permission free of charge on the condition that:

This permission is limited to non exclusive English language rights for this usage only.

This permission does not cover any third party copyrighted work which may appear in the material requested.

No alterations may be made to our work without written consent.

All reasonable efforts must be made to contact the author(s) to notify them of your intentions and confirm they are happy with the permission being granted.

Full acknowledgement must be included showing publisher, article title, author, full Journal title, the credit line 'in press' and publisher (Taylor & Francis Ltd, http://www.tandf.co.uk/journals), reprinted by permission of the publisher.

Thank you for your interest in our Journal.

Yours sincerely

Huw Nesbitt
Permissions Administrator
Huw.Nesbitt@informa.com

Vita

Candidate's full name: Gang Hong

Universities attended:

2002.5- now
University of New Brunswick, Canada
Studying for PhD degree

2004.9- 2005.5
University of New Brunswick, Canada
University Teaching Diploma

1996-1999
Chinese Academy of Surveying and Mapping, China
Master's Degree

1992-1996
Liao Ning Technical University, China
Bachelor's Degree

Publications:

Journal Papers:

Zhang, Y. and **G. Hong** (2005)**.** "An IHS and wavelet integrated approach to improve pan-sharpening quality of IKONOS and QuickBird images." *International Journal of Information Fusion,* Vol. 6, No. 3, pp. 225-234.

Hong, G. and Y. Zhang (2006). "A comparative study on radiometric normalization using high resolution satellite images." *International Journal of Remote Sensing,* in press.

Hong, G. and Y. Zhang **(**2007**).** "Comparison and improvement of wavelet-based image fusion." *Submitted to International Journal of Remote Sensing*, in press.

Hong, G., Y. Zhang, J.B. Mercer (2006). "A robust technique for fusing SAR data and multisource multispectral images." *Submitted to Photogrammetric Engineering and Remote Sensing*, in reviewing process.

Hong, G. and Y. Zhang (2006). "The wavelet-based image registration technique for high resolution remote sensing image." Submitted to *Computers & Geosciences*, in reviewing process.

Conference Papers:

Lavigne, D.A., **G. Hong**, Y. Zhang, (2006). "Performance assessment of automated feature extraction tools on high resolution imagery." *MAPPS/ASPRS, 2006 Specialty Conference*, San Antonio, Texas, 6-10 November, 2006

Hong, G., Y. Zhang, D.A. Lavigne (2006). "Object-based change detection in high resolution image." *ASPRS 2006 Annual Conference*, Reno, Nevada, 1-5 May, 2006.

Hong, G., Y. Zhang, D.A. Lavigne (2006). "Comparison of car extraction techniques for high resolution airborne images." *1st workshop of the EARSeL Special Interest Group Urban Remote Sensing*, Berlin Adlershof, Germany, 2-3 March, 2006.

Mercer, J. B., D. Edwards, **G. Hong**, J. Maduck, Y. Zhang (2005). "Fusion of InSAR high resolution imagery and low resolution Multi-Spectral optical imagery." *ISPRS Hannover Workshop 2005*, Hannover Germany, 17-20 May, 2005.

Mercer, J.B., D. Edwards, **G. Hong**, J. Maduck, Y. Zhang (2005). "Fusion of high resolution Radar and low resolution multi-spectral optical imagery." *IGARSS 2005*, Seoul, Korea, 25-29 July, 2005.

Zhang, Y., **G. Hong**, J.B. Mercer, D. Edwards, J. Maduck (2005). "A wavelet approach for the fusion of radar amplitude and optical multispectral images." *The 9th World Multi-Conference on Systemics, Cybernetics and Informatics*, Florida, USA, July 10-13, 2005, Orlando.

Zhang, Y. and **G. Hong** (2005). "A wavelet integrated image fusion approach for target detection in very high resolution satellite imagery." *SPIE Defense& Security Symposium*, Florida USA, March 28 – April 1, 2005.

Hong, G. and Y. Zhang (2005). "Radiometric normalization of IKONOS image using QuickBird image for urban area change detection." *URS 2005*, Tempe Arizona, USA, 14-16 March, 2005.

Hong, G. and Y. Zhang (2005). "The image registration technique for high resolution remote sensing image in hilly area." *URBAN 2005*, Tempe, Arizona, United States, 14-16 March, 2005.

Hong, G. and Y. Zhang (2004). "The effects of different types of wavelets on image fusion." *Proceedings of the XXth ISPRS congress*, Istanbul, Turkey, 12-23 July, 2004.

Zhang, Y. and **G. Hong** (2004). "Improvement of image fusion quality by integrating wavelet transform into band substitution fusion techniques." *ASPRS Annual Conference Proceedings*, Denver, Colorado, America, May, 2004.

Hong, G., Y. Zhang and D. Fraser (2004). "A new image registration technique in urban change detection." *ASPRS Annual Conference Proceedings*, Denver, Colorado, May, 2004.

Hong, G. and Y. Zhang (2003). "High resolution image fusion based on Wavelet and IHS transformations." *In: Proceedings of the IEEE/ISPRS joint*

Workshop on "Remote Sensing and Data Fusion over Urban Areas", Berlin, 2003.

Conference Presentations:

Hong, G. and Y. Zhang (2005). "Radiometric normalization of IKONOS image using QuickBird image for urban area change detection." *URS 2005*, Tempe Arizona, USA, 14-16 March, 2005.

Hong, G. and Y. Zhang (2005). "The image registration technique for high resolution remote sensing image in hilly area." *URBAN 2005*, Tempe, Arizona, United States, 14-16 March, 2005.